INTERMEDIATE AND HIGH – ENERGY COLLISIONS

Experimental 1

Chairman	J. OREAR
Rapporteur	G. BELLETTINI
Discussion Leader	I. MANNELLI
Secretaries	M. FIDECARO
	S. KULLANDER

TWO-BODY PROCESSES

G. Bellettini

Istituto di Fisica dell' Università, Pisa and Istituto Nazionale di Fisica Nucleare, Sezione di Pisa

1. ELASTIC SCATTERING AND TOTAL CROSS-SECTIONS

1.1 Proton-proton elastic scattering

As you know, the pp elastic differential cross-section depends a priori on two variables, for instance the energy and the scattering angle. However, up to one year ago the experimentalists working in high-energy pp scattering were accustomed to presenting their data as a function of a single variable. Such a variable thus contained both an energy and an angle dependence, and it was chosen in such a way that data at many angles and energies were distributed along a single simple pattern. This procedure is justified by the idea that in this way the single variable -- if it exists -- on which the interaction depends will be naturally indicated by the data. The most popular example of this is Orear's plot of $s\, d\sigma/d\Omega$ versus $p_\perp$ [1] (s = c.m. total energy squared, $p_\perp$ = $= p \sin\theta$ = transverse momentum). Several other presentations of the data have recently been proposed[2-4].

The most successful approach was made by Krisch[3], who was able to display all data available up to about one year ago in the fashion shown in Fig. 1. Krisch interpreted the existence of three "slopes" separated by "breaks" in this picture as evidence for the existence of structure within the proton. Much discussion on the significance of these structures has recently been continued in the literature[5]. However, in order to obtain this presentation use was made of an ideal cross-section $d\sigma^+/dt$ for distinguishable protons; it is this "true" cross-section which, in the idea of Krisch, is likely to show a simple pattern. The function needed to derive such a "true" cross-section depends on the unknown cross-section itself

$$d\sigma(\theta) = d\sigma^+(\theta) + d\sigma^+(\pi-\theta)$$

$$d\sigma^+(\theta) = f(\theta)\, d\sigma(\theta)$$

$$f(\theta) = \frac{d\sigma^+(\theta)}{d\sigma^+(\theta) + d\sigma^+(\pi-\theta)}$$

(θ = c.m. scattering angle), and therefore the construction of $d\sigma^+/dt$ from the experimental data is

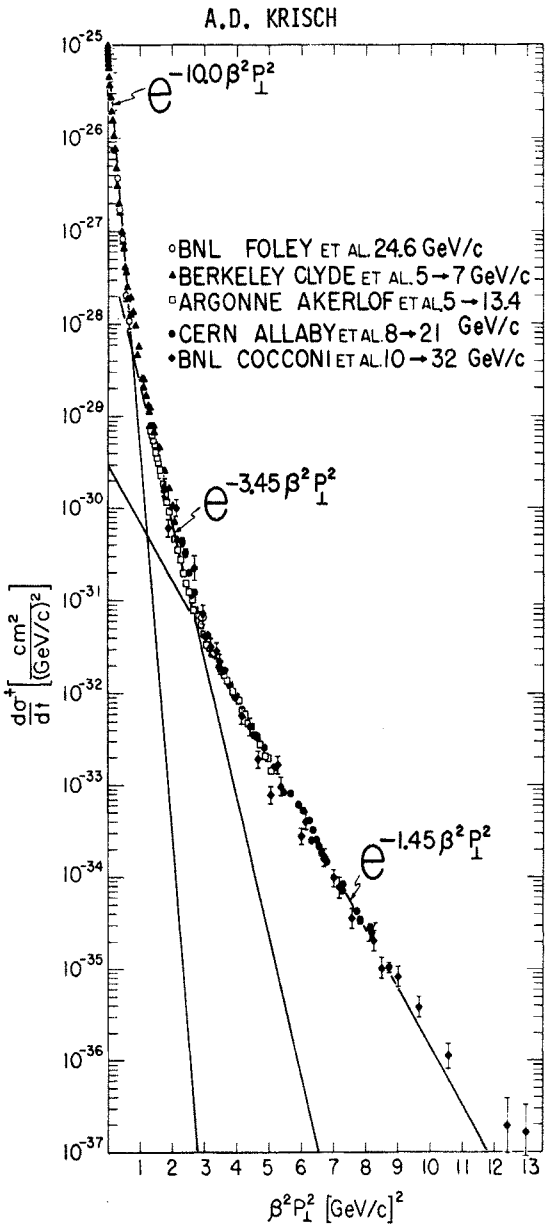

Fig. 1 Plot of $d\sigma^+/dt$ versus $\beta^2 p_\perp^2$ (β = proton velocity in the c.m., $p_\perp$ = p sin θ = transverse momentum) for all high-energy proton-proton elastic scattering data (Ref. 3). For references on the experimental data and for further discussions on this presentation, see Ref. 3.

arbitrary and made ad hoc in view of obtaining the simple pattern. While $d\sigma/dt$ is symmetrical with respect to 90°, $d\sigma^+/dt$ is a decreasing function of θ through 90°. However, the function chosen by Krisch was not able to accommodate on the exponentials of Fig. 1 the data from several precise angular distributions between 40° and 90° and from 8 to 12 GeV/c, measured at CERN last year, to better than a factor of two or so[6]. Also in Krisch's approach one would identify $d\sigma^+/dt$ with the differential cross-section for np elastic scattering (n and p are indeed distinguishable). This would imply at $\theta = 90°$ $d\sigma(np) = 1/2\, d\sigma(pp)$, whilst at this angle there is a clear indication for $d\sigma(np) \approx d\sigma(pp)$ (see Section 1.1).

As a matter of fact, if one abandons the search for a special presentation, one can notice several interesting features in the data. An example of this situation is seen in Fig. 2, which contains some of the recent CERN data, presented as $d\sigma/dt$ versus $p_\perp$. Some data from other groups are also included. The curves at each energy end at $\theta = 90°$. With increasing energy, a wider and wider $p_\perp$ interval is explored, and some new structure appears to be brought in. At $\theta = 90°$, the distributions at different energies end

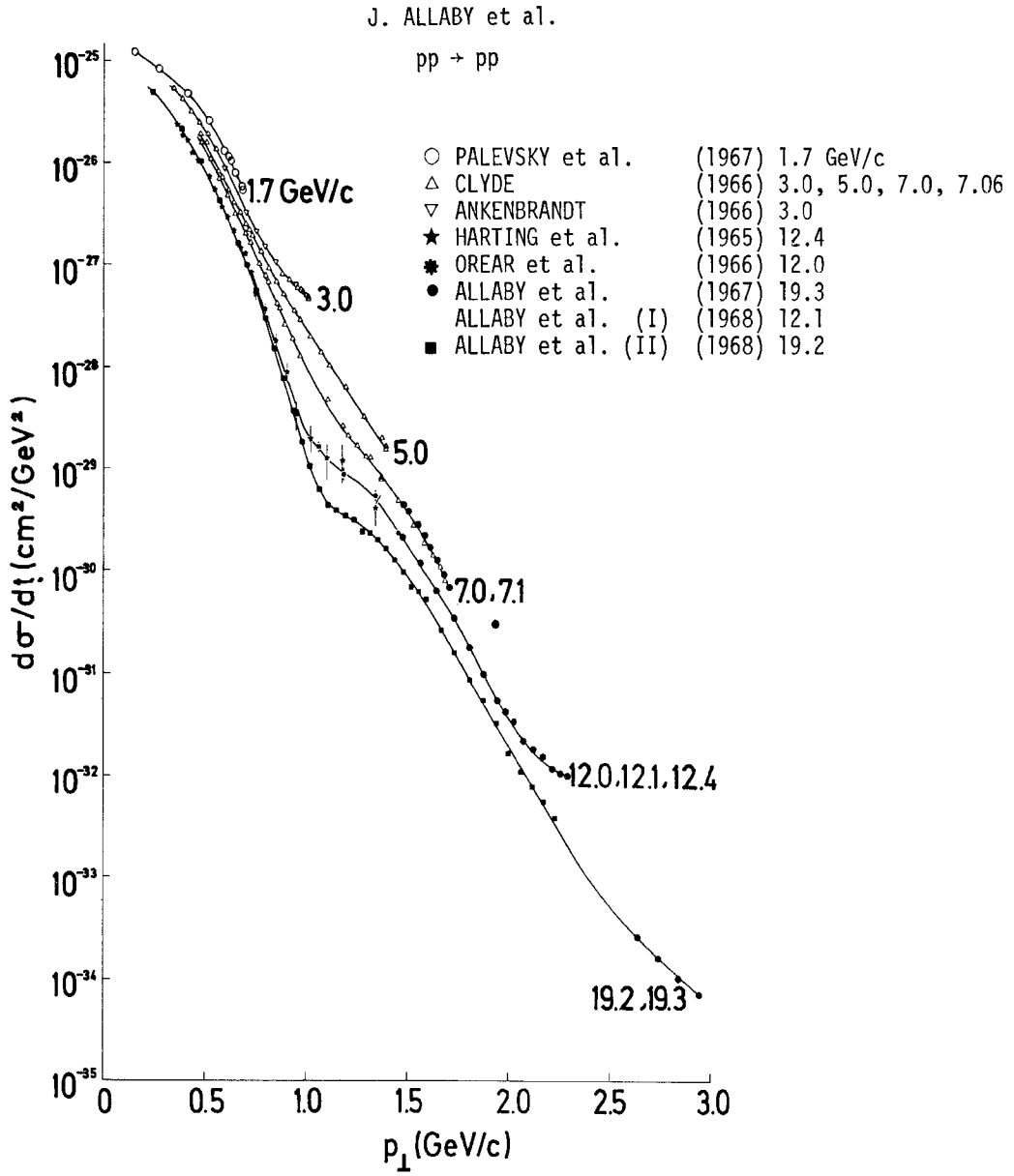

Fig. 2 Proton-proton elastic scattering differential cross-sections $d\sigma/dt$ as functions of $p_\perp$ (Ref. 6). The curves joining the experimental points are hand-drawn to guide the eye. For references on the experimental data, see Ref. 6.

at different positions along such a structure. The main structure is a shoulder at $p_\perp \sim 1$ GeV/c that becomes more and more prominent with increasing energy.

In Fig. 3 all the new CERN data[7] are presented versus $|t|$, together with some previously existing data. The large $|t|$ data at all energies were taken with a double-arm spectrometer; the data at $|t| \leq 6$ $(GeV/c)^2$ at 19.2 GeV/c were taken with a single-arm high-precision spectrometer.

The main structure which develops with increasing energy is at $|t| \sim 1$ $(GeV/c)^2$. One may also note a tendency of $d\sigma/dt$ to become almost energy independent from $|t| = 0$ over a wider and wider $|t|$ interval with increasing energy. This picture may indicate the existence of some "saturated" energy-independent (non-shrinking) cross-sections at infinite energy. As we heard from Dr. Chan's talk[8], some recent theoretical models[9] can naturally explain such a picture, including the increase of structure in the data with increasing energy[10-12]. Another model, however[13], which is in good qualitative agreement with these data, predicts that the decrease of the cross-section at fixed $|t|$ with increasing energy will continue up to infinite energy.

Looking at Fig. 3, one can also understand how one may find "breaks" in cross-sections. In a hypothetical experiment at fixed large θ, for example $\theta = 90°$, one would find a break at about 8 GeV/c, since the waving structure has some variation of phase at 90° at about this energy.

The experiment by Akerlof et al. at Argonne[2], where the first striking example of breaks in $d\sigma/dt$ was found, was in fact done precisely in these conditions. The results from this experiment are shown in Fig. 4. It is clear that since these data came before most of the precise high-energy data shown in

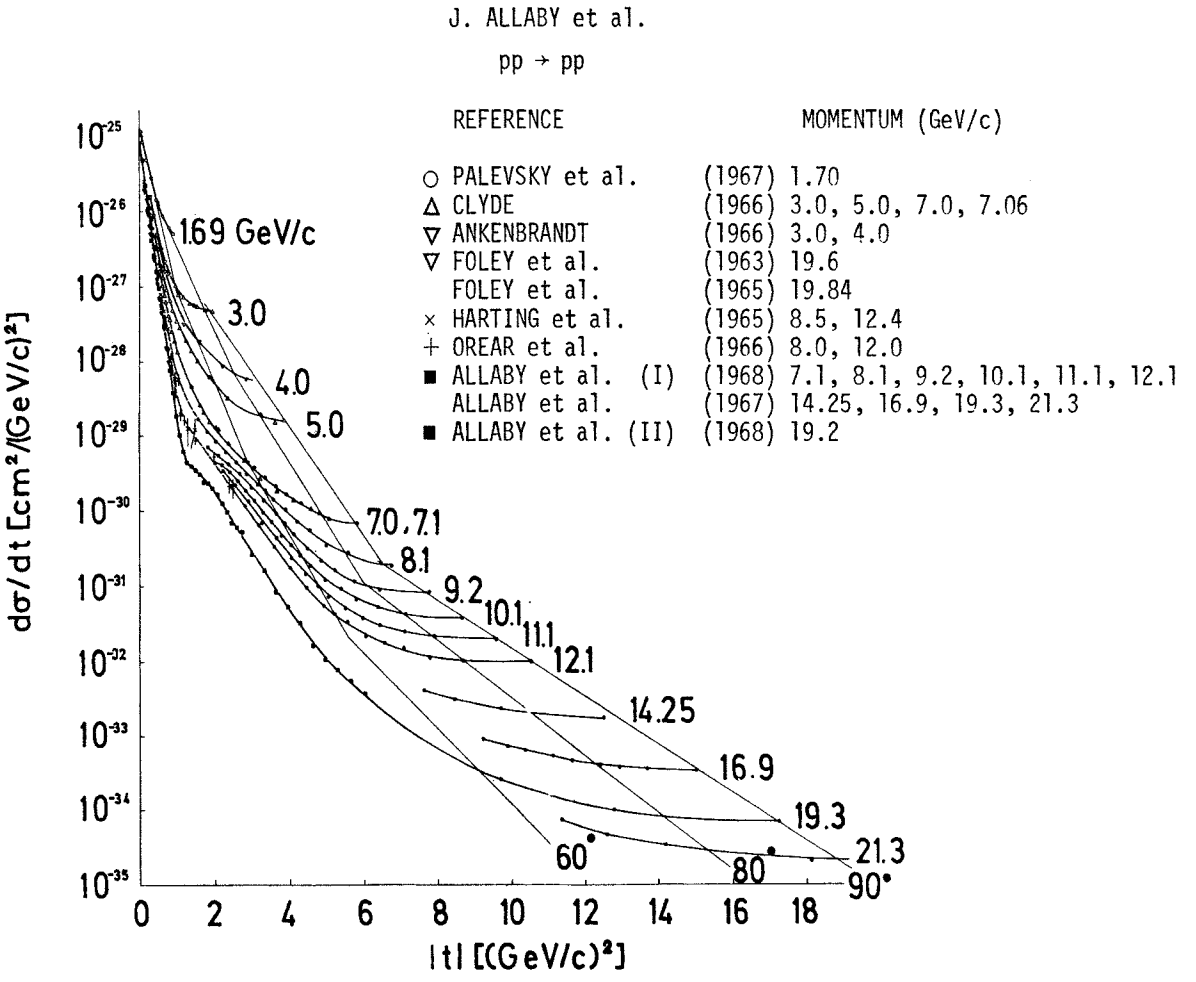

Fig. 3 Proton-proton elastic scattering differential cross-sections as functions of $|t|$ (Ref. 6). The curves joining the experimental points are hand-drawn to guide the eye. The loci of cross-sections for fixed c.m. angle are indicated for 60°, 80°, and 90°. For references on the experimental data, see Refs. 6 and 7.

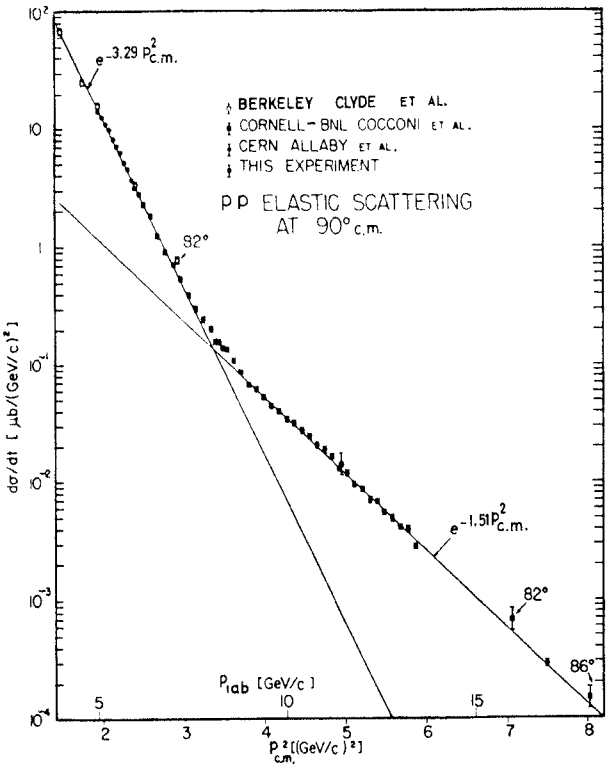

Fig. 4 Plot of $d\sigma/dt$ versus $p^2_{c.m.}$ for proton-proton elastic scattering at 90° in the centre-of-mass system (Ref. 2). The lines drawn are straight line fits to the low-energy and the high-energy data. Data from the experiment by Akerlof et al. are added to some data from other experiments, as quoted in Ref. 2.

Figs. 2 and 3, it was very natural at that time to place great emphasis on the significance of this break.

1.2 Total and elastic differential neutron-proton cross-sections

A Michigan-Princeton-Stanford group working at Berkeley and at BNL and a Karlsruhe group working at CERN have presented new data on neutron-proton total cross-sections and differential elastic cross-sections. These groups used neutron beams and a transmission technique.

In Fig. 5 the total cross-section results of the Karlsruhe group at 4.3, 6.5, and 10.0 GeV/c [14], and of the Michigan-Princeton group at 14.6, 17.8, 21.6, and 27.0 GeV/c [15] [which we shall call $\sigma(np)$] are compared with data obtained from total pd and pp cross-section measurements [16-18] [which we shall call $\sigma(pn)$]. The total proton-proton cross-section is also shown as a full line.

At momenta between 5 and 20 GeV/c, $\sigma_t(pn)$ is consistently higher than $\sigma_t(np)$, whilst $\sigma_t(pp)$ lies between the two. These differences (of the order of at most 5%) can be easily accounted for by systematic errors in the experiments. In particular, the point at 3.0 GeV/c by Bugg et al. [16] has recently been measured at BNL using the same technique [19]. The result is about 2.5 mb lower than that by Bugg et al.

All these data are averages over a rather wide and not too well-known energy interval, due to the Fermi motion of the neutron for $\sigma_t(pn)$ and to the wide neutron beam spectrum in $\sigma_t(np)$. This fact introduces some uncertainty when making a comparison with $\sigma_t(pp)$. In such a situation, one can make the statement that above 5 GeV/c, $\sigma_t(np)$ [or $\sigma_t(pn)$] is equal to $\sigma_t(pp)$ to a few per cent.

The Michigan-Stanford-Princeton group has also measured angular distributions for elastic np cross-section up to $|t| \simeq 1$ (GeV/c)^2, at several energies from 8 to 30 GeV/c [20]. As an example, the differential np cross-section at (23.4 ± 2) GeV/c is shown in Fig. 6 and compared with pp data at 24.6 GeV/c by Foley et al. [21]. The situation at the other energies is practically the same. One concludes that up to the highest available energies the forward diffraction peak for neutron-proton scattering is very similar to the peak in pp scattering. Preliminary data by the Karlsruhe group [22] at momenta between 4 and 15 GeV/c also support this conclusion.

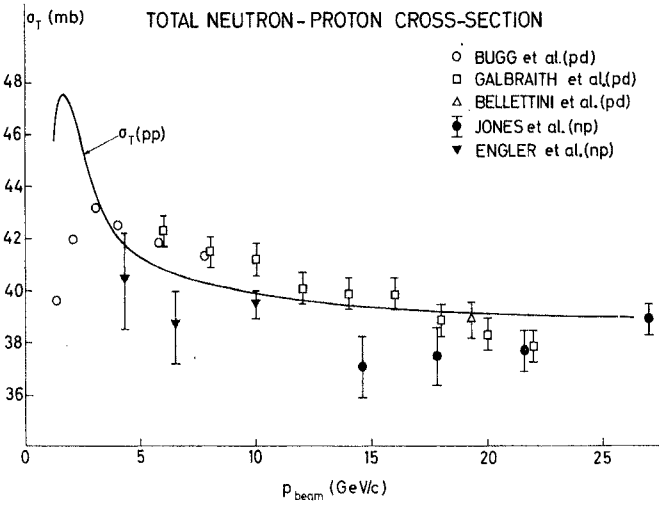

Fig. 5 Compilation of high-energy data on neutron-proton total cross-sections [data obtained indirectly from $\sigma_t(pd)$ and $\sigma_t(pp)$ are shown with open symbols, Refs. 16-18. Cross-sections measured directly by means of a neutron beam are shown with black symbols]. The full line is a smooth curve through the existing pp total cross-section data.

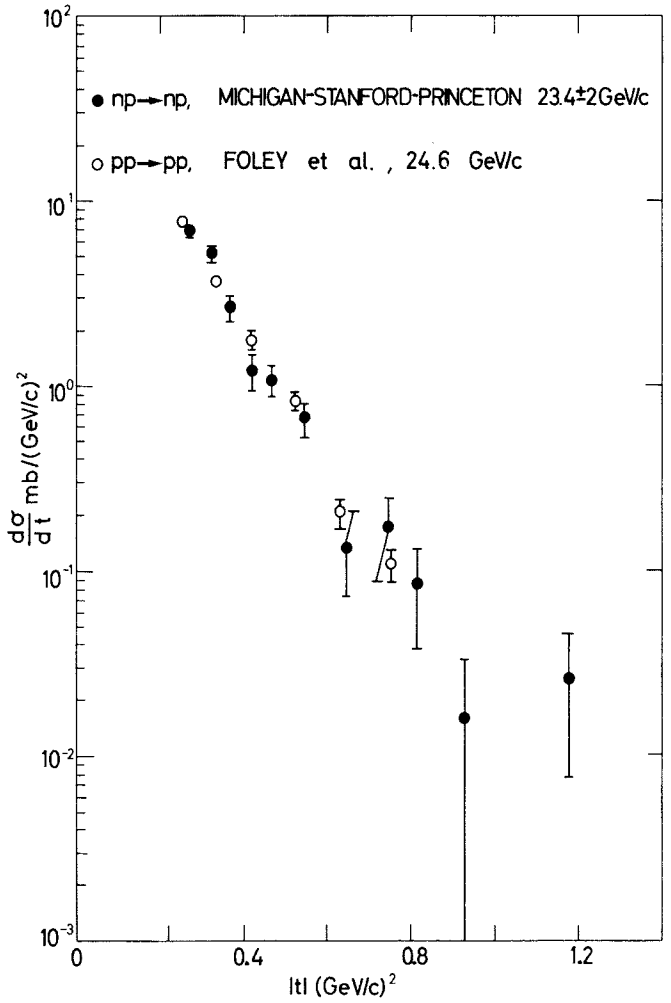

Fig. 6 The np elastic scattering differential cross-section (Ref. 20) for neutron momenta between 21.4 and 25.4 GeV/c (full points). The pp data at 24.6 GeV/c by Foley et al. (Ref. 21) are shown for comparison.

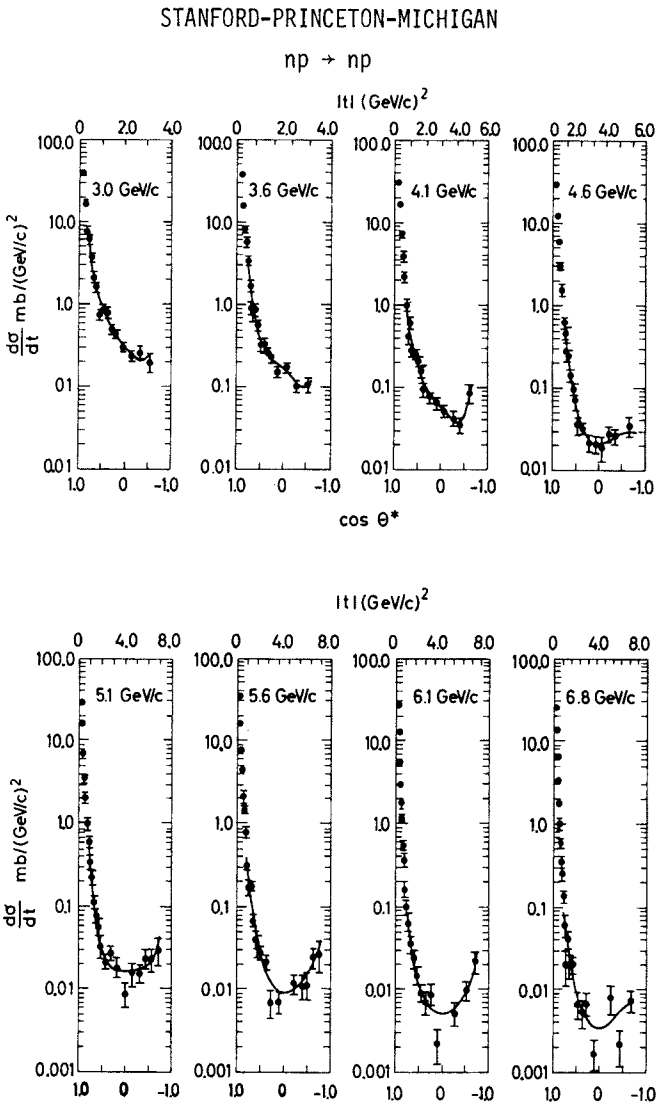

Fig. 7 The np elastic scattering differential cross-sections from 3.0 to 6.8 GeV/c, as functions of the cosine of the neutron c.m. scattering angle (Ref. 23). The full lines are polynomial fits to the large-angle data.

Away from the diffraction peak and through the 90° region, data are available up to about 7 GeV/c. These data (Fig. 7) have been measured at the Lawrence Radiation Laboratory by the Stanford-Princeton-Michigan group[23]. The cross-sections at 4.6 GeV/c and higher energies look rather symmetrical with respect to 90°. The full curves are polynomial fits to the large-angle points. From these fits one can deduce the 90° cross-section. The conclusion of the authors is that

$$\frac{d\sigma(np)}{d\sigma(pp)}(90°) = 1.1^{+0.13}_{-0.10},$$

as an average between 4 and 7 GeV/c. Even if the quoted error on this ratio may look somewhat optimistic, there is a clear indication that at 90° $d\sigma(np) \sim d\sigma(pp)$. This is what one would obtain if at 90° the nucleon-nucleon interaction is spin independent. Such a result implies that at 90° the isospin zero cross-section is approximately three times as large as the isospin one (pp) cross-section[24]. This result is also in contrast with the speculation by Wu and Yang[25] that at high energies and at $\theta \approx 90°$ $d\sigma(pp) = 2\, d\sigma(np)$.

1.3 Neutron total cross-sections on nuclei

New data from the Karlsruhe group[26] and from the Michigan-Princeton-Stanford group[27] on high-energy total neutron cross-sections on several nuclei are shown in Fig. 8. Although the CERN data are at an average momentum of 10 GeV/c and the BNL data are at

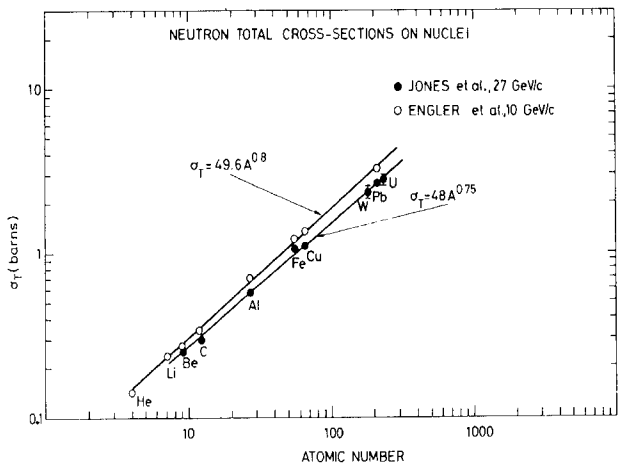

Fig. 8 Comparison of the n-nuclei total cross-section data at ∿ 10 GeV/c by the Karlsruhe group (Ref. 26)(Engler et al., open points) with the ∿ 27 GeV/c data by the Michigan-Princeton-Stanford group (Ref. 27)(Jones et al., open points). The full lines are hand-fits to the data. However, Engler et al. report that their data are well fitted by the formula $\sigma_t = 2\pi(1.3A^{1/3} - 0.5)^2$ fm^2, which is the same formula that also fits the e$^-$-nuclei total cross-section data, after substituting 1.2 for the 1.3 numerical factor.

∿ 27 GeV/c, the difference between the data is too large to be due to the difference in incoming beam momentum.

Since we know that $\sigma_t(np) \approx \sigma_t(pp)$ (Section 1.1) one would also expect that σ_t(n Nucleus) $\approx \sigma_t$(p Nucleus). This consideration would favour the Karlsruhe data, since it agrees very well with previous CERN results on total proton-nuclei cross-sections at ∿ 20 GeV/c [28]. However, the proton-nuclei data can be brought into better agreement with the Michigan-Princeton-Stanford data if one assumes[15] that an important real part is present in the proton-nucleus (strong interaction) scattering amplitude. Also, some older data by Pantuev and Khachaturyan[29] on neutron total cross-sections on copper and lead at 8.3 GeV/c agree better with the Michigan-Princeton-Stanford data. It appears that only new measurements can possibly clarify the situation.

1.4 Antiproton-proton and antiproton-neutron elastic scattering

New data on $\bar{p}p$ elastic scattering at 8 and 16 GeV/c and $|t| \lesssim 1$ (GeV/c)^2 have been presented at this Conference by the BNL-Carnegie Mellon group[30]. In this experiment, the forward-scattered particle is momentum-analysed with a high resolution magnet spectrometer with wire spark chambers. The results are shown

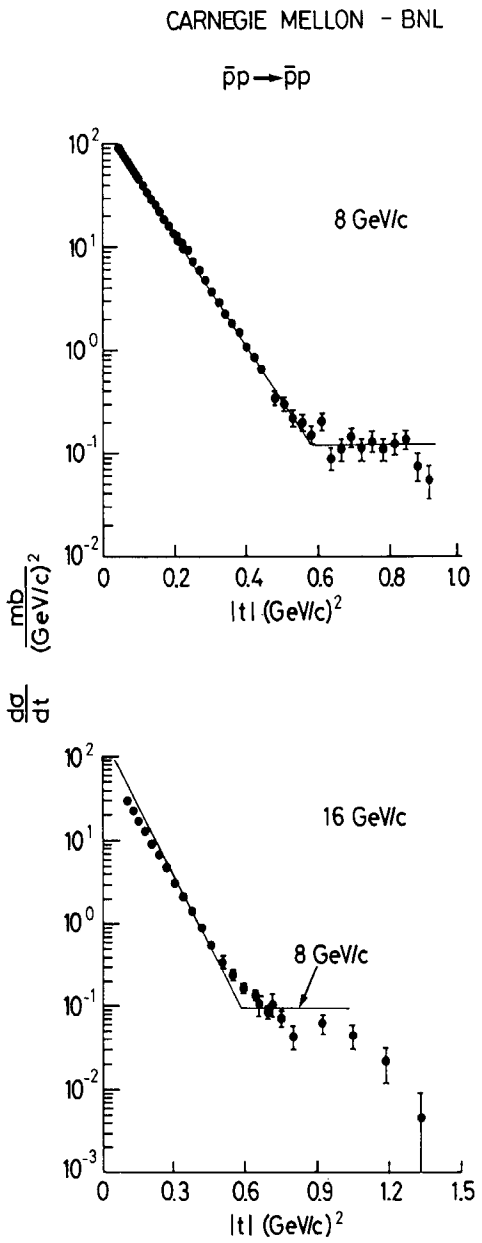

Fig. 9 Differential cross-sections for $\bar{p}p$ elastic scattering at 8 and 16 GeV/c (Ref. 30). The full curve on both plots shows the behaviour of the 8 GeV/c data.

in Fig. 9. One observes that the forward peak ends at $|t| \simeq 0.6$ (GeV/c)^2, and that a shoulder develops at larger $|t|$'s. A line drawn through the 8 GeV/c data, and reproduced on the 16 GeV/c graph, helps to note that the forward peak continues expanding with increasing energy even at such high energies, and that the cross-section at the shoulder decreases slowly with increasing energy (not more than a factor of 2 when going from 8 to 16 GeV/c).

The Cornell-BNL group, using two magnet spectrometers with optical spark chambers, measured the $\bar{p}p$ differential cross-section data at 5.8 and 9.7 GeV/c

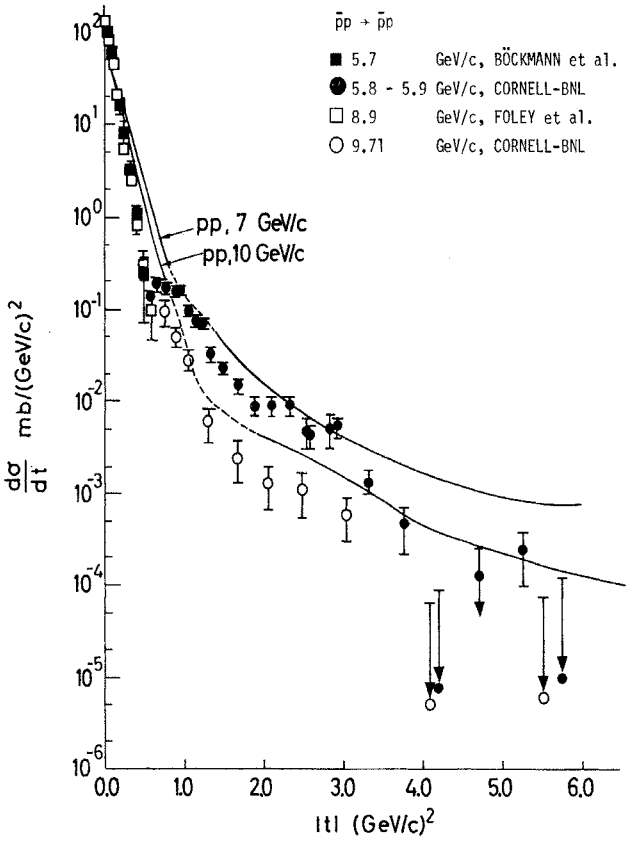

Fig. 10 Differential cross-section for $\bar{p}p$ elastic scattering at ∿ 5.8 and ∿ 9.7 GeV/c (Refs. 31 and 32). Full squares are representative points from Ref. 33, and open squares are representative points from Ref. 34. The pp cross-sections at ∿ 7 and ∿ 10 GeV/c are also shown for comparison.

over a $|t|$ range from ∿ 0.5 to ∿ 5.5 $(GeV/c)^2$ [31,32]. These data are shown in Fig. 10, together with some existing data at comparable energies and smaller angles[33,34].

The structure at $|t| \sim 0.6 (GeV/c)^2$ is again seen clearly, whilst an additional shoulder may be present at $|t| \sim$ 2-3 $(GeV/c)^2$, possibly followed by a drop in the cross-section at $|t| \geq 4$ $(GeV/c)^2$.

In Fig. 10 the pp differential cross-section at ∿ 7 and ∿ 10 GeV/c is also plotted for comparison. One observes that the forward peak in $\bar{p}p$ is sensibly steeper than in pp [with slopes of ∿ 10-12 $(GeV/c)^{-2}$]. The secondary structure seems to become less pronounced for $\bar{p}p$ with increasing energy, whilst it definitely behaves in the opposite sense in the pp case.

At $|t| \geq 1$ $(GeV/c)^2$ the $\bar{p}p$ cross-section is always below the pp one, but the general behaviour of the two cross-sections is more or less the same. However, it is possible that the indications mentioned above for some structure in the $\bar{p}p$ case at $|t| \geq 2$ $(GeV/c)^2$ are due to statistical fluctuations.

At this Conference, a paper by Berryhill and Cline[35] has been presented which allows a comparison of $\bar{p}p$ and $\bar{p}n$ elastic scattering above 1 GeV/c at $|t| \leq 1$ $(GeV/c)^2$. The data are shown in Fig. 11. In order to reduce the relative systematic errors, both reactions were measured on the same film from an exposure of a deuterium bubble chamber to antiprotons. One sees that the peak-bump structure in the $\bar{p}p$ differential cross-section is present even at such a low energy, and that $\bar{p}n$ is very similar to $\bar{p}p$. However, the forward peak in $\bar{p}n$ is steeper than in $\bar{p}p$, and the two cross-sections cross twice. $\bar{p}n$ is larger than $\bar{p}p$ at very small $|t|$ and at $|t| \geq 0.4$ $(GeV/c)^2$.

In a Regge-pole model the existence of such differences would imply that I = 1 exchanges, such as ρ or A_2, give appreciable contributions, since the I = 0 terms such as P, P', ω are symmetrical in the two reactions. This may be of some interest, because current Regge-pole models of forward nucleon-nucleon scattering[36] assume that only the I = 0 trajectories are strongly coupled to the nucleon-nucleon system. On the other hand, the energy is very low, and it is

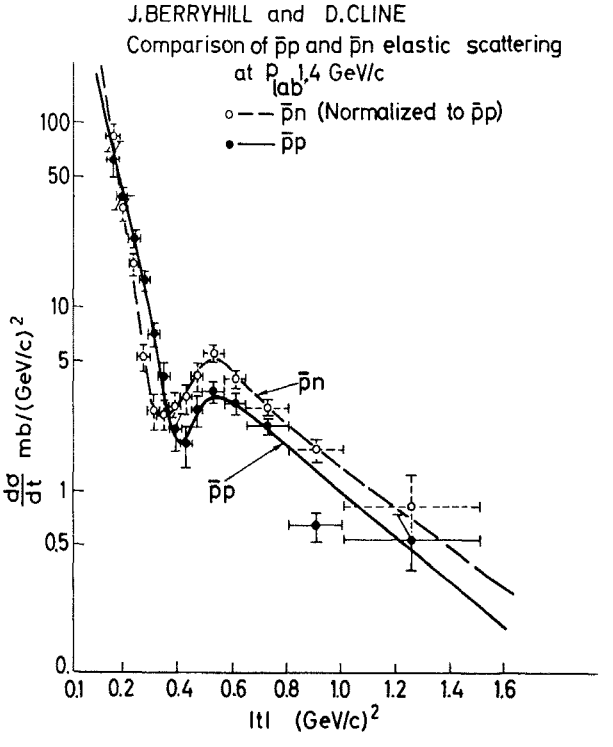

Fig. 11 The $\bar{p}p$ (full circles) and $\bar{p}n$ (open circles) differential cross-sections at 1.4 GeV/c (Ref. 35). Hand-drawn curves through the points are also shown.

possible that there are other interpretations of these data.

1.5 Pion-nucleon elastic scattering

The differential cross-sections for $\pi^- p$ and $\pi^+ p$ elastic scattering are known to be rather similar at high energies and in the forward region, showing the usual forward peak, followed by a structure at $|t| \approx$ ≈ 0.6 (GeV/c)^2. This structure is a dip followed by a broad maximum at 2-3 GeV/c incident momentum, which quickly dies into a smooth shoulder at 4-6 GeV/c[37,38]. New $\pi^- p$ data[31,32] from $\sim$ 6 to $\sim$ 14 GeV/c by the Cornell-BNL group are shown in Fig. 12. From these data one sees that the structure at $|t| \approx 0.6$ GeV/c becomes smoother and smoother with increasing energy, while a second minimum is present at $|t| \approx 3$ GeV/c, which seems to be rather energy independent.

At large $|t|$ the cross-section drops very fast with energy. At $|t| \sim 2$ (GeV/c)^2 it drops like $\sim s^{-3.2}$, and at $|t| \sim 2.4$ (GeV/c)^2 like $\sim s^{-4}$ [32]. At $|t| \lesssim 2$ (GeV/c)^2 the energy dependence becomes very weak. One may notice a tendency for the cross-section

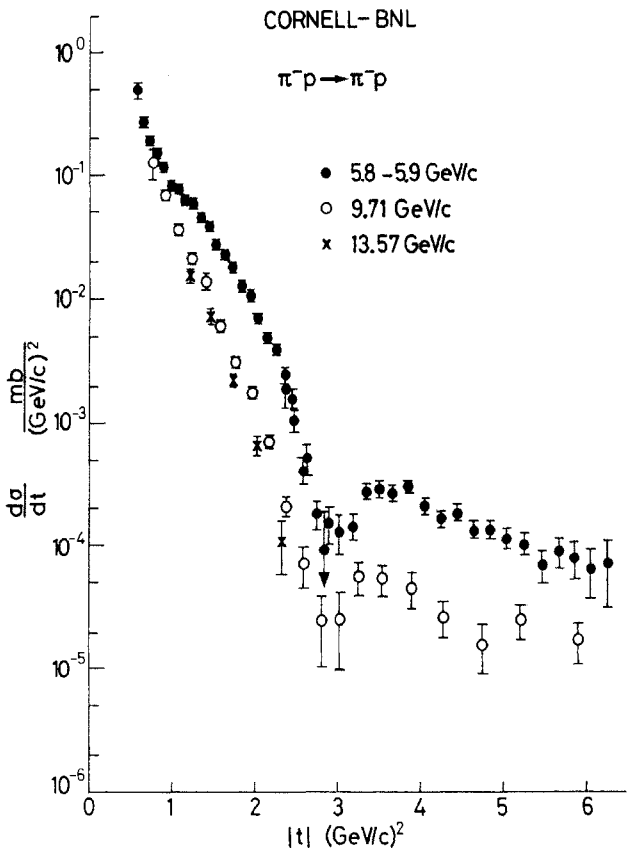

Fig. 12 Differential cross-section for $\pi^- p$ scattering between $\sim$ 6 and $\sim$ 13.5 incident momentum, and for 0.6 (GeV/c)^2 $\lesssim |t| \lesssim$ 6 (GeV/c)^2 (Refs. 31 and 32).

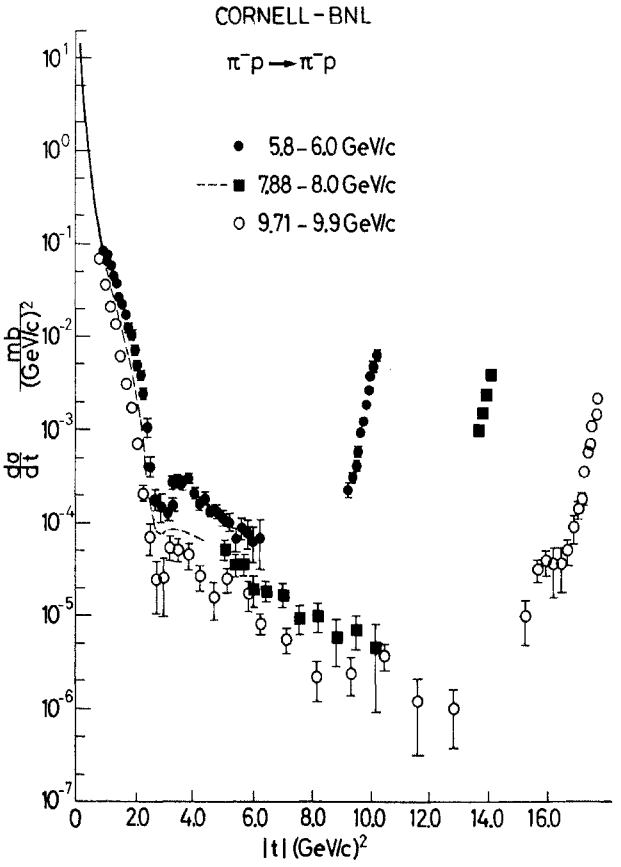

Fig. 13 Full $\pi^- p$ angular distributions at $\sim$ 6, $\sim$ 8, and $\sim$ 10 GeV/c incident momentum[32]. The rough shape of the cross-sections at $|t| \lesssim 0.8$ (GeV/c)^2 is shown as a full line. To allow a clear presentation, the data at $\sim$ 8 GeV/c for $|t| \lesssim 5$ (GeV/c)^2 are not shown, and are replaced by a broken line.

to approach a "saturated" energy-independent cross-section, over a range of $|t|$ that becomes wider and wider with increasing energy. As observed in Section 1.1, indication of a similar phenomenon was noticeable also in the case of pp elastic scattering.

The new Cornell-BNL data provide us with an almost complete angular distribution for $\pi^- p$ scattering at $\sim$ 10 GeV/c, as shown in Fig. 13. The backward peaks are about 10^4 times smaller in cross-section than are the forward ones. At 10 GeV/c there is a clear indication for some structure also in the backward peak.

Such backward peaks are a very general, although not absolutely general, property of the two-body or quasi-two-body hadron collisions at high energies[39]. Consequently, we shall discuss the backward data in further detail.

The backward $\pi^- p$ data by the BNL-Carnegie Mellon[40] group and by the Cornell-BNL group[41] are shown in Fig. 14, plotted versus u on an expanded scale. As

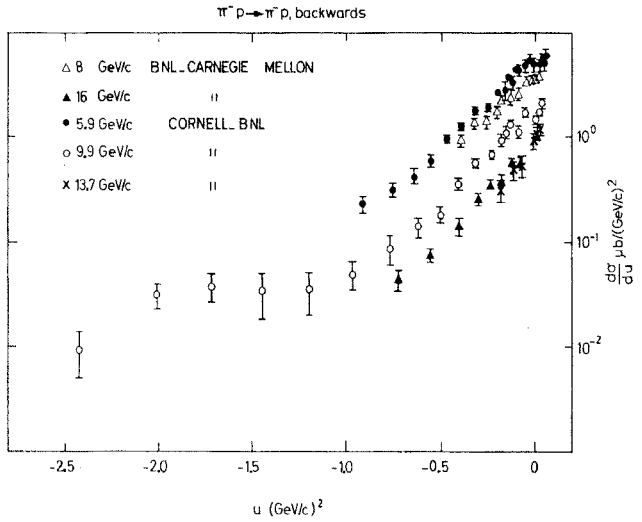

Fig. 14 Backward π^-p scattering data from Refs. 40 and 41.

a whole, the data at each energy for $|u| \lesssim 1$ (GeV/c)^2 are consistent with pure exponentials in u with slopes of ~ 4 (GeV/c)$^{-2}$. For $|u| \gtrsim 1$ (GeV/c)^2, a secondary shoulder develops in the 10 GeV/c Cornell-BNL data.

Although separate data from each experiment show a clear energy dependence of the cross-section [such as $\sim p_{lab}^{-2}$, as an average between 8 and 16 GeV/c, according to Anderson et al.[40]], the combined data may give the impression that the cross-section at $u = u_{max}$ is rather constant above 10 GeV/c. When allowing for some possible relative normalization error,

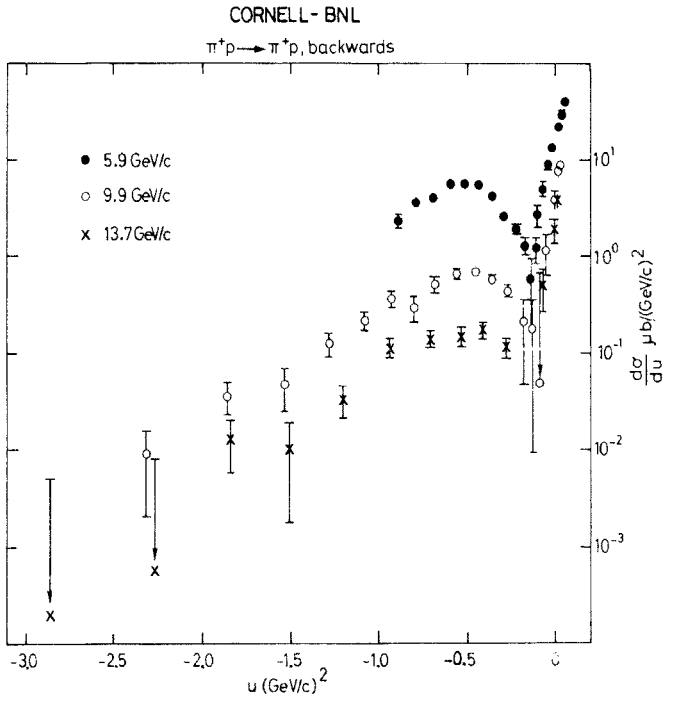

Fig. 15 Backward π^+p differential cross-section between ~ 6 and ~ 14 GeV/c (Ref. 41).

one may perhaps accommodate the energy dependence that is predicted by the baryon-exchange model.

The Cornell-BNL group has also extended its measurements to backward π^+p scattering. The results at 5.9, 9.9, and 13.7 GeV/c [41] are shown in Fig. 15. The sharp dip at $u \approx -0.15$ (GeV/c)^2 is the most striking feature of the data. The 10 and 13.7 GeV/c data do not contain any indication for a reduction of this phenomenon with increasing energy. The slope of the peak shrinks from ~ 13 (GeV/c)$^{-2}$ to ~ 18 (GeV/c)$^{-2}$ when going from 6 to 14 GeV/c.

Such impressive features of backward πp scattering, including the striking difference between π^- and π^+, are currently explained in the Regge-pole model by assuming that the backward scattering is dominated by baryon exchanges in the u channel. Using the Δ and the N_α trajectories only, Barger and Cline[42] obtain a rather good fit to the combined π^+ and π^- data of the Cornell-BNL group. The fit in the π^+p case is shown in Fig. 16. In this model the dip is due to a

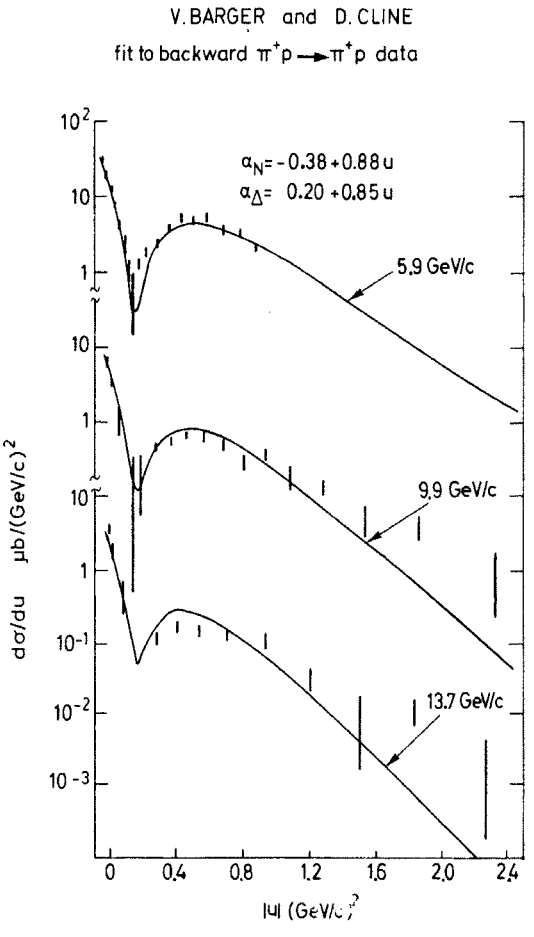

Fig. 16 Regge-pole model fits to backward π^+p scattering data, by Barger and Cline (Ref. 42). The indicated α_N and α_Δ trajectories are as obtained in the fit to both π^-p and π^+p data.

zero in the N_α exchange amplitude at $\alpha_N = -1/2$. At the dip, where the isospin 1/2 exchange amplitude is zero, the model predicts 1/9 for the ratio of the π^+p and π^-p cross-sections, which is very near to the experimental value of $\sim 1/7$. However, a similar dip at $\alpha_\Delta = -3/2$ in the π^-p case does not appear, which is somewhat disappointing. The trajectories obtained in the fit, as quoted in Fig. 16, go nicely through the existing isobars in the Chew-Frautschi plot.

A similar Regge-pole model, but allowing for an important contribution by the N_γ trajectory, has been proposed by Contogouris et al.[43]. The rather weak energy-dependence of the backward π^-p cross-section above 10 GeV/c, as noticed before, might create some problems for all such Regge-pole models.

Diffraction-type models have also recently been proposed to interpret the main features of backward πp scattering[44].

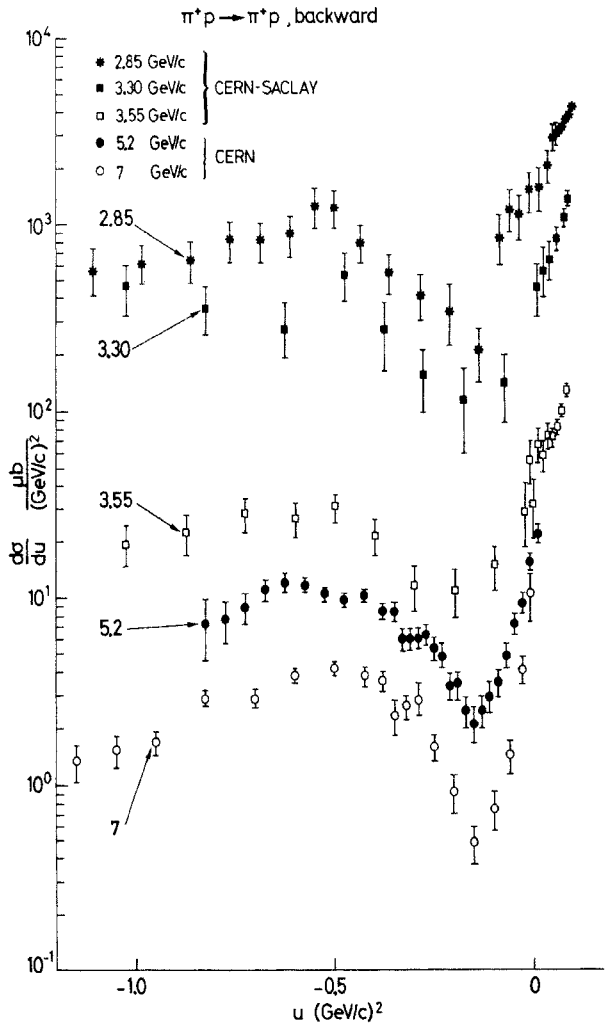

Fig. 17 Combined π^+p backward elastic scattering data by the CERN-Saclay (Ref. 45) and CERN (Ref. 46) experiments, from 2.85 to 7 GeV/c laboratory momentum.

V.D. ANTOPOLSKY et al.

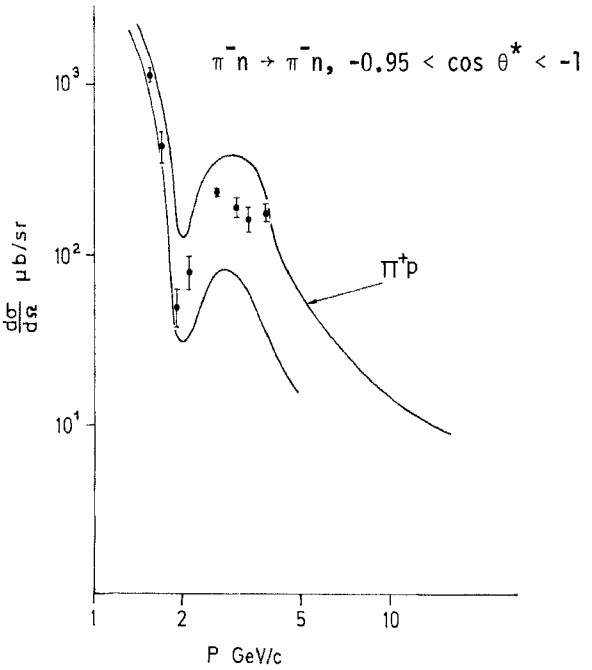

Fig. 18 Preliminary results by Antopolsky et al. (Ref. 48) on backward ($-0.95 < \cos\theta^* < -1$) π^-n elastic scattering. According to charge symmetry, the points should lie inside the band within the full lines. Such lines have been drawn to enclose the region covered by the existing π^+p scattering data.

The peak-dip structure in backward π^+p scattering develops at surprisingly low energy. This is seen in Fig. 17, which shows data at 2.85, 3.30, and 3.55 GeV/c from a Saclay-CERN experiment[45], and data at 5.2 and 7.0 GeV/c from a CERN experiment[46].

One observes a strong energy-dependence of the cross-section all over the backward region (such as $\sim s^{-2}$), but the peak-dip structure is practically the same down to 2.85 GeV/c. It is also interesting to observe that the formulas by which Barger and Cline fit the high-energy data, as shown previously, predict such a behaviour rather well[47].

Aiming to check charge symmetry, Antopolsky et al.[48] at Dubna have measured π^-n scattering at the backward direction and at several energies between 1.5 and 3.8 GeV/c. They used an optical spark chamber system surrounding a deuterium target. Preliminary data from this experiment are shown in Fig. 18. The full lines enclose the region covered by the existing π^+p scattering data.

1.6 Kaon-proton elastic scattering

At $|t| \lesssim 1.2$ (GeV/c)^2, K^-p and K^+p differential cross-sections are known to show (as usual) forward

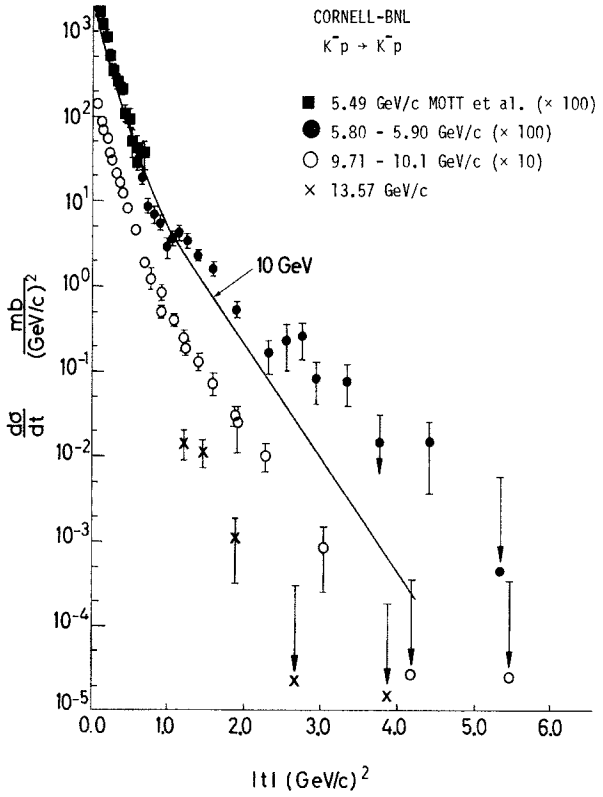

Fig. 19 Cornell-BNL data (Refs. 31 and 32) on elastic K^-p scattering; the 5.49 GeV/c by Mott et al. (Ref. 49) are also included. The ∿ 6 GeV/c data are plotted after multiplying by 100, and the ∿ 10 GeV/c data after multiplying by 10. The full line shows the qualitative behaviour of the 10 GeV/c data, after multiplying by 100.

peaks, the K^-p one being somewhat steeper[34]. New K^-p data by the Cornell-BNL group at ∿ 6, ∿ 10, and ∿ 13.5 GeV/c [31,32] are shown in Fig. 19. Data at 5.49 GeV/c by Mott et al.[49] are also included.

In order to allow a better presentation, the 10 GeV/c points in Fig. 19 are multiplied by ten, and the 6 GeV/c points by one hundred. The full line represents the 10 GeV/c cross-section multiplied by one hundred, to allow comparison with the 6 GeV/c data. Thus one can observe that the forward peak at $|t| \lesssim 1$ (GeV/c)^2 expands with increasing energy. For 1 (GeV/c)$^2 \lesssim |t| \lesssim 2$ (GeV/c)^2 there is appreciable energy dependence; the rather narrow structure present in the 6 GeV/c data is washed down to a change in slope at 10 GeV/c. At $|t| \gtrsim 2$ GeV/c, the cross-section appears to drop fast with increasing energy.

At the backward direction, the K^-p differential cross-section drops extremely quickly with increasing energy. This is very different from backward π^+ and π^- scattering, as we have seen in Section 1.4, and also from backward K^+p scattering which has a backward peak, as we shall see in a moment.

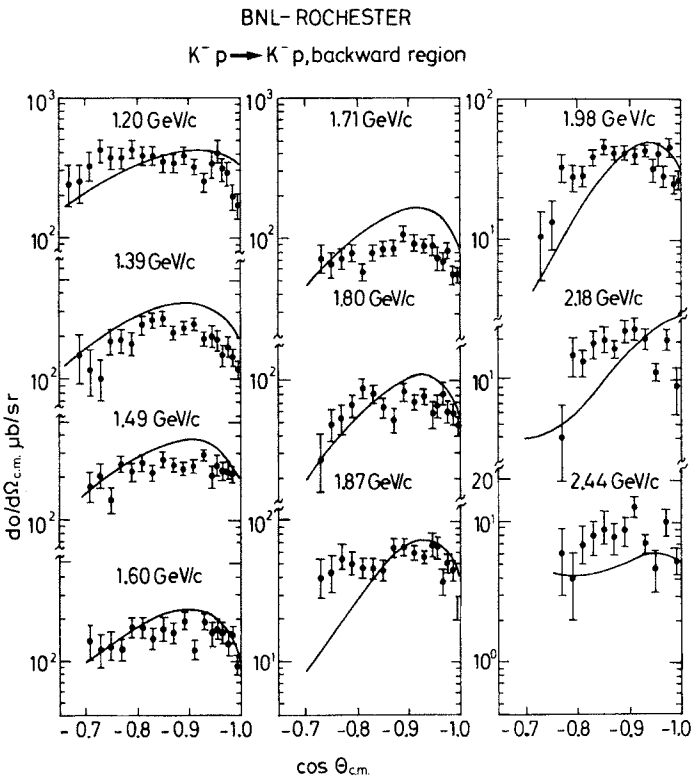

Fig. 20 K^-p elastic scattering differential cross-sections in the backward region between 1.2 and 2.44 GeV/c (Ref. 50). The full curves are best fit curves using a superposition of the known s-channel resonances.

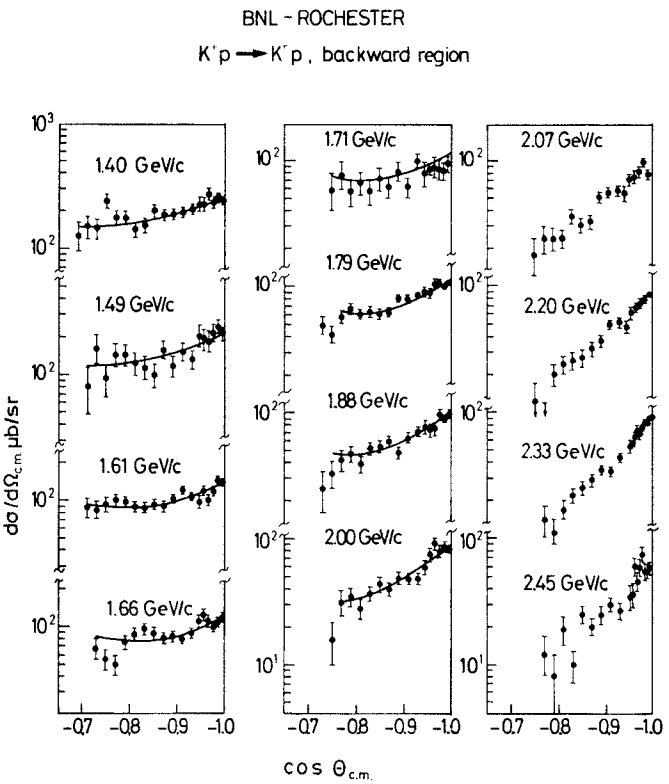

Fig. 21 K^+p elastic scattering differential cross-sections in the backward region, between 1.40 and 2.45 GeV/c (Ref. 52). The full lines are hand-drawn curves through the data.

Figure 20 shows data from a BNL-Rochester counter experiment with wire spark chambers[50]. At these energies the contribution from s-channel resonances is enough to explain the cross-section (as shown in the figure by the continuous curves). The situation is not very different from the $\pi^- p$ case[51]: in particular, the backward dip is similar in both cases. However, whilst at higher energies a backward peak develops in $\pi^- p$, the $K^- p$ cross-section continues to drop quickly with energy. In the baryon exchange model of the backward cross-sections, this fact is naturally explained if one assumes that there is no strangeness +1 baryon.

New data by the BNL-Rochester group have been presented at this Conference, also on backward $K^+ p$ scattering[52]. These data are shown in Fig. 21. In general they are rather flat, but with a trend to peak backwards with increasing energy. The curves shown are calculated from an energy-dependent phase-shift fit to all the available $K^+ p$ data.

The CERN group of Baker et al. has also measured backward $K^+ p$ elastic scattering at 5.2 and 7 GeV/c [46].

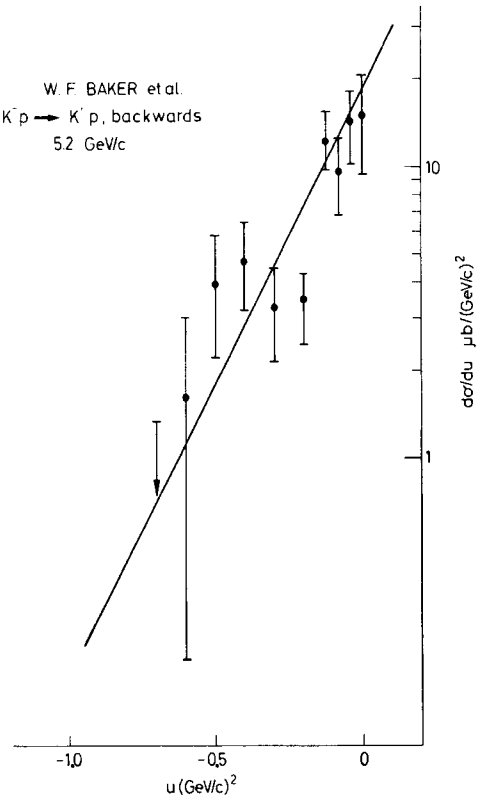

Fig. 22 Backward $K^+ p$ data by Baker et al. (Ref. 46). The full line shows the forward differential cross-section [slope ~ 5 $(GeV/c)^{-2}$] divided by 1000 and plotted at $|u| = |t|$.

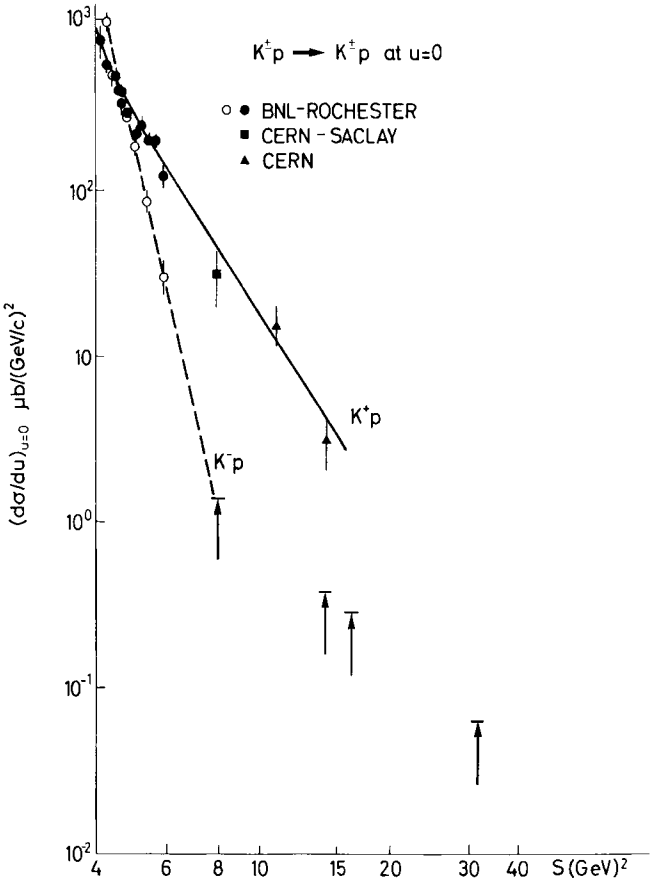

Fig. 23 Energy behaviour of the $u = 0$ $K^- p$ and $K^+ p$ elastic scattering cross-section (data from Refs. 50, 52, 54 and 55).

The 5.2 GeV/c data show a clear backward peak, as shown in Fig. 22. The existence of such a peak has been interpreted[39,53] as being due to some $S = -1$ baryon exchange in the u-channel. The full line in Fig. 22 represents the forward cross-section divided by one thousand and plotted at $|u| = |t|$. One observes that the slopes of both peaks [~ 5 $(GeV/c)^2$] are practically identical.

The backward peak drops fast with increasing energy. This is seen in Fig. 23 which shows the energy dependence of $d\sigma/du$ $(u = 0)$ for both $K^+ p$ and $K^- p$ scattering. Data at 7 GeV/c or below come from the BNL-Rochester[50,52] and CERN experiments[46] discussed before, and from a CERN-Saclay experiment at 3.55 GeV/c[54]. The two upper limits, 0.18 μb at 8 and 0.08 μb at 16 GeV/c, for the average backward cross-section have been measured by the BNL-Carnegie Mellon group at BNL[55]. The rate of decrease for the $K^+ p$ case is $\sim s^{-4}$, consistent with the interpretation of these backward peaks as being due to the exchange of the low-lying strange baryon trajectories. Without

any connection to possible theoretical models, one may observe that the u = 0, K^-p cross-section below 2.5 GeV/c decreases roughly as s^{-10}.

In Fig. 24 the qualitative features of the backward $\pi^{\pm}p$ and K^+p scattering are compared. The K^+p cross-section at 7 GeV/c is of the same magnitude as the π^-p cross-sections, but it is dropping faster with increasing energy. One sees that if one forgets the dip in π^+p (!), all slopes are very similar.

1.7 Backward $\pi^- + p \to \rho^- + p$

Although the $\pi^- + p \to \rho^- + p$ reaction should not be quoted below the "elastic scattering and total cross-sections" heading, I would like to mention it before leaving the argument of the backward peaks, because the Carnegie Mellon-BNL group has reported on an interesting peak in the backward region of this reaction[56]. This group measured the momentum of the forward recoil proton with the wire spark chamber spectrometer, and separated the ρ^-p final state by a missing-mass technique.

These data at 8 and 16 GeV/c are shown in Fig. 25, and compared with backward π^-p elastic scattering data and with the angular distribution for the background near the ρ mass in the missing-mass distribution. One sees that at 8 GeV/c the ρ^-p differential cross-section is steeper than at 16 GeV/c, and that the background is not to be suspected of being responsible for such a difference.

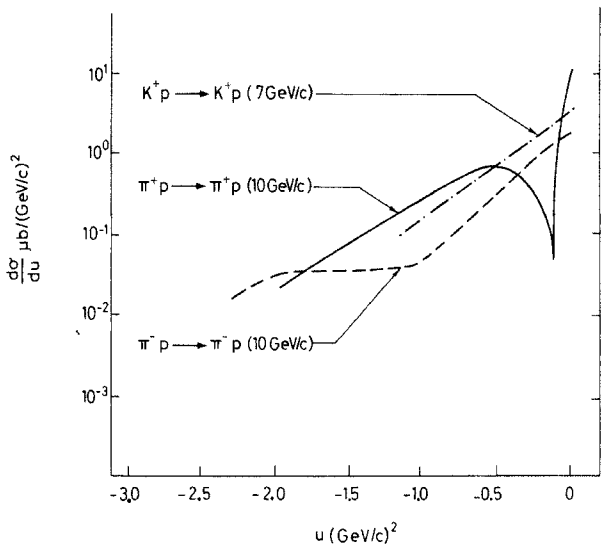

Fig. 24 Comparative behaviour of the K^+p (at ∿ 7 GeV/c), π^+p (at ∿ 10 GeV/c), and π^-p (at ∿ 10 GeV/c) differential cross-sections in the backward region.

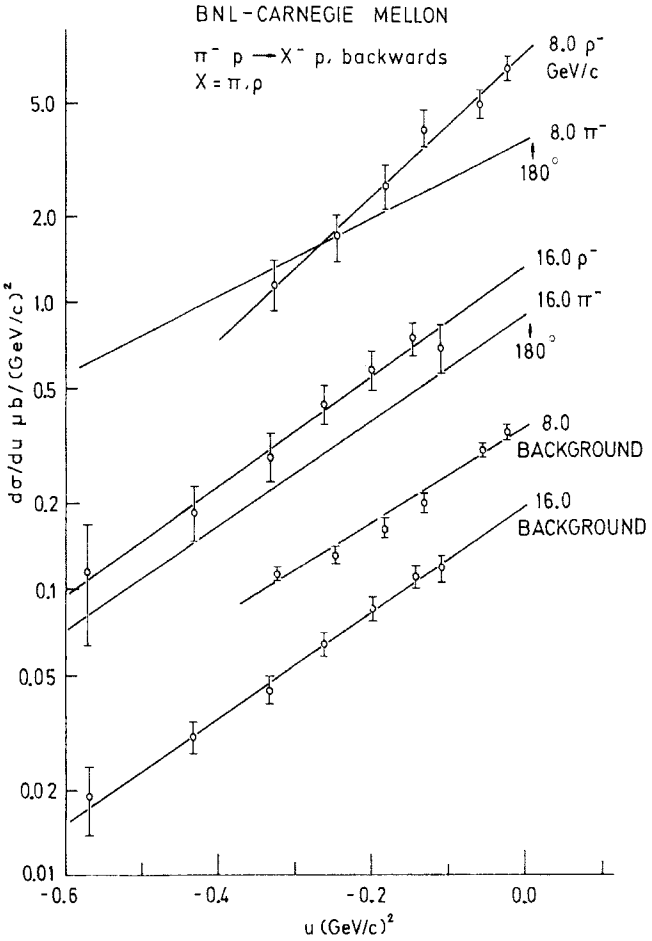

Fig. 25 Backward angular distribution for the reaction $\pi^- + p \to \rho^- + p$ at 8 and 16 GeV/c (Ref. 56). The angular distributions for π^- elastic scattering and for the reaction $\pi^- + p \to X^- + p$, with the X^- mass outside and near the ρ^- mass peak ("background"), are also shown for comparison. All slopes are very similar, except for the ρ^-p reaction at 8 GeV/c.

The exchange of the Δ trajectory should dominate this reaction, as in the π^-p case. At first sight one could consequently be brought to believe that these two reactions should be very similar at these energies. However, this is not necessarily so, because there are new complications in this reaction -- in particular the fact that the ρ has a spin.

Data on the backward differential cross-sections (showing backward peaks) for the reactions $\pi^- + p \to A_1^- + p$ and $\pi^- + p \to A_2^- + p$ at 16 GeV/c were also obtained in this experiment.

1.8 Coherent πd elastic scattering

A few papers on coherent pion elastic scattering on deuterium have been presented at this Conference. In Fig. 26 is shown the angular distribution for π^-d coherent scattering at $|t| \lesssim 1$ (GeV/c)² at 3.75 GeV/c,

as measured by a Minnesota-Iowa group in a spark chamber and counter experiment[57]. It is worth noticing how the picture greatly resembles some of the forward peaks and secondary bumps previously reviewed in hadron-hadron scattering. Some recent theoretical models seem to have taken this similarity very seriously [see, for example, Harrington and Pagnamenta[5], and Chou and Yang[10]].

The data are compared to the Glauber theory of scattering on deuterons, in which the secondary shoulder is attributed to the double scattering term predominating on the single scattering one, and the dip to the interference of these two terms[58,59]. The full curve is the prediction of the Glauber formula when taking the pion-nucleon scattering amplitudes to have the form (for both $\pi^+ p$ and $\pi^- p$ scattering, with appropriate values for the parameters)

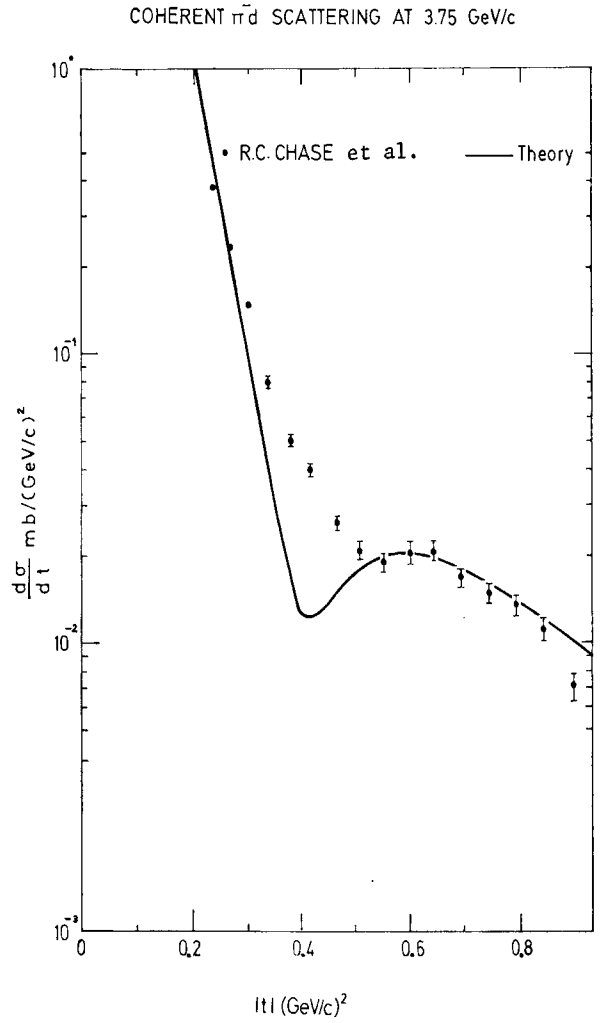

Fig. 26 Differential cross-section for $\pi^- d$ coherent elastic scattering at 3.75 GeV/c (Ref. 57). The full curve represents the Glauber formula prediction, after assuming spin-independent pion-nucleon scattering amplitudes with a constant phase.

$$f_N = (i + \alpha_N) \frac{k\sigma_N}{4\pi} e^{At/2}$$

(σ_N = total pion-nucleon cross-section, A = slope of the diffraction peak, k = centre-of-mass momentum). The fraction of the real part α_N was taken to be constant with $|t|$ and to be equal to the forward value. From the agreement between the main features of the data and of the calculated curve, one may conclude that the Glauber double-scattering mechanism is at work.

The results of a bubble chamber experiment by Hsiung et al.[60] on $\pi^+ d$ coherent scattering at 3.65 GeV/c are in good agreement with those of Chase et al. However, the theoretically predicted curve is rather different in the region of the dip and even at larger $|t|$. From what one can read in the submitted papers, the only difference between these two calculations is that they make use of different wave functions for the deuteron.

When analysing their data, Hsiung et al. made an attempt to measure the real part of the pion-nucleon scattering amplitude away from t = 0 (where it is known from the Coulomb interference measurements), by the amount of filling of the interference dip[61]. In fact for $\alpha_N = 0$, the cross-section drops to zero at the minimum, and for $\alpha_N \neq 0$ the dip is progressively filled in.

Although such an approach is interesting, it seems that one needs some more theoretical work before one can say if this can be done with a good level of confidence. In fact, the basic problem of proving that the Glauber formula is a suitable approximation to the cross-section is still open. The effects of choosing a particular deuterium wave function, and of including spin effects, need some more careful investigation[62].

One way to check Glauber's theory is to do an experiment at an energy such that the pion-nucleon scattering amplitudes are known from phase-shift analysis, to calculate the deuteron cross-section with the Glauber formula, and then see whether it is able to reproduce the data.

Such an attitude has been taken by a CERN-Trieste group working at CERN, who performed an experiment of $\pi^- d$ coherent scattering at 900 MeV/c [63]. Results from this experiment are shown in Fig. 27. As one can

see, the picture is very much the same as before. The full curve shows the results of a calculation by Alberi and Bertocchi[64] which includes spin dependence but not the effect of Fermi motion. Indeed, owing to the resonances lying nearby, it turns out that it is very difficult to take the internal motion of the nucleon into account properly. Consequently, one cannot rely very much on the results of the calculation, and the problem of checking Glauber's formula is left open.

2. CHARGE EXCHANGE

2.1 π^-p charge exchange

At this Conference, results from several measurements have been presented on backward π^-p charge exchange at high energies.

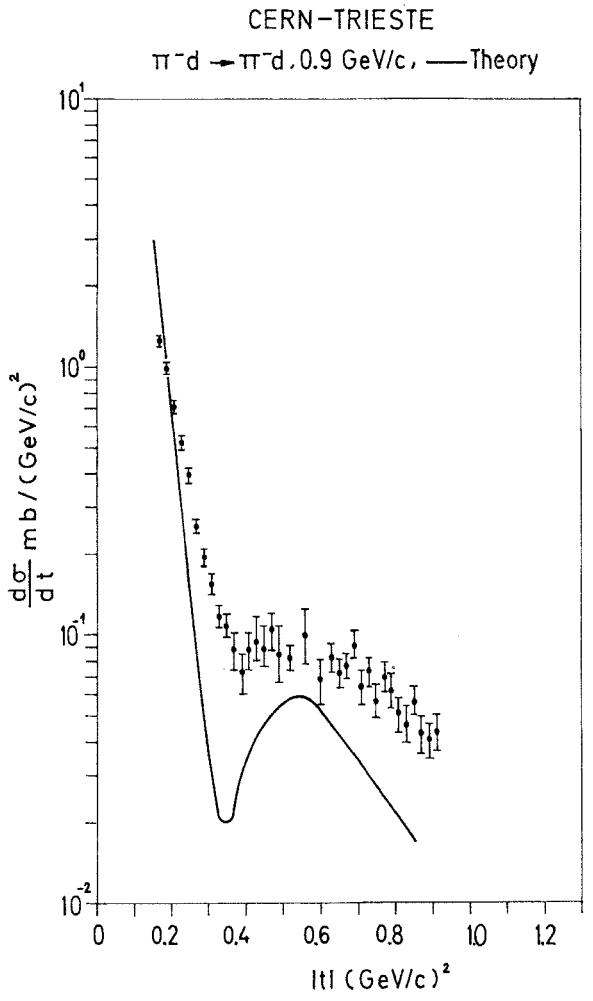

Fig. 27 Differential cross-section for π^-d coherent scattering at 900 MeV/c (Ref. 63). The full curve shows the prediction by the Glauber formula by making use of the measured pion-nucleon phase shifts. The spin dependence of the amplitudes is taken into account.

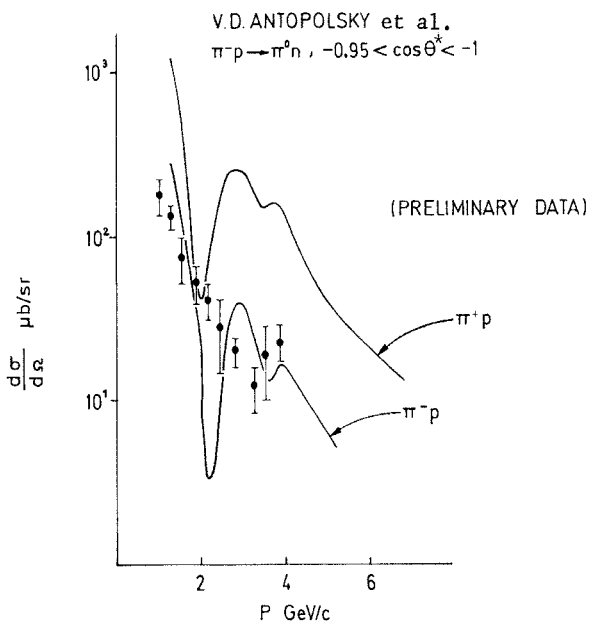

Fig. 28 Preliminary data for backward ($-0.95 < \cos\theta^* < -1$) π^-p charge exchange, by Antopolsky et al. (Ref. 65). The full lines give the qualitative behaviour of the backward π^-p and π^+p cross-sections.

In Fig. 28 are shown preliminary data on this reaction by Antopolsky et al.[65]. In the same run with a deuterium target in which data on backward π^-n scattering were taken[48], charge-exchange data were taken at several momenta between 1.5 and 3.8 GeV/c. No indication is seen in these data of the strong dip at $\sim$ 2 GeV/c laboratory momentum, which is observed as a function of momentum in both π^-p and π^+p 180° differential cross-sections (full curves in Fig. 28). It should be observed, however, that in this experiment the Fermi motion produces a strong spread in c.m. energy.

Figure 29 shows preliminary results of an optical spark chamber experiment on backward charge exchange performed at Argonne by a Minnesota group[66]. Qualitatively, the most evident feature is the dip at $u \sim -0.2$ (GeV/c)^2. This is very near to that predicted by Barger and Cline in their baryon exchange model[67]. In the framework of this model the data favour a negative value for the ratio of the pole residue of the Δ and the N_α trajectories.

Also, preliminary data at 4, 6, 8, and 11 GeV/c have been presented by the Orsay-Saclay group working at CERN[68]. These data cover only the very backward peak, and at 4 GeV/c are in excellent agreement with the Argonne data, as shown in Fig. 29. The 6 GeV/c

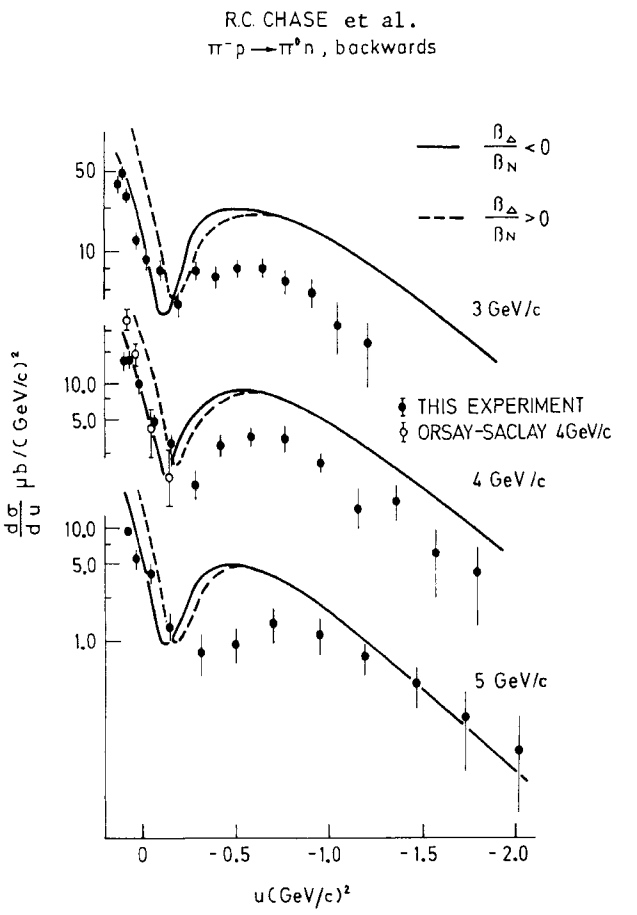

Fig. 29 Preliminary results by the Minnesota experiment (Ref. 66) on π^-p charge exchange in the backward region at 3, 4, and 5 GeV/c. The full and broken curves show predictions (Ref. 67) by the Barger and Cline Regge-pole model for the two indicated signs for the ratios of the pole residues of the Δ and N_α trajectories. Preliminary data at 4 GeV/c by the Orsay-Saclay group (Ref. 68) are also shown.

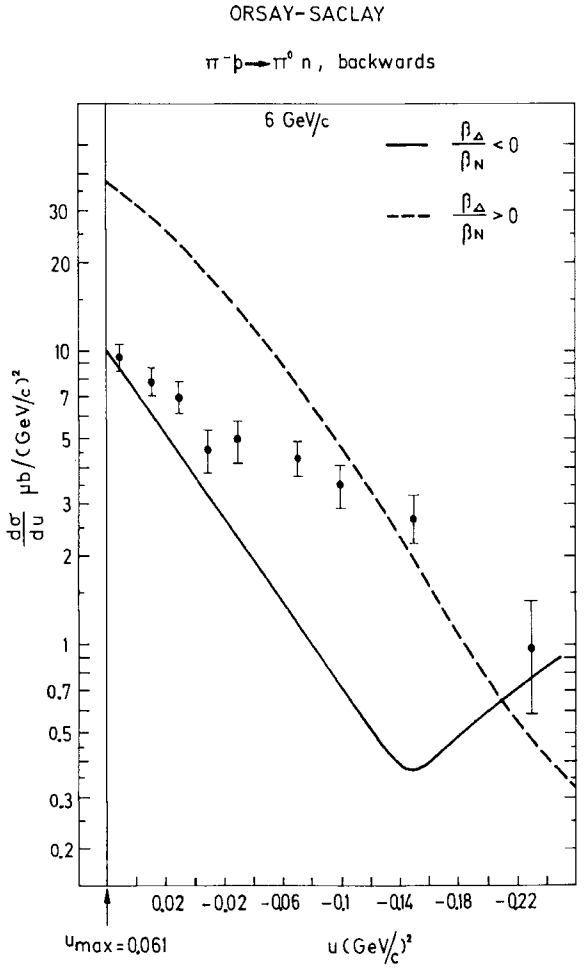

Fig. 30 Preliminary results by Schneider et al. (Ref. 68) on backward $\pi^- + p \to \pi^0 + n$ at 6 GeV/c. The curves are the Barger and Cline predictions, as in Fig. 29.

data from this experiment are shown in Fig. 30, together with the prediction by Barger and Cline[67]. At this energy the data and the theoretical prediction disagree rather clearly.

An extensive study of the π^-p charge-exchange reaction has been made in a spark chamber experiment by a Brown University-Harvard-Padova-Rehovoth-MIT collaboration[69]. The result of this experiment is expressed by giving the coefficients of the Legendre polynomials expansion of the angular distributions, and their errors at many energies between 1.4 and 4 GeV/c. An example of such results is shown in Fig. 31. The dotted curves show the error limits associated with the fits.

Forward cross-section data by Sonderegger et al.[70] and backward preliminary data by Chase et al.[66] at comparable energies are also plotted in this figure for comparison. There is a rather strong discrepancy at the backward direction.

2.2 K^+n charge exchange

A couple of bubble chamber experiments on the charge-exchange reaction $K^+ + n \to K^0 + p$ [at 3 GeV/c by the CERN-Bruxelles-Munich collaboration[71], and at 5.5 GeV/c by Cline et al.[72]] have been performed, aimed mainly at checking the validity of the Regge-pole and SU(3) sum rules by Barger and Cline[73]. The results for the total cross-section are shown in Fig. 32, together with the sum-rule predictions. Due to the steep energy dependence of the cross-section, the sum rule that was badly violated at 2.3 GeV/c seems to be satisfied at 5.5 GeV/c. Such a steep energy dependence of the total cross-section does not fit with Morrison's scheme[74] on the relationship between exchanged particles in a reaction (ρ and A_2 in

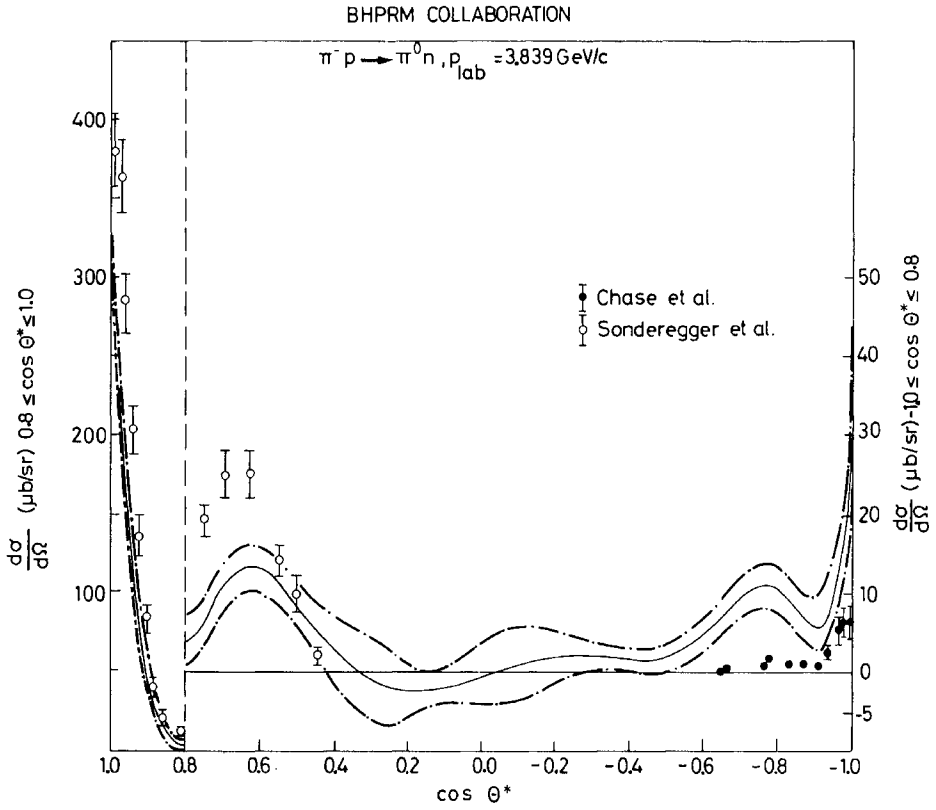

Fig. 31 Unfolded full angular distribution (full line) for $\pi^- p$ charge exchange at ∿ 3.84 GeV/c (BHPRM collaboration, Ref. 69). The dotted lines show the error limits as obtained in the fitting procedure. The 3.67 GeV/c forward data by Sonderegger et al. (Ref. 70) and the 4 GeV/c backward data by Chase et al. (Ref. 66) are also shown for comparison.

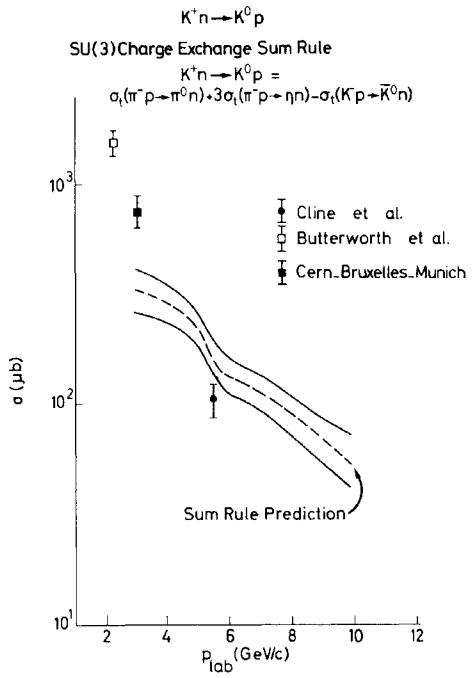

Fig. 32 $K^+ + n \rightarrow K^0 + p$ total cross-section at 2.3, 3.0, and 5.5 GeV/c (Refs. 75, 71, and 72, respectively). The broken curve represents the sum rule prediction (Ref. 73), as calculated by Cline et al. (Ref. 72). The full lines show the errors associated to the prediction.

this case) and the decrease of total cross-sections with increasing energy.

3. POLARIZATION EFFECTS

3.1 Polarization parameter in forward elastic scattering

It is known[76] that appreciable polarization, of the order of 5%, exists in pp elastic scattering at $|t| \lesssim 0.7$ (GeV/c)^2 up to 12 GeV/c incident momentum. New data at 5.15 GeV/c from a hodoscope counter experiment on a polarized target by a Chicago-Argonne group[77] extended the explored $|t|$ interval to about 1.8 (GeV/c)^2. These data are shown in Fig. 33, together with some older data by Grannis et al.[78]. The most interesting feature of the data is the increase of the polarization to values of ∿ 20% at $|t| > 0.6$ (GeV/c)^2. Whilst this behaviour is easily fitted by the optical model of Durand and Lipes[11], it cannot be reproduced by the P + P' + ω Regge-pole model of Rarita et al.[36].

It is interesting to observe that indications for a similar behaviour for the polarization -- a first positive broad maximum at $|t| \lesssim 0.7$ (GeV/c)^2 followed by a possible second broad maximum -- are found by a CERN-Holland group in an antiproton scattering experiment on a polarized target, at energies of about 2-3 GeV/c [79]. Part of these data are shown in Fig. 34. The fitted curves are obtained in an optical model, in which the structure in the polarization is closely bound to the structure in the differential cross-section.

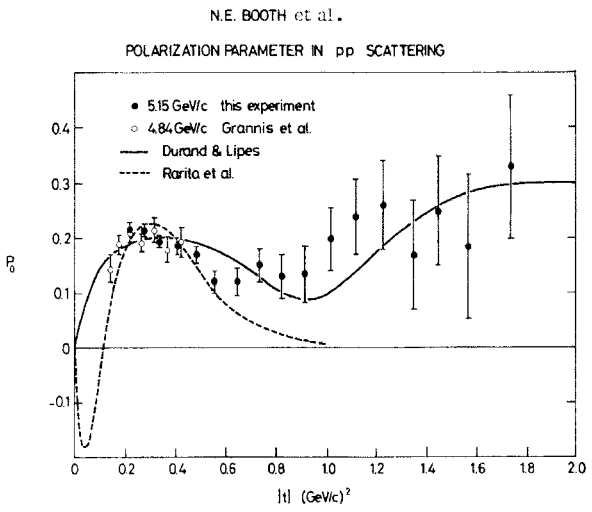

Fig. 33 The pp polarization data at 5.15 GeV/c by the Chicago-Argonne group (Ref. 77). Data by Grannis et al. (Ref. 78) at 4.84 GeV/c are in good agreement with these data. However, some normalization problem (Ref. 37) seems to exist on comparing with the 6 GeV/c data by Borghini et al. (Ref. 76 and Fig. 35). The theoretical curves are predictions by the models of Durand and Lipes, and Rarita et al. (Refs. 11 and 36, respectively).

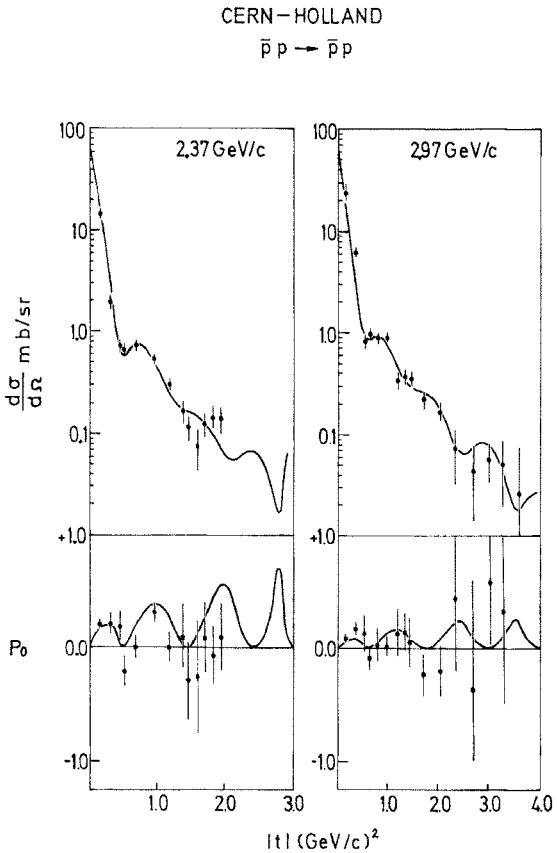

Fig. 34 Differential elastic cross-sections and polarizations at 1.73 and 2.13 GeV/c (Ref. 79). The full curves are fitted to the data. The model used is the Frahn and Venter (Ref. 80) model, modified to be applicable to the (spin ½-spin ½) case.

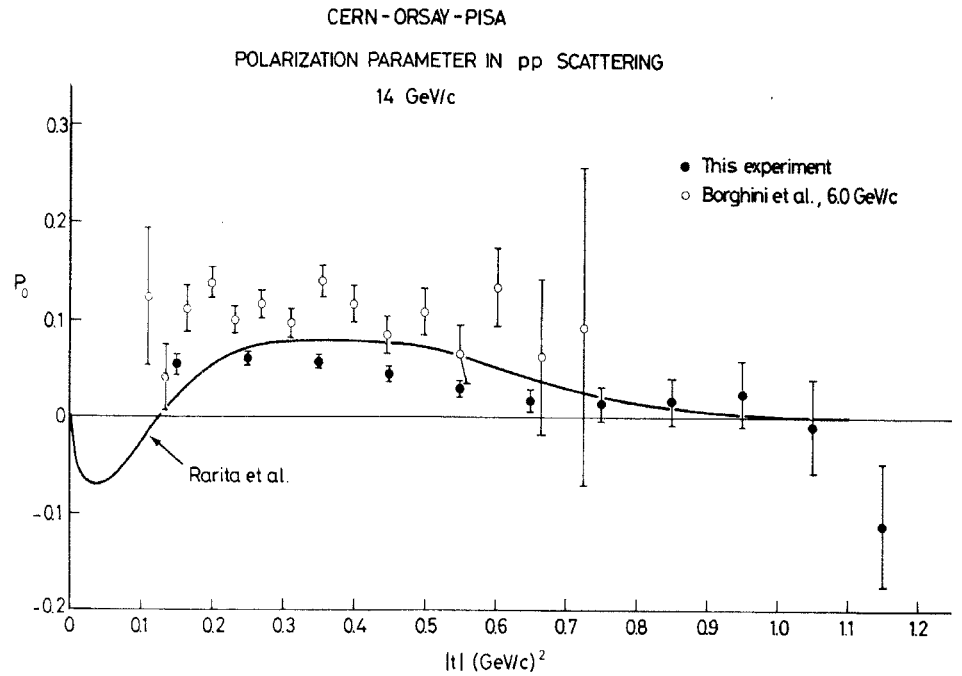

Fig. 35 Preliminary results for the polarization parameter in pp scattering at 14 GeV/c (Ref. 81). Data by Borghini et al. (Ref. 76) at 6.0 GeV/c are also shown for comparison.

Preliminary polarization data at 14 GeV/c for pp scattering have been presented by the CERN-Orsay-Pisa group[81]. These data are compared to the previous data by Borghini et al.[76] at 6 GeV/c and to the predictions by the Regge-pole model of Rarita et al.[36] in Fig. 35. The data show that the decrease of the polarization with increasing energy[37] continues smoothly. However, these data do not show any increase of P_0 at $|t| > 0.6$ GeV/c, as found at 5.15 GeV/c by Booth et al.[77].

The Chicago-Argonne group has also measured the polarization parameter for π^+p and π^-p at 5.15 GeV/c up to $|t| \sim 1.8$ (GeV/c)^2 [82]. The P + P' + ω Regge-pole model by Rarita et al.[36] gives predictions in qualitative agreement with the structures in P_0 at $|t| \gtrsim 0.7$ (GeV/c)^2 which are seen in Fig. 36.

Preliminary data on P_0 at the highest energy available up to now (14 GeV/c) for π^+p scattering at $|t| \lesssim 1$ (GeV/c)^2 has been reported by the CERN-Orsay-Pisa group[81]. These data are shown in Fig. 37, together with previous data by Borghini et al.[76] at lower energies. The polarization has qualitatively the same behaviour as at lower energies, with an absolute value which decreases rather slowly with increasing energy.

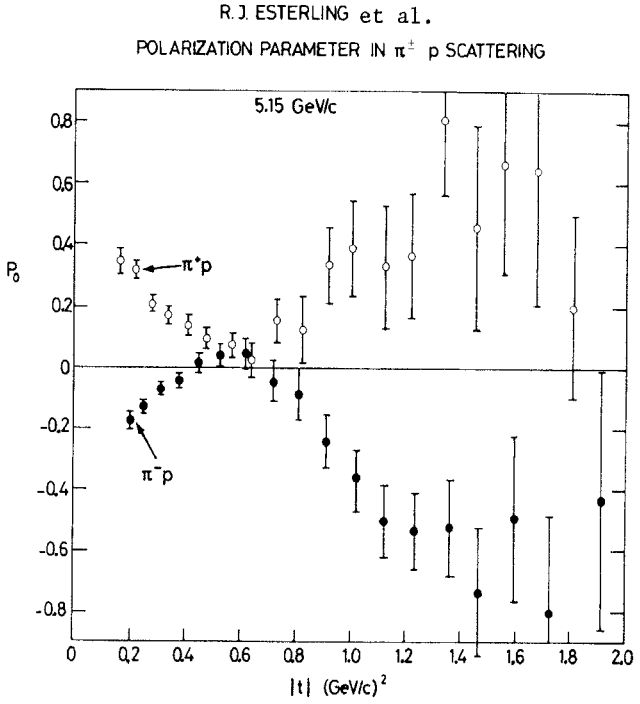

Fig. 36 Polarization parameter in $\pi^{\pm}p$ scattering at 5.15 GeV/c (Ref. 82).

The same group has also reported preliminary data on the polarization in K^+p scattering at 14 GeV/c. Although the statistical accuracy is still very poor, there is a clear indication for P_0 being positive at

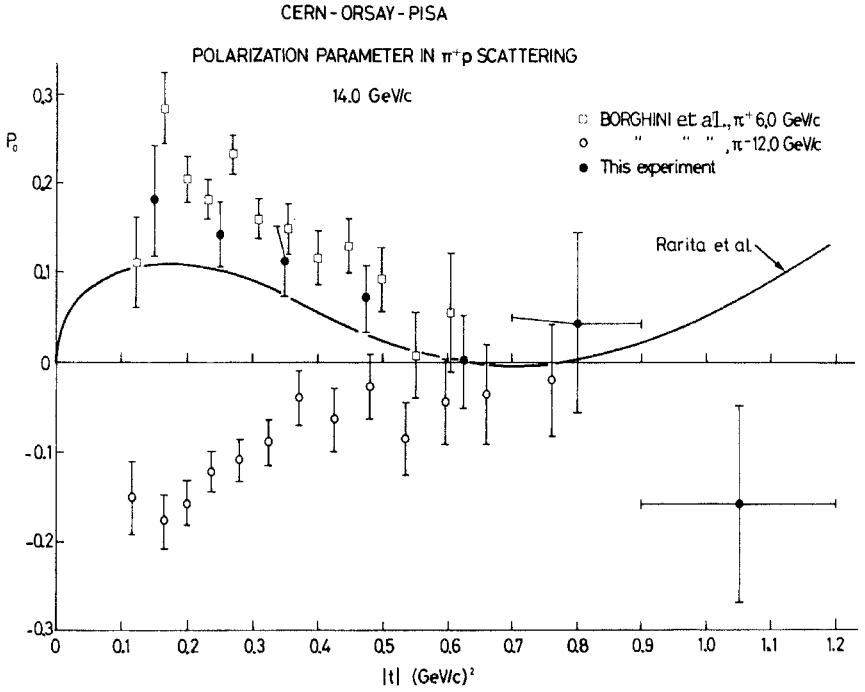

Fig. 37 Preliminary results for the polarization parameter in π^+p scattering at 14 GeV/c (full points) (Ref. 81). π^+p and π^-p data by Borghini et al. (Ref. 76) at lower energies are also shown for comparison. The curve represents the theoretical prediction of Rarita et al. (Ref. 36) for P_0 in π^+p scattering at 14 GeV/c.

$|t| < 0.7$ (GeV/c)^2. In the same $|t|$ region and at energies of the order of 3 GeV/c, the polarization is known to be positive also for K^-p scattering[83].

3.2 Polarization in backward peaks

If polarization exists in the forward peaks, one can naively expect it to be present also in the backward peaks. Very preliminary data from the Chicago-Argonne group[84] (shown in Fig. 38) on backward π^+p scattering on a polarized target at 2.75 GeV/c indeed give evidence for a strong peak in the polarization at $u \sim -0.1$ (GeV/c)^2, in the region of the dip in the differential cross-section. Polarization effects in backward πp scattering at these energies have been discussed, for example, by Barger and Cline, and by Dar and Kozlowsky[85], and at somewhat higher energies by Contogouris et al.[43] and by Barger[86].

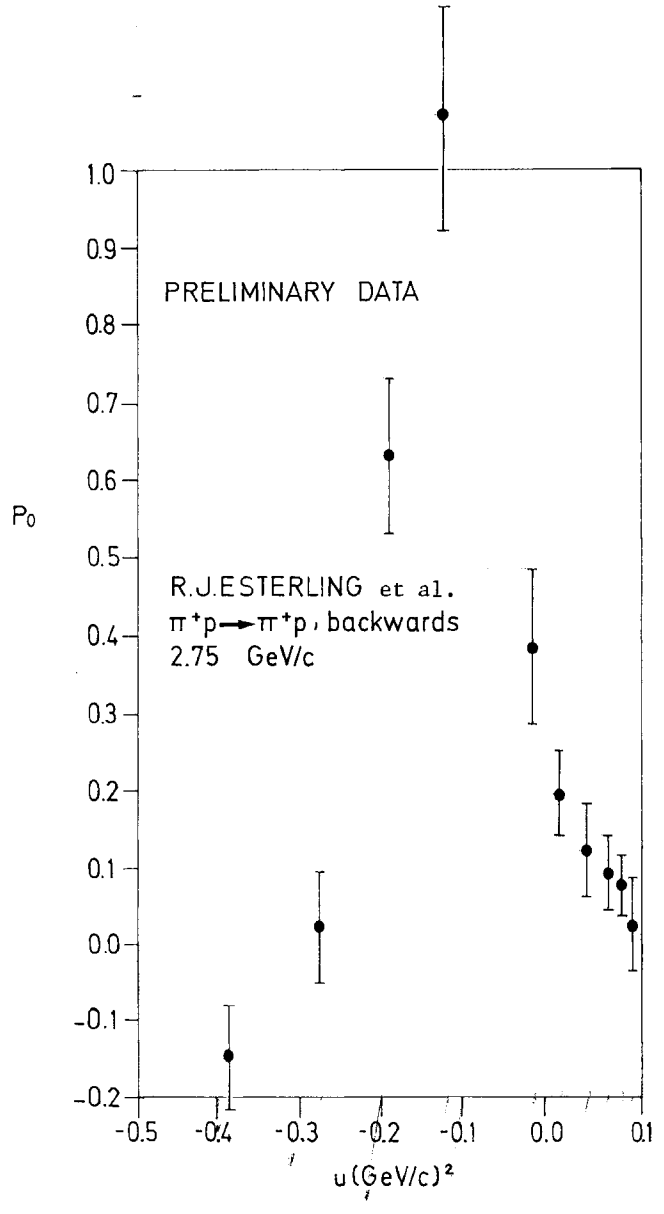

Fig. 38 Very preliminary data by the Chicago-Argonne group (Ref. 84) on the polarization in backward π^+p scattering at 2.75 GeV/c.

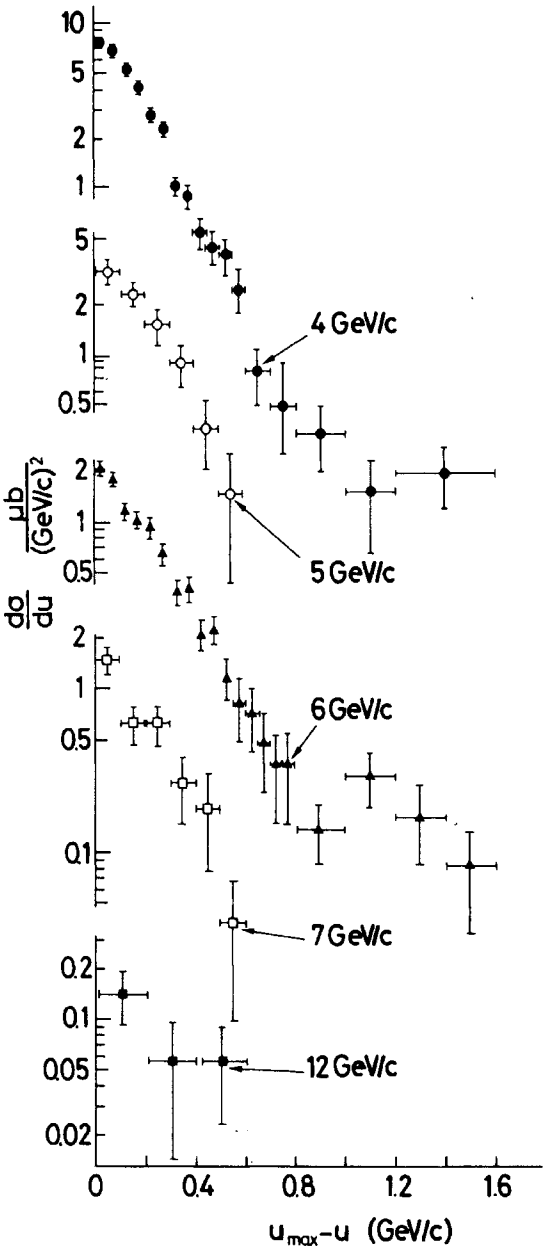

Fig. 39 Differential cross-sections for the associated production reaction $\pi^- + p \to K^0 + \Lambda$ in the backward region (Ref. 87), between 4 and 12 GeV/c incoming momentum.

A beautiful example of polarization in a backward peak is also provided by associated production $\pi^- + p \to K^0 + \Lambda$. Backward differential cross-section data between 4 and 12 GeV/c are presented in Fig. 39. These data have been measured at CERN by the CERN-ETH-Imperial College group, using optical spark chambers in a magnetic field[87]. One notices some flattening

in the distributions at $u = u_{max}$, and an indication of a dip or a change in slope at $(u - u_{max}) \sim 1$ $(GeV/c)^2$, in the 4 and 6 GeV/c data. The cross-section at $u = u_{max}$ decreases like $\sim s^{-3.4}$.

The results for the polarization at 4 and 6 GeV/c, as measured from the Λ decay, are shown in Fig. 40.

The polarization (which is bound to be zero at $u = u_{max}$ in the backward direction) away from $u = u_{max}$ increases very rapidly at about maximum positive value, and remains sensibly constant up to $u - u_{max} \sim 0.4$ $(GeV/c)^2$. At larger $u - u_{max}$, P_0 shows a tendency to decrease.

Barger reported[86] that the baryon exchange model of Barger and Cline can easily interpret these data. In this reaction the baryon exchanged in the u-channel must have isospin 1. Making use of linear Σ_α and Σ_δ trajectories [the strange baryon trajectories associated to the Σ and to the $Y_1^*(1385)$] in an approach very similar to that used for elastic πp scattering,

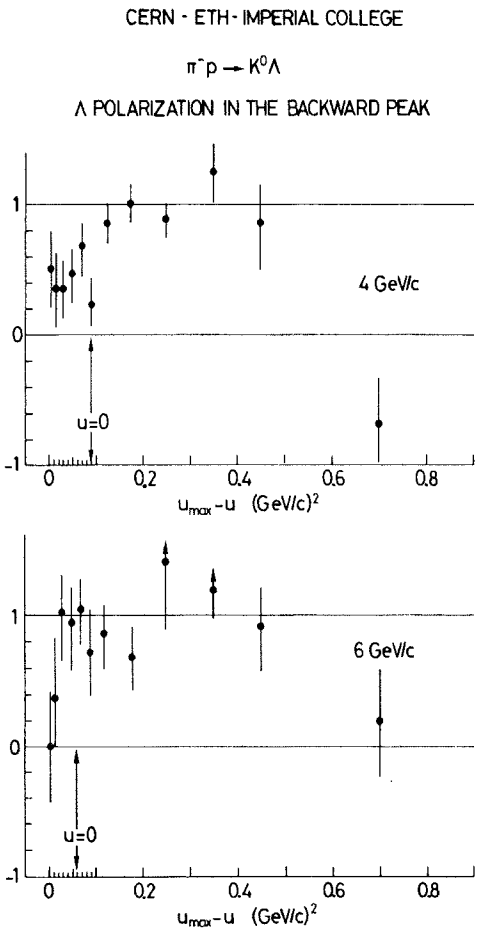

Fig. 40 Polarization in backward associated production, at 4 and 6 GeV/c (Ref. 87).

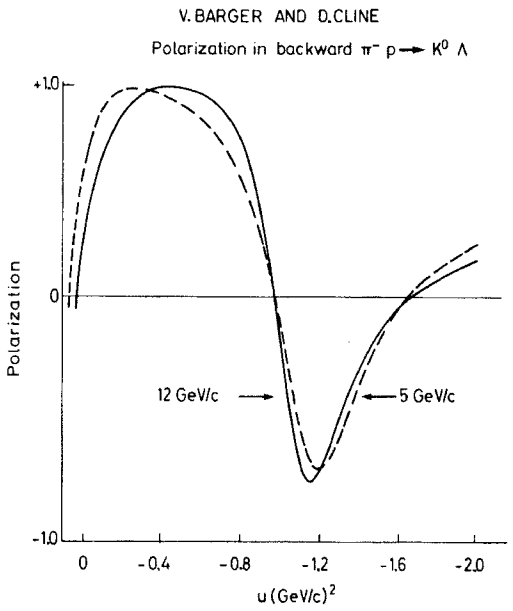

Fig. 41 Predicted polarization in backward $\pi^- + p \to K^0 + \Lambda$, in the Σ_α and Σ_δ exchange model by Barger and Cline (Ref. 86).

Barger and Cline were able to fit preliminary differential cross-section data from this experiment, and to predict the polarization, as shown in Fig. 41. This prediction is almost identical to that actually found in the experiment. Polarization effects in backward associated production have also been discussed by Högaasen[88].

4. INELASTIC TWO-BODY COLLISIONS IN pp REACTIONS

4.1 $p + p \to p + N^*(1518)$ and $p + p \to p + N^*(1688)$

It was shown by Anderson et al. at BNL[89] that the total cross-section for excitation of the two I = 1/2 isobars N*(1518) and N*(1688) in the reaction $p + p \to p + N^*$ is rather constant above 10 GeV/c. This peculiar behaviour is similar to that of elastic scattering. This fact is commonly explained by observing that these reactions, as the elastic scattering one, can proceed without any change of internal quantum numbers -- except spin and parity -- from the original to the produced particles.

In the forward region, however, the differential cross-section for excitation of such isobars is appreciably different from pp elastic scattering, showing peaks with slopes[89,90] of ~ 5 $(GeV/c)^{-2}$, which is about half the slope of the elastic peak. In addition, production of the N*(1518) seems to be suppressed in the very forward direction. Data have re-

cently become available on the large-angle behaviour of such cross-sections.

The differential cross-section for $p + p \to p + N^*(1518)$ up to a centre-of-mass angle $\theta \sim 90°$, as measured in two counter missing-mass experiments by Ankenbrandt et al. at Berkeley[91] and by Allaby et al. at CERN[92], are shown in Fig. 42. The most forward peaks are not indicated in the figure. The behaviour of the pp elastic scattering cross-sections at ~ 4, ~ 7, and ~ 19 GeV/c is also shown for comparison.

It is seen that at 4 GeV/c the isobar cross-section is much flatter than pp, at 7 GeV/c it is almost as steep, and that at 19 GeV/c and at large $|t|$ it is sensibly parallel to pp. At $\theta \sim 90°$ and below 7 GeV/c, the pN* cross-section has comparable magnitude to or is slightly larger than the pp, whilst at 19 GeV/c it is definitely smaller than the pp cross-section by almost an order of magnitude.

One may find some indication in this picture for the isobar differential cross-sections to tend to some energy-independent $d\sigma/dt$, as appears to be the case for pp and πp elastic scattering.

In Fig. 43, data from the same experiments for N*(1688) excitation are presented. This figure is impressively similar to the previous one.

A hint about the understanding of such phenomena can be found, for example, in the multiple scattering model by Frautschi and Margolis[93,94], and in an extension of the Chou and Yang model[10] to diffractive isobar excitation[95], as well as in the original papers on diffraction dissociation processes by Feinberg and Pomeranchuk, and by Good and Walker[96].

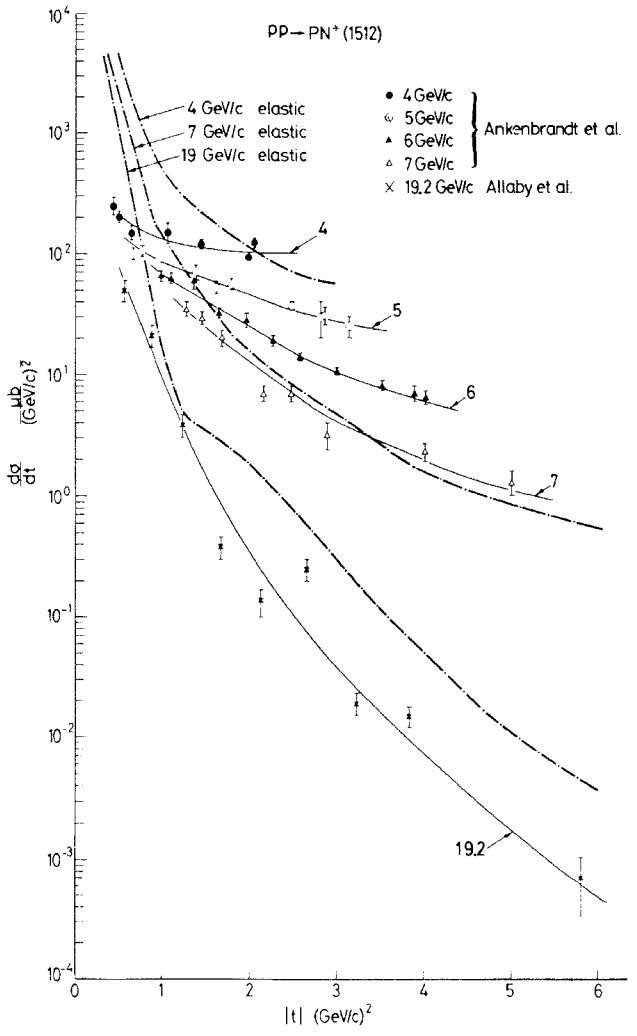

Fig. 42 Differential cross-section for the reaction pp → → pN*(1518) at 4, 5, 6, 7 (Ref. 91), and 19.2 (Ref. 92) GeV/c, and at large $[|t| \gtrsim 0.5\ (\mathrm{GeV/c})^2]$ momentum transfers. The behaviour of the ~ 4, ~ 7, and ~ 19 GeV/c pp elastic scattering cross-section is also shown for comparison.

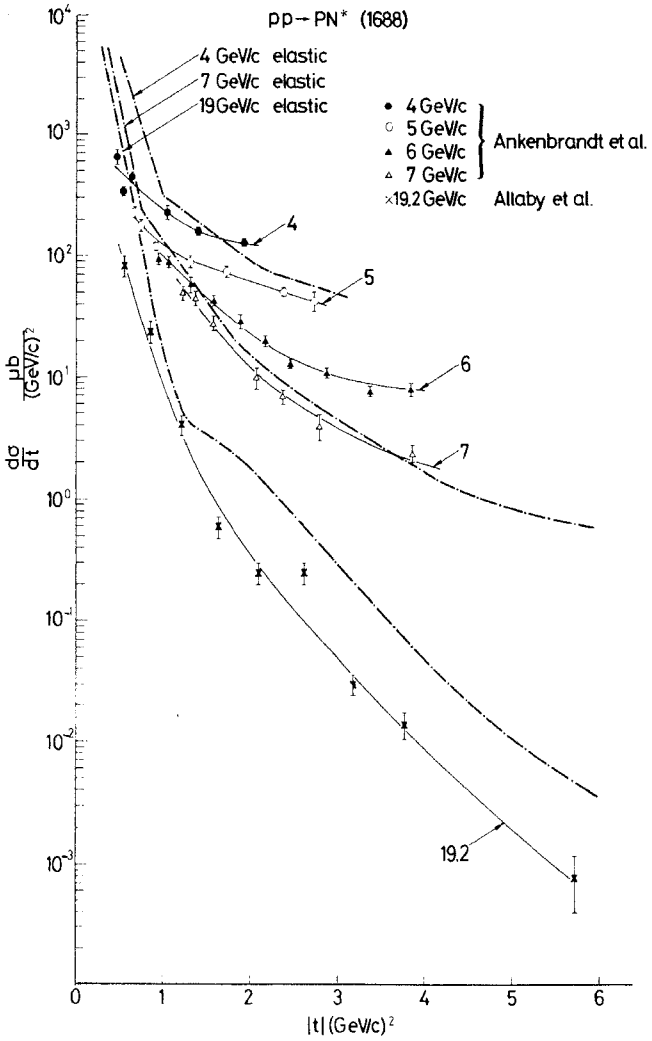

Fig. 43 Differential cross-section for the reaction pp → → pN*(1688) at 4, 5, 6, 7 (Ref. 91), and 19.2 (Ref. 92) GeV/c, and at large $[|t| \gtrsim 0.5\ (\mathrm{GeV/c})^2]$ momentum transfers. The behaviour of the ~ 4, ~ 7, and ~ 19 GeV/c pp elastic scattering cross-section is also shown for comparison.

4.2 p + p → p + N*(1400)

A very interesting result concerning the reaction p + p → p + N*(1400) has been reported by a BNL bubble chamber group from an experiment at 28.5 GeV/c [97]. The missing-mass M spectra for the reaction p + p → p + X_M, when X_M decays into one or three charged prongs, is shown in Fig. 44a (2 prong + 4 prong, upper histogram). A cut at $|t| = 0.06$ (GeV/c)^2 is applied in order to avoid scanning biases.

The over-all spectrum is extremely similar to that obtained (after integration over angle) by Anderson et al. in a missing-mass counter experiment at 30 GeV/c [89]. The Anderson et al. data are shown as a full curve in Fig. 44a. The bubble chamber experiment is able to show that the broad peak ranging from M ∿ 1.3 to M ∿ 1.8 GeV comes mostly from the two-prong final state (X_M → one charged prong).

Ellis et al.[97] studied the X_M → one-prong sample separately (Fig. 44b) in the small |t| - range, $|t| < 0.12$ (GeV/c)^2, since the cross-section for excitation of the N*(1400) is known to be very strongly peaked in the forward direction[98]. By studying the missing-mass m in the decay X_M → one charged prong + x_m, they were able to separate the $X_M \to \pi^+ + n$ cases from the rest. These events are shown as a shadowed histogram at the bottom of Fig. 44b. In this sample one notices a broad peak centred at M ∿ 1400 MeV.

Finally, Ellis et al. compared the ratio of events in the region around M = 1400 MeV, in the $\pi^+ n$ sample and in the full two-prong sample. If the isospin of the isobar is 1/2, one expects the $\pi^+ n$ decay to be twice as frequent as the $\pi^0 p$ one. This is consistent with the data if almost all the two-prong sample is assumed to be $\pi^0 p$ plus $\pi^+ n$. If I = 3/2, the $\pi^0 p$ decay should be predominant by a factor of two over the $\pi^+ n$ decay and this is inconsistent with the data. The authors conclude that in the missing-mass peak seen in high-energy counter experiments[89,90,98] at small momentum transfers, for M ∿ 1400 MeV, there was indeed excitation of an I = 1/2 nucleon resonance.

By inspection of the $\pi^+ n$ spectrum at $|t| > 0.12$ (GeV/c)^2 (Fig. 44c), one sees that the N*(1400) excitation is strongly reduced, whilst on the other hand excitation of some other isobar of higher mass [pos-

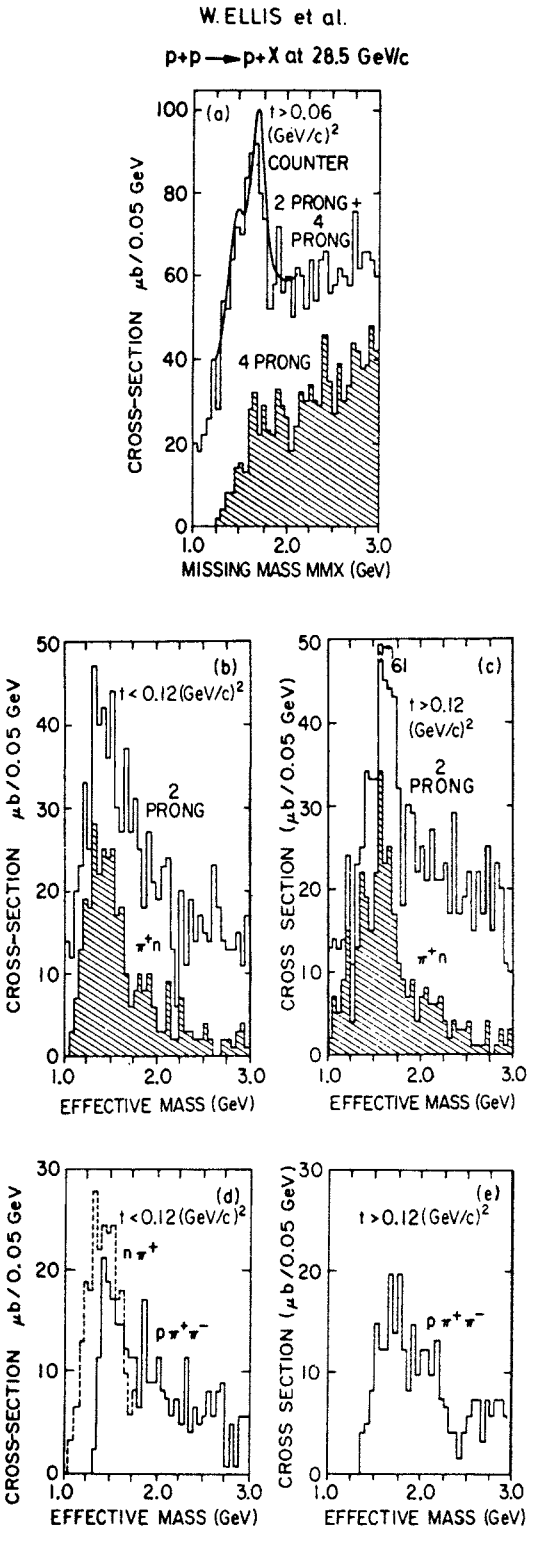

Fig. 44 Missing-mass M spectra for the reaction p + p → p + X_M at 28.5 GeV/c (Ref. 97). The very forward region [$|t| < 0.06$ (GeV/c)^2] where scanning losses would be important is excluded. (a) The upper histogram comprises all two and four charged prong (X_M → one charged prong and X_M → three charged prong) events. The shadowed histogram comprises only the four-prong events. The integrated counter data by Anderson et al. at 30 GeV/c (Ref. 89) are also shown for comparison. (b),(c) two-prong (X_M → one prong) events only (shadowed histogram: only $X_M \to \pi^+ n$ events), at $|t| < 0.12$ and at $|t| > 0.12$ (GeV/c)^2, respectively. (d),(e) four-prong (X_M → three prongs) only, at $|t| < 0.12$ and at $|t| > 0.12$ (GeV/c)^2. The $\pi^+ n$ sample is shown as a broken line histogram in (d).

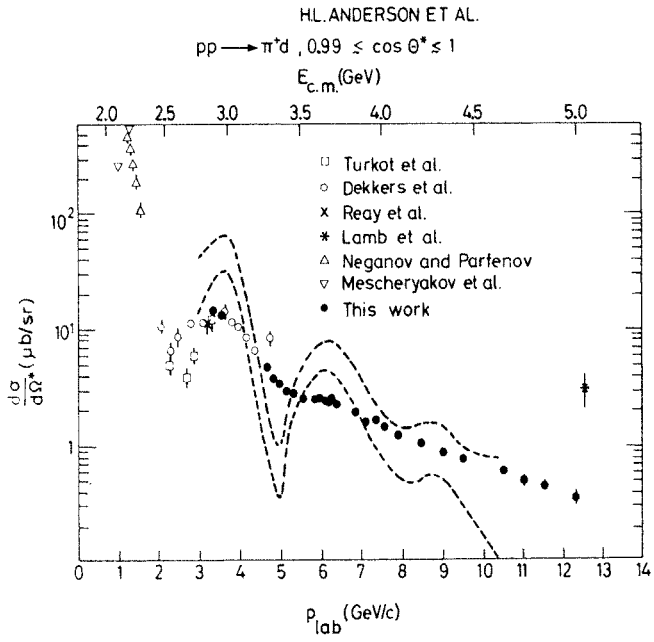

Fig. 45 Forward ($0.99 < \cos\Theta^* < 1$) differential cross-section for the reaction $p + p \to d + \pi^+$ as a function of the incident momentum p_{lab} and of the total c.m. energy ($E_{c.m.}$, upper scale) (Ref. 104). Experimental points from other works are from Refs. 103, 107. The dashed curves are calculated according to the model of Yao (Ref. 106). The upper and lower bounds correspond to the lack of knowledge on the pion charge-exchange cross-section.

sibly the N*(1512)] has increased. These different mechanisms are therefore probably responsible for the distorted 1400 spectra observed in counter experiments[98].

The connections of such a 1400 MeV isobar with the P_{11} Roper resonance[99] are not very clear. Inspection of the $X_M \to$ three charged prong ($p\pi^+\pi^-$) at $0.06 < |t| < 0.12$ (GeV/c)^2 and at $|t| > 0.12$ (GeV/c)^2 (full histograms in Figs. 44c and 44d) shows an enhancement at a mass of $\sim$ 1450 MeV, which is washed down quickly with increasing $|t|$. The mass of this object is nearer to that found for the P_{11} resonance in phase-shift analyses[99] ($\sim$ 1470 MeV). It is possibly an I = 1/2 state, since evidence for a $p\pi^+\pi^-$ enhancement at a mass M $\sim$ 1470 MeV coherently produced by protons on neon -- an isospin zero nucleus -- has been reported at this Conference[100]. However, its origin as a $\pi^-\pi^+p$ resonance, a $\pi\Delta$ resonance, or neither of these, is under discussion[101].

4.3 $p + p \to d + \pi^+$

A most typical (one might even say the only true) inelastic two-body pp reaction is $p + p \to d + \pi^+$. This reaction[102] or the inverse one $\pi^+ + d \to p + p$ [103] have been studied rather extensively at momenta of $\sim$ 3.5 GeV/c and below. Data have been presented at this Conference on the energy behaviour of the forward*) cross-section between 3.4 and 12.3 GeV/c by Anderson et al.[104], and on the differential cross-section in the forward angular region at 21.1 GeV/c by Allaby et al.[105].

Anderson et al.[104] used a magnet spectrometer and time-of-flight system to separate the backward-emitted deuterons. Their results are shown in Fig. 45 together with experimental points from other works[103,107]. A theoretical treatment by Yao[106], in the framework of the one-pion exchange model, predicts the forward cross-section to be essentially proportional to backward π^+p scattering. Intuitively, one can understand this by thinking that the zero-angle reaction can proceed by a proton emitting a π^+ in the forward direction, and recoiling backwards as a neutron bound to the other proton in the deuteron. As a matter of fact there is also a pion backward charge-exchange diagram contributing to the reaction. Disregarding this contribution, and allowing for the known experimental uncertainties in the πp data, what Yao's theory predicts is that the $p + p \to d + \pi^+$ cross-section would lie in between the broken lines shown in Fig. 45. It is seen that the data are much smoother than the predicted curve, but nevertheless resemble it. In particular there is an indication for a structure at $\sim$ 6 GeV/c laboratory momentum.

Allaby et al.[105] separated the $p + p \to d + \pi^+$ reaction by a missing-mass technique, in an accurate measurement of the momentum spectrum of deuterons emitted at small laboratory angles (12.5 to 60 mrad) from a hydrogen target hit by 21.1 GeV/c protons. Their missing-mass spectrum at 40 mrad is shown in Fig. 46. The peak at the highest momentum is associated to a recoiling pion, and the other structures at lower momenta to a recoiling ρ^+ (also the differential cross-section for the reaction $p + p \to d + \rho^+$ was in fact measured in this experiment), and possibly to recoiling A_1, A_2, ... The angular distribution as obtained from such measurements at several angles is shown

*) Forward and backward directions, although kinematically distinguishable, are physically equivalent in this reaction.

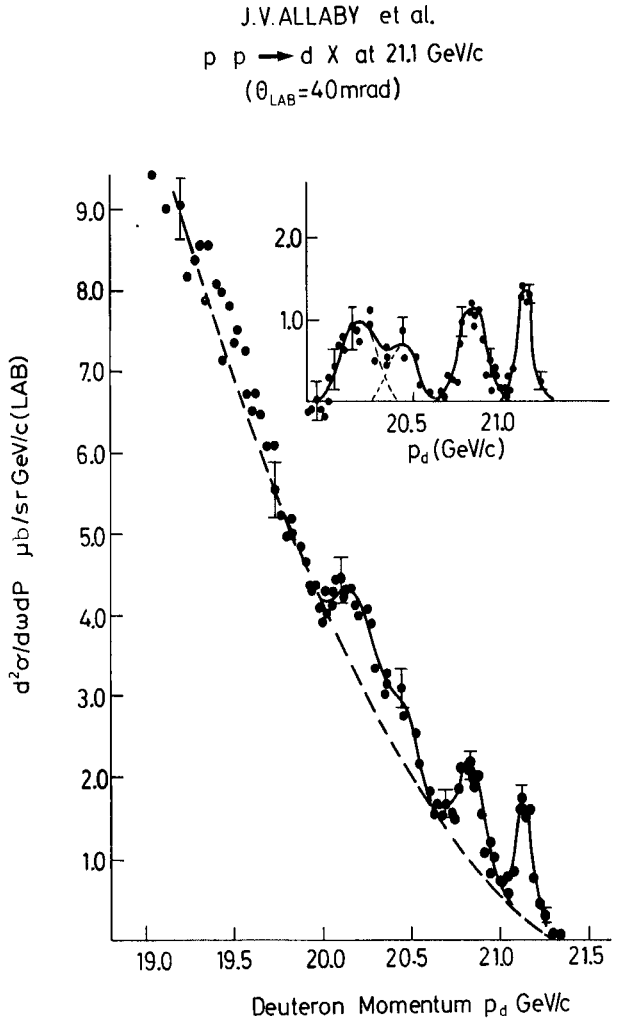

Fig. 46 Deuteron momentum spectrum obtained in the experiment of Allaby et al. (Ref. 105) at a laboratory angle of 40 mrad. The broken line indicates the hand-drawn fit to the smooth continuum used to extract the two-body differential cross-sections. The insert shows the spectrum after subtraction of this continuum.

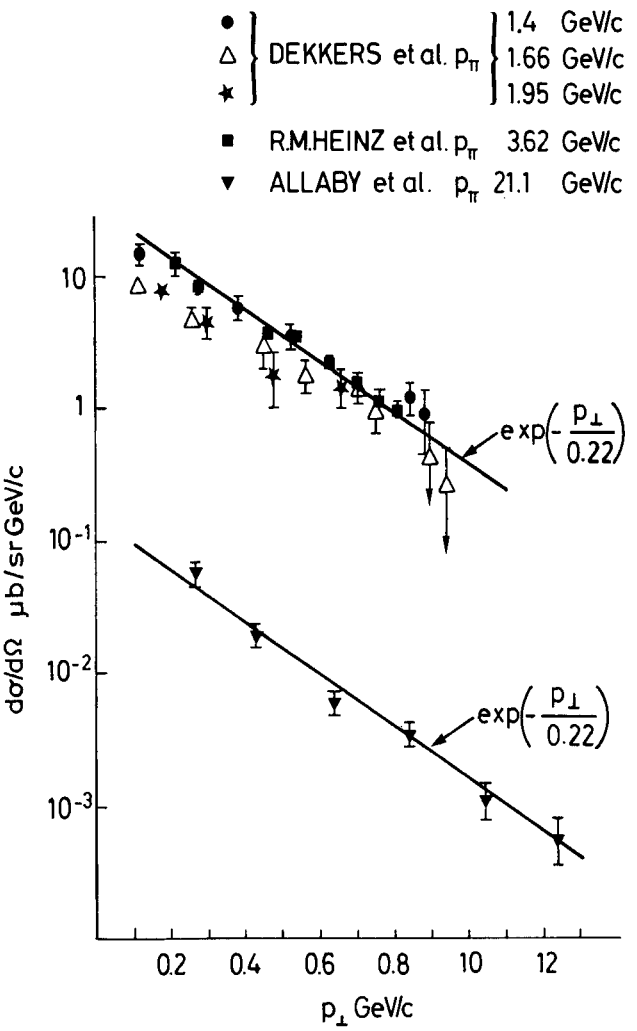

Fig. 47 A comparison by Allaby et al. (Ref. 105) between their data on the p + p → d + π^+ reaction at 21.1 GeV/c and the data by Heinz et al. (Ref. 102) at 3.62 GeV/c. The data of Dekkers et al. (Ref. 103) on the inverse reaction π^+ + d → p + p are also displayed.

in Fig. 47. It is well fitted by an exponential in $p_\perp$, $e^{-p_\perp/b}$, with a constant b of a rather universal value ($\sim$ 220 MeV/c), very similar to that exhibited by the data at much lower energy.

5. INELASTIC TWO-BODY COLLISIONS IN MESON-NUCLEON SCATTERING

5.1 K scattering

The following empirical rules are known to be approximately valid for all inelastic quasi-two-body hadron reactions at high energies.

a) The total cross-sections decrease to a first approximation as an inverse power of the incident momentum p_{lab}:

$$\sigma_t \sim p_{lab}^{-n} .$$

The exponent n varies from reaction to reaction. An empirical rule has been proposed connecting the values of n to the nature of the particle which is supposed to be exchanged in the reaction[74]. A discussion of the experimental evidence for the validity of this rule can be found elsewhere[108].

b) There is a forward peak, where roughly $d\sigma/dt \sim e^{-A|t|}$. The slope A does not change much with energy. For reactions in which the width of the produced particles is large enough to make the forward momentum transfer, t_{min}, vary appreciably from event to event, spurious changes in shape at small |t| are avoided if the variable $t' = |t-t_{min}|$ is calculated for each individual event, and the angular distributions are presented as functions of t'[109]. For these reactions $d\sigma/dt' \sim e^{-At'}$.

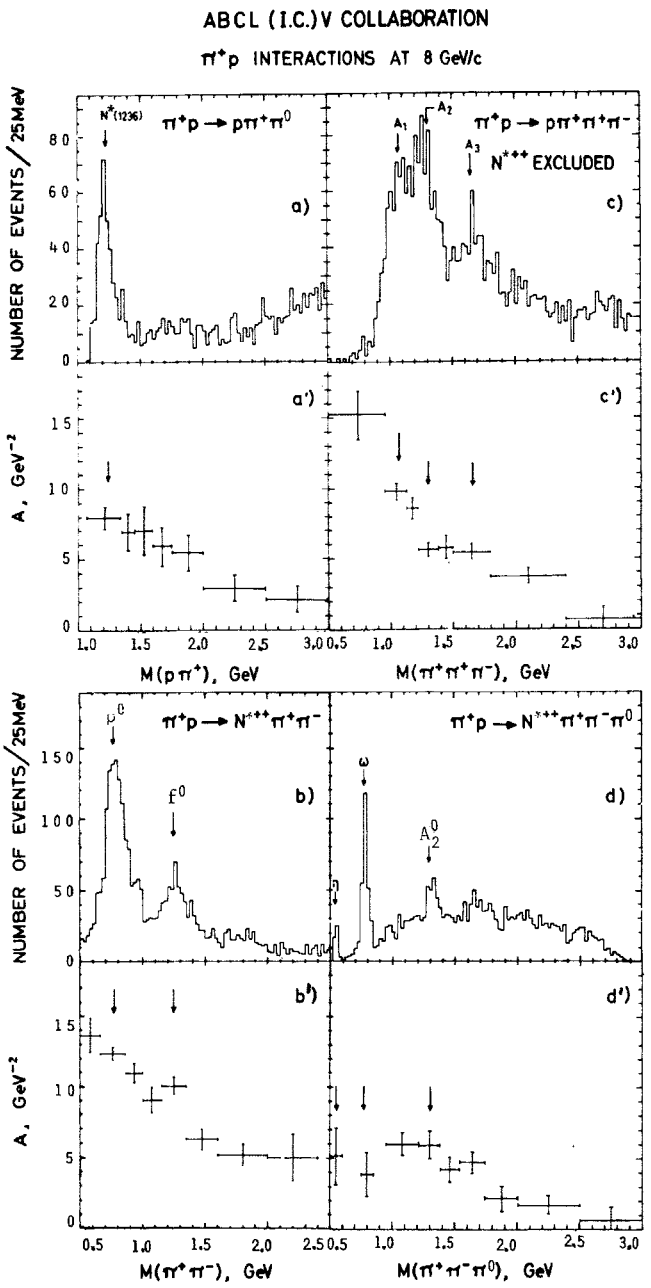

Fig. 48 Effective mass distributions and slope of the differential cross-sections for several π^+p inelastic two-body reactions at 8 GeV/c (Ref. 110). For each indicated reaction, the top part of the figure shows the effective mass distribution of the system considered (as indicated on the horizontal axis): the bottom part of the figure shows the variation with the effective mass, M, of the coefficient A in the expression: $d\sigma/dt' = K \exp(At')$ fitted to the data up to $t' = 0.4$ (GeV/c)^2.

c) The slope A of the forward peaks seems to be a decreasing function of the mass of the produced particles. Furthermore, strong evidence for an extremely interesting empirical rule has been presented at this Conference by the Aachen-Berlin-CERN-London (I.C.)-Vienna Collaboration. It appears that the exponential t-dependence of the differential cross-section and the dependence of the slope on the mass of the produced systems are valid irrespectively of whether the produced system is in a resonant state or not[110].

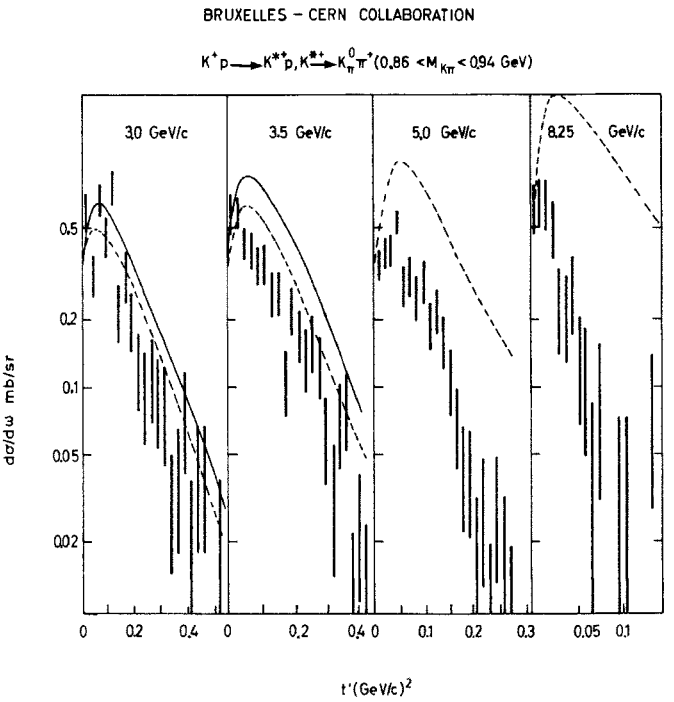

Fig. 49 Angular distributions for the reaction $K^+ + p \to K^{*+}(890)p$ at 3.0, 3.5, 5.0, and 8.25 GeV/c (Ref. 111). The curves are the prediction of the one-particle (1^-) exchange model with absorption, for two different choices of the relevant parameters.

An example of such a situation is shown in Fig. 48, which contains data from a 10 GeV/c π^+ run on hydrogen[110]. One sees that when the mass M of the produced systems sweeps through the isobar or the meson masses, the slope A of the differential cross-section continues to decrease smoothly.

Also, the statistical accuracy of the experiments has improved to the extent that it is now possible to study some finer details of the differential cross-sections. Besides this, the energy at which many data are taken is sufficiently high (5-10 GeV/c) for one to believe that one is looking at phenomena which will no longer change quickly with energy.

A very interesting "detail" is that most cross-sections behave in a peculiar way at small $|t|$ (or t'), typically $|t| \lesssim 0.2$ (GeV/c)^2. As a first example of this, data by the Bruxelles-CERN group on the reaction $K^+ + p \to K^{*+}(890)p$ [111] at 3.0, 3.5, 5.0, and 8.25 GeV/c are shown in Fig. 49. In this case the structure consists of a flattening or even a dip at $t' = 0$.

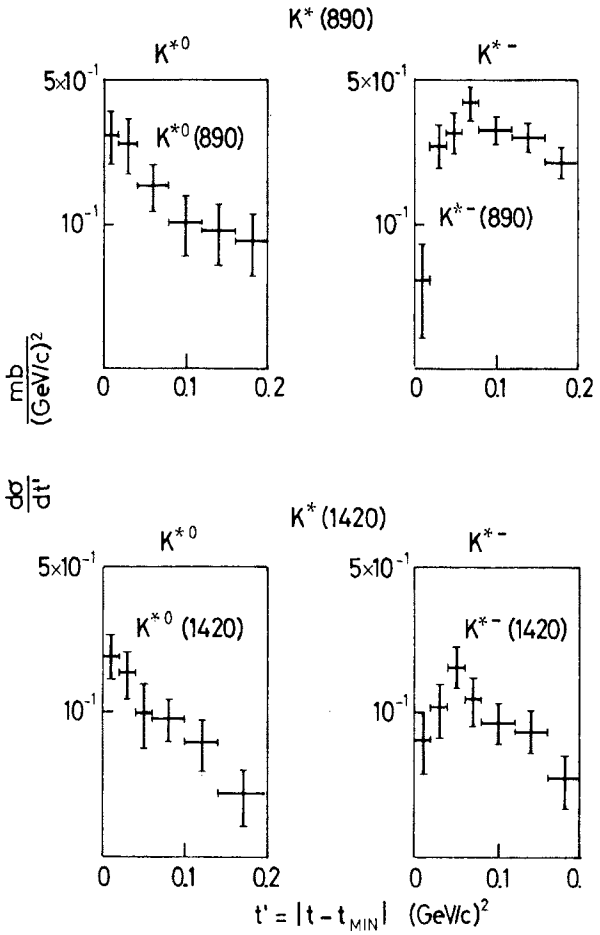

Fig. 50 Differential cross-sections at $t' < 0.2$ (GeV/c)^2 for K*(890) and K*(1420) excitation in $K^- + p \to K^*N$ reactions at 10 GeV/c (Ref. 112).

In Fig. 50 the differential cross-sections at $t' < 0.2$ (GeV/c)^2 for K*(890) and K*(1420) production in the reaction $K^- + p \to K^* + N$ at 10 GeV/c are shown. These data were contributed to this Conference by the ABCL(I.C.) Collaboration[112]. As in the previous figure, forward dips are observed in K^{*-}(890) and K^{*-}(1420) production. On the other hand, one sees that the charge-exchange reactions $K^- + p \to K^{*0} + n$ have a forward peak.

Traditionally, these differences are understood in the sense that the above no-charge-exchange reactions are dominated by ω exchange, and the charge-exchange reactions are dominated by pion exchange.

The evidence for many π or K initiated charge-exchange two-body inelastic reactions to be dominated by π exchange (at least up to ∿ 5 GeV/c) is rather convincing[113]. However, this model does not work any more for the $K^- + p \to K^{*-}(890) + n$ reaction at 10 GeV/c [112]. The evidence for vector-meson exchange to be dominating in $K^{\pm} + p \to K^{*\pm}(890) + p$ is based on the angular decay distributions[114]. On the other hand, this model -- one vector meson exchange plus absorption -- does not fit at all the angular distributions above a few GeV/c. An example of such a situation is given by the calculated curves shown in Fig. 49.

Some experiments of K*(890) coherent production on deuterium are in progress[115-117], and these could possibly help in clarifying this situation. The ω exchange should be the dominant contribution to this reaction, since the exchange amplitude must have I = 0. From these results one may possibly work out how much of the production on protons is actually due to ω exchange.

The complete K*(890) and K*(1420) differential cross-section data from Ref. 112 are shown in Fig. 51. Whilst in general all cross-sections are very similar, with slopes of ∿ 5 $(GeV/c)^{-2}$, at $t' < 0.5$ $(GeV/c)^2$ there is a difference in the K^{*-}(890) and K^{*0}(890) cross-sections that is not noticed in the K*(1420) case.

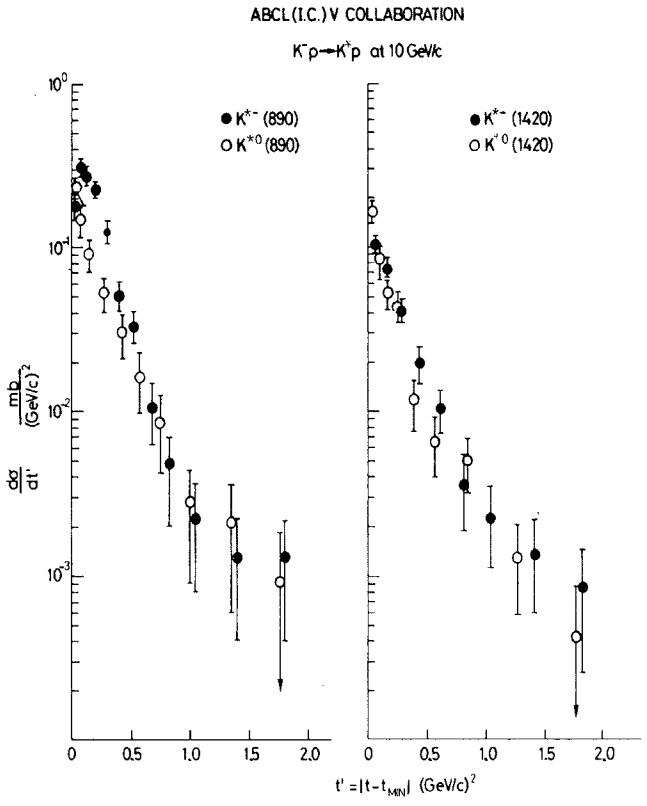

Fig. 51 Differential cross-sections for the reactions $K^- + p \to K^{*-} + p$, $K^- + p \to K^{*0} + n$ for K*(890) and K*(1400) at 10 GeV/c (data from Ref. 112).

5.2 π scattering

Structures at $t' \lesssim 0.2$ (GeV/c)^2 exist also in reactions involving non-strange mesons. This is seen, for example, in Fig. 52, which shows preliminary data by the Bari-Bologna-Florence-Orsay Collaboration[118] at 5.1 GeV/c, and by the Bari-Bologna-Florence Collaboration[119] at 9 GeV/c.

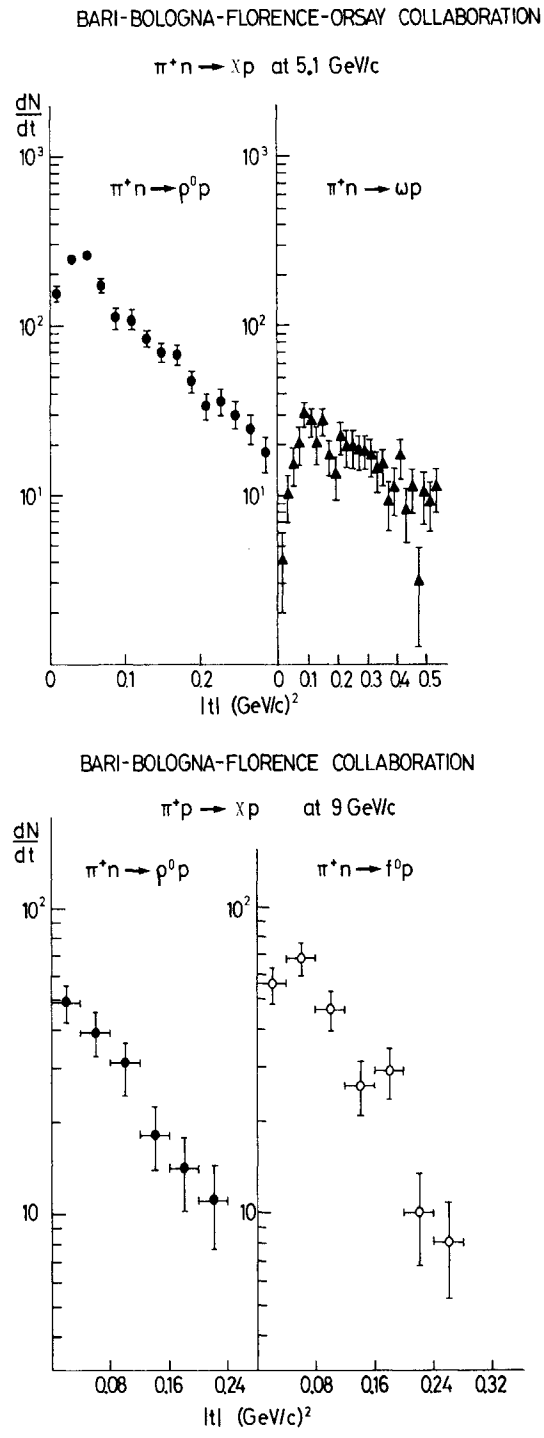

Fig. 52 Differential cross-sections for the indicated reactions, from a deuterium bubble chamber experiment at two energies of the Orsay-Bari-Bologna-Florence Collaboration (Ref. 118), and the Bari-Bologna-Florence Collaboration (Ref. 119).

The forward dips in all cross-sections distinguish these charge-exchange reactions from those for excitation of K^{*0}'s, previously discussed. It is also interesting to observe that whilst all dips are very similar to each other, π exchange is not allowed in $\pi^+ + n \to \omega + p$. The 9 GeV/c $\pi^+ + n \to \rho^0 + p$ cross-section does not show any forward dip. However, the statistical errors at this energy are very large. In addition, an experiment[120] on the charge-symmetric reaction $\pi^- + p \to \rho^0 + n$ at 11.2 GeV/c shows evidence for a forward dip.

The ABC collaboration has submitted data with good statistics for the reactions $\pi^+ + p \to \rho^0(f^0) + \Delta^{++}$ at 8 GeV/c [121], as shown in Fig. 53. In the insert one sees that the forward peaks are now back. The situation looks rather complicated. An attempt at finding some rule connecting such forward structures to the type of exchange is made in Ref. 121.

If one feels confused from the behaviour of such charge-exchange cross-sections in the very forward region, one may on the other hand be pleased to observe that the picture in Fig. 53 resembles very much as a whole what we have been seeing in elastic hadron-hadron scattering with a first peak and some secondary structures. This is not the only example of

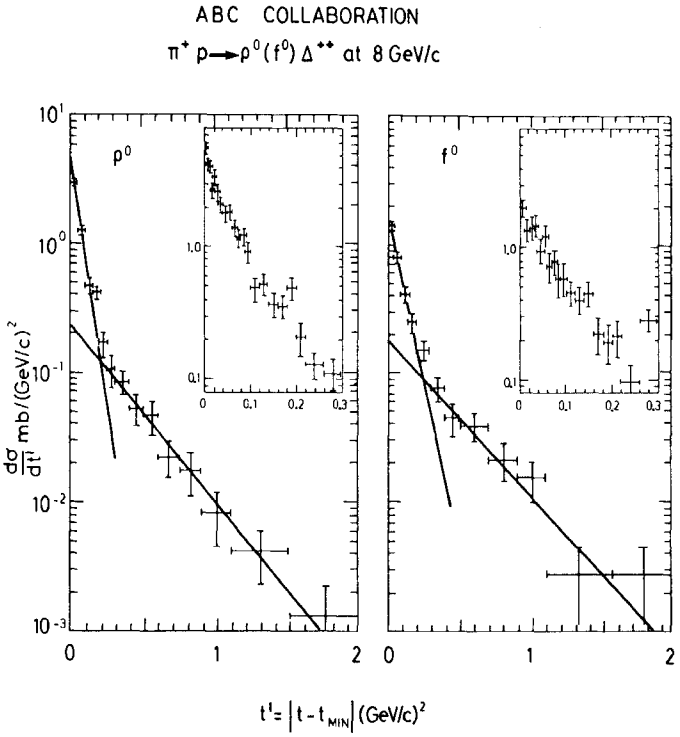

Fig. 53 Differential cross-sections for the reaction $\pi^+ + p \to \rho^0(f^0) + \Delta^{++}$ at 8 GeV/c (Ref. 121). The insert shows the small t' region in detail.

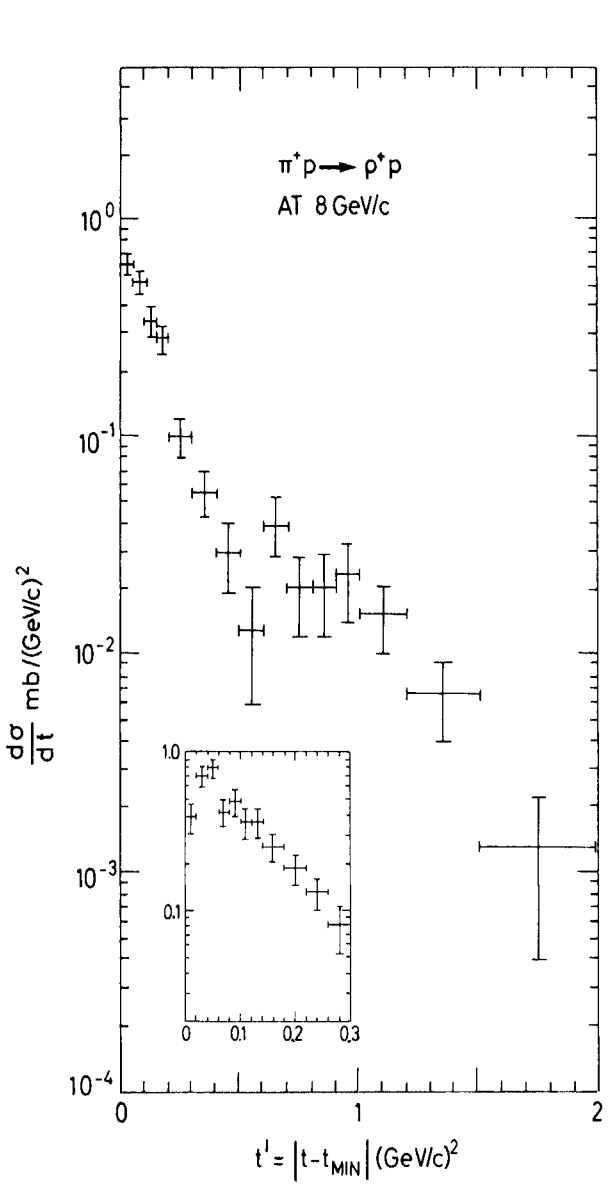

Fig. 54 Differential cross-section for the reaction $\pi^+ + p \to \rho^+ + p$ at 8 GeV/c (Ref. 121). The insert shows the small t' region in detail.

such a situation. It appears, in fact, that when good data are available, secondary structures appear in the inelastic two-body cross-sections which are similar to those found in elastic hadron scattering.

To illustrate this point even further, data by the Aachen-Berlin-CERN group are shown in Fig. 54 on the reaction $\pi^+ + p \to \rho^+ + p$ at 8 GeV/c [121]. There is again a forward dip, over a t' interval of ~ 0.05 $(GeV/c)^2$, consistent with what we saw in the previously considered no-charge-exchange reaction. The most impressive feature is, however, the structure at $t' \sim 0.5$ $(GeV/c)^2$ and the broad bump at larger t' values.

Finally, another example of such a situation is given by the results of an experiment on $\pi^+ + p \to \pi^0 + \Delta^{++}$ by a Berkeley-Riverside group [122], as shown in Fig. 55. Qualitatively, this cross-section is very similar to the previous one. In terms of Regge poles these data constitute a beautiful example of a reaction dominated by ρ exchange.

The $\pi^+ + p \to \rho^+ + p$ cross-section shown in Fig. 54 is compared to the $\pi^- p$, pp, and $\bar{p}p$ cross-section data at similar energies in Fig. 56. The presentation probably exaggerates the importance of the bump in the $\rho^+ p$ cross-section. In any case, it appears that all structures develop at comparable t values. This is likely to be true for many -- if not all -- effective two-body reactions. These facts are likely to be interpreted in the framework of several models. The simplest one will be the most welcome.

5.3 Strangeness-exchange scattering

The peculiar behaviour of structures is also present in strangeness-exchange reactions. A reaction

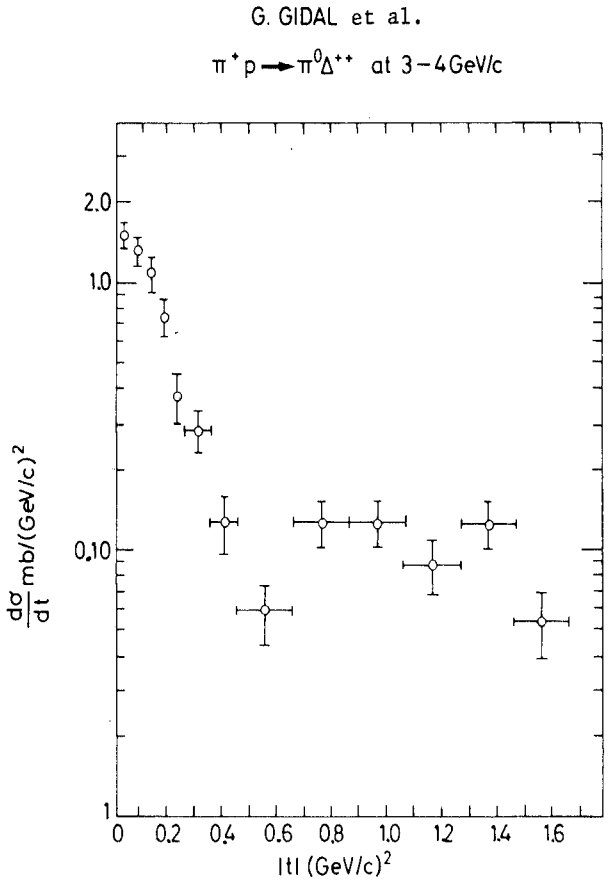

Fig. 55 Differential cross-section for the reaction $\pi^+ + p \to \pi^0 + \Delta^{++}$ (Ref. 122). Data at five momenta between 2.95 and 4.08 GeV/c have been averaged.

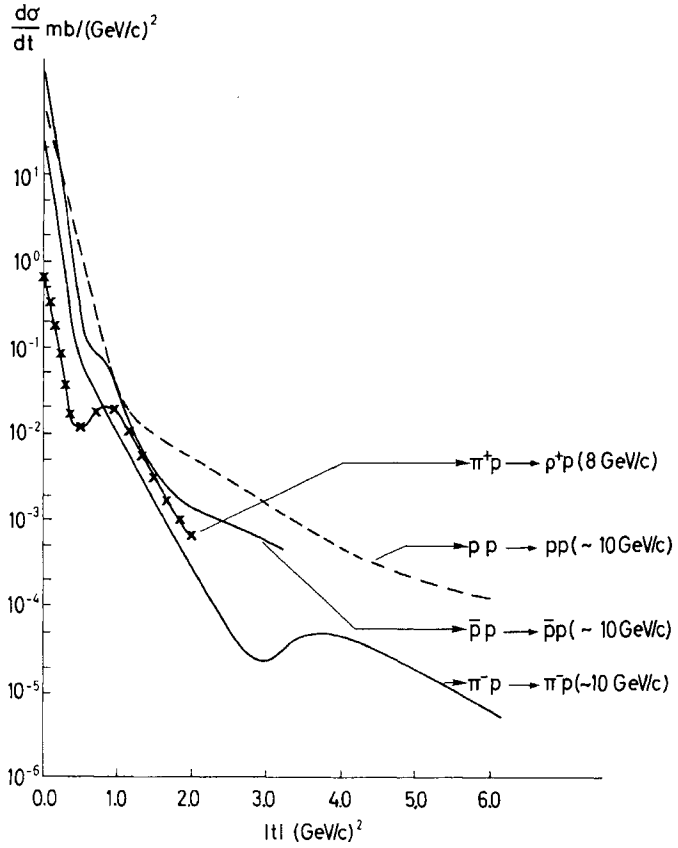

Fig. 56 Comparative behaviour of the pp, $\bar{p}p$, π^-p, and $\pi^+ + p \to \rho^+ + p$ cross-sections at 8-10 GeV/c laboratory momentum.

which behaves in a simple way, however, is the π^-p associated production in the forward region. Figure 57 shows the final data by the Pisa-Orsay spark chamber experiment, in which the differential cross-section at $|t| \lesssim 1$ $(GeV/c)^2$ between 6 and 11.2 GeV/c was measured[123]. The data are nicely fitted in a reggeized K* exchange model[124].

The Carnegie Mellon-BNL group has submitted to this Conference preliminary data on 8 and 16 GeV/c differential cross-sections for the reactions $K^- + p \to \pi^- + \Sigma^+$ and $K^- + p \to \pi^- + Y_1^{*+}(1385)$ [125]. The forward peaks, as seen in Fig. 58, show approximately the same energy dependence in both reactions, but the $\pi^-\Sigma^+$ slopes are much steeper. This is consistent with the empirical rule discussed in Section 5.1c above.

The SABRE bubble chamber group has studied the reaction $K^- + n \to \pi^-$ + an isospin-zero hyperon, at 3 GeV/c [126]. Their results for Λ, $Y_0^*(1405)$, $Y_0^*(1520)$, and $Y_0^*(1820)$ are shown in Fig. 59. In terms of exchange, the forward peak in these reactions should be due to K^* exchange, and the backward ones to baryon

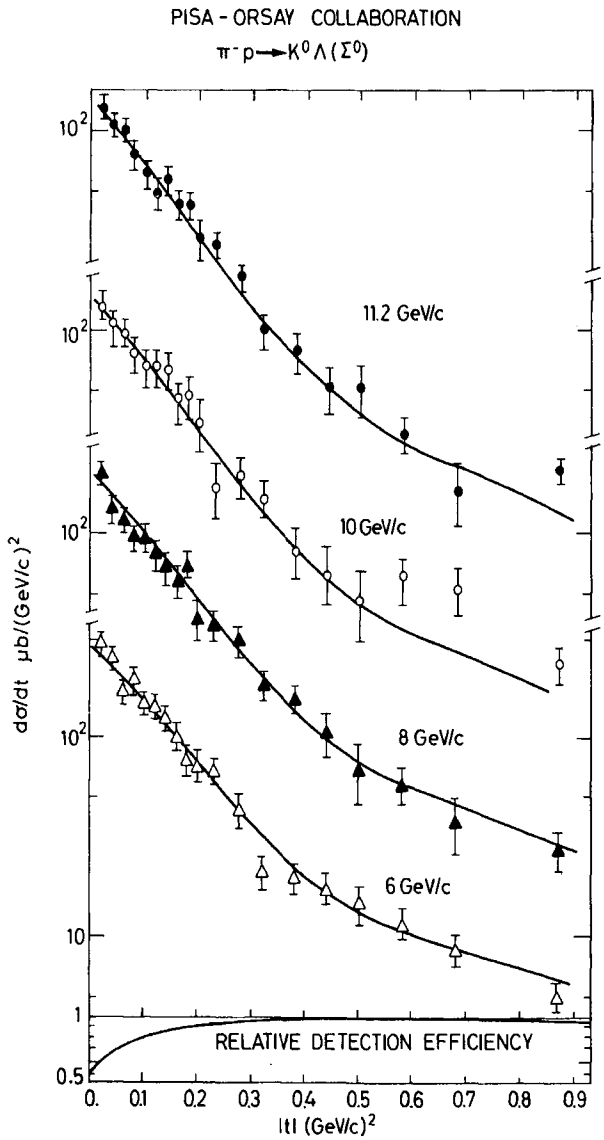

Fig. 57 Differential cross-sections for the reaction $\pi^- + p \to K^0 + \Lambda$ (or Σ^0) at $|t| \lesssim 1$ $(GeV/c)^2$ (Ref. 123). The theoretical curves are fitted to the data and have been calculated in the model by Reeder and Sarma (Ref. 124).

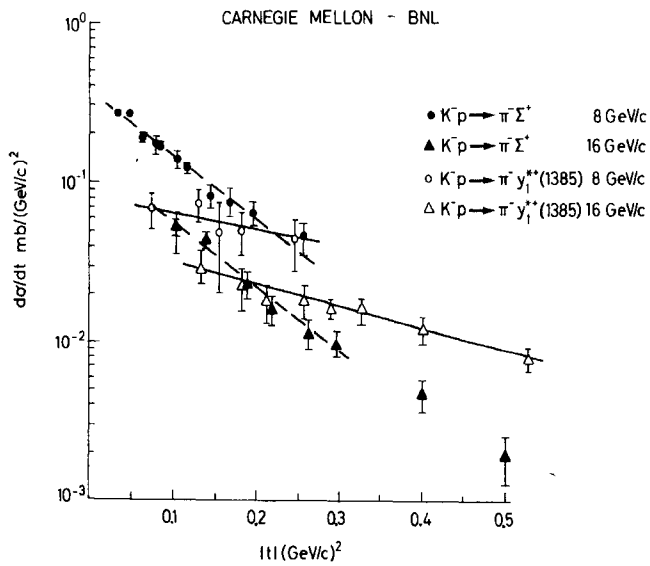

Fig. 58 Forward differential cross-sections for the reactions $K^- + p \to \pi^- + \Sigma^+$ and $K^- + p \to \pi^- + Y_1^{*+}(1385)$ at 8 and 16 GeV/c (Ref. 125).

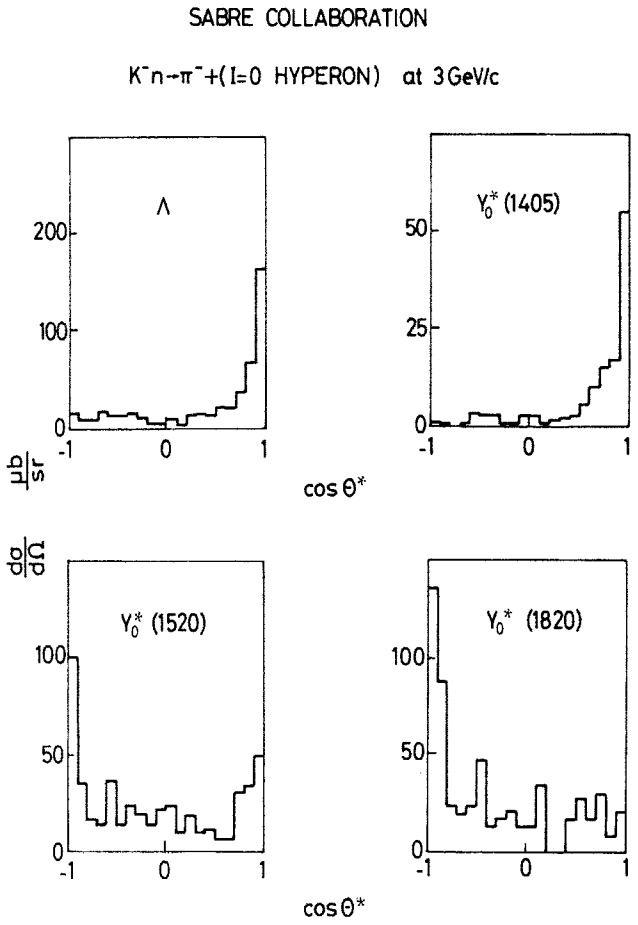

Fig. 59 Differential cross-sections for four I = 0 hyperon production reactions in $K^- + n \to \pi^- + Y$ at 3.0 GeV/c.

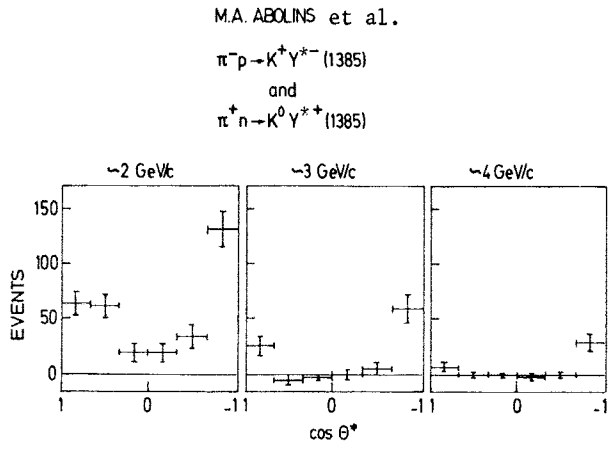

Fig. 60 $Y_1^*(1385)$ production angular distributions in the reactions $\pi^- + p \to K^+ + Y^{*-}$ or $\pi^+ + n \to K^0 + Y^{*+}$ at ~ 2, ~ 3, and ~ 4 GeV/c (Ref. 127). Data at several momenta, with relative differences of the order of 10% about the quoted values, have been combined.

exchange. As far as quantum numbers are concerned, all reactions are very similar. However, the results are rather different from one reaction to another. Whilst one can see an indication that the forward peak decreases regularly with increasing hyperon mass, the backward peak in the $\pi^-\Lambda$ and $\pi^- Y_0^*(1405)$ is just absent. It is not easy to understand this effect in the framework of the baryon exchange model.

Surprising features are also present in the reactions $\pi^- + p \to K^+ + Y^{*-}(1385)$ and $\pi^+ + n \to K^0 + Y^{*+}(1385)$ (which are two isospin projections of the same reaction), that have been studied by a Berkeley group group[127]. One sees in Fig. 60 that a forward peak is present up to 4 GeV/c. There is no known existing doubly charged K^* whose exchange could give rise to such a peak. One may argue that the energy at which this experiment was performed is not high enough for the reaction to be dominated by exchange processes in the crossed channels. Also the statistical errors are large. As a matter of fact, the data are consistent with the forward peak decreasing with increasing energy.

Acknowledgements

The warm and perfect hospitality of CERN, and the invaluable technical assistance of its Document Reproduction Service and MSC Drawing Office, are gratefully acknowledged. Useful discussions with many colleagues, in particular with Drs. G. Cocconi, V.T. Cocconi, L. di Lella, B. Margolis, I. Mannelli, D.R.O. Morrison and J. Orear, are also acknowledged. The active assistance of the scientific secretary Dr. M. Fidecaro has been of the greatest help.

REFERENCES AND FOOTNOTES

1. J. Orear, Phys. Letters 13, 190 (1964).
2. C.W. Akerlof et al., paper 547; Phys. Rev. 159, 1138 (1967).
3. A.D. Krisch, paper 545; Phys. Rev. Letters 19, 1149 (1967).
4. J.V. Allaby, G. Cocconi, A.N. Diddens, A. Klovning, G. Matthiae, E.J. Sacharidis and A.M. Wetherell, Phys. Letters 25 B, 156 (1967).

5. See, for example, J.V. Allaby, G. Cocconi, A.N. Diddens, A. Klovning, G. Matthiae, E.J. Sacharidis and A.M. Wetherell, Phys. Letters 25 B, 156 (1967).
J.G. Asbury et al., paper 549; Phys. Rev. Letters 21, 830 (1968).
A.D. Krisch, Phys. Rev. 135 B, 1456 (1964).
D.R. Harrington and A. Pagnamenta, Phys. Rev. Letters 18, 1147 (1967).
J.J.J. Kokkedee and L. Van Hove, Phys. Letters 25 B, 228 (1968).

6. J.V. Allaby, A.N. Diddens, A. Klovning, E. Lillethun, E.J. Sacharidis, K. Schlüpmann and A.M. Wetherell, Proc. of the CERN Topical Conf. on High-Energy Collisions of Hadrons, CERN (1968), CERN 68-7, p. 580.

7. J.V. Allaby et al., paper 605a (submitted to Phys. Letters).

8. H.M. Chan, Rapporteur's talk.

9. H.D.I. Abarbanel et al., paper 682; Phys. Rev. Letters 20, 280 (1968); SLAC-PUB-476.

10. T.T. Chou and C.N. Yang, Phys. Rev. 170, 1591 (1968), and Phys. Rev. Letters 20, 1213 (1968).

11. L. Durand III and R. Lipes, Phys. Rev. Letters 20, 637 (1968).

12. C.B. Chiu and J. Finkelstein, CERN preprint TH 892 (to be published in Nuovo Cimento).

13. S. Frautschi and B. Margolis, paper 727; Nuovo Cimento 56 A, 1155 (1968).

14. J. Engler et al., paper 391a (submitted to Phys. Letters).

15. M.N. Kreisler, L.W. Jones, M.J. Longo and J.R. O'Fallon, Phys. Rev. Letters 20, 468 (1968).

16. D.V. Bugg, D.C. Salter, G.H. Stafford, R.F. George, K.F. Riley and R.J. Tapper, Phys. Rev. 146, 980 (1966).

17. W. Galbraith, E.W. Jenkins, T.F. Kycia, B.A. Leontic, R.H. Phillips, A.L. Read and R. Rubinstein, Phys. Rev. 138 B, 813 (1965).

18. G. Bellettini, G. Cocconi, A.N. Diddens, E. Lillethun, G. Matthiae, J.P. Scanlon and A.M. Wetherell, Phys. Letters 19, 341 (1965).

19. R.J. Abrams, R.L. Cool, G. Giacomelli, T.F. Kycia, B.A. Leontic, K.K. Li and D.N. Michael, BNL 12454 (submitted to Phys. Rev. Letters).

20. B.G. Gibbard et al., paper 482.

21. K.J. Foley, R.S. Gilmore, S.J. Lindenbaum, W.A. Love, S. Ozaki, E.H. Willen, R. Yamada and L.C.L. Yuan, Phys. Rev. Letters 15, 45 (1965).

22. J. Engler et al., paper 390.

23. J. Cox et al., paper 487; Phys. Rev. Letters 21, 641 (1968).

24. J. Cox et al., paper 488 (submitted to Phys. Letters); SLAC-PUB-408, April 1968.

25. T.T. Wu and C.N. Yang, Phys. Rev. 137 B, 708 (1965).

26. J. Engler et al., paper 391b (submitted to Phys. Letters).

27. L.W. Jones et al., paper 348; Phys. Letters 27 B, 328 (1968).

28. G. Bellettini, G. Cocconi, A.N. Diddens, E. Lillethun, G. Matthiae, J.P. Scanlon and A.M. Wetherell, Nucl. Phys. 79, 609 (1966).

29. V.S. Pantuev and M.N. Khachaturyan, Zh. Eksper. Teor. Fiz. 42, 909 (1962); Soviet Phys. - JETP 15, 626 (1962).

30. D. Birnbaum et al., paper 719.

31. A. Ashmore, C.J.S. Damerell, W.R. Frisken, R. Rubinstein, J. Orear, D.P. Owen, F.C. Peterson, A.L. Read, D.G. Ryan and D.H. White, Phys. Rev. Letters 21, 387 (1968).

32. J. Orear et al., paper 513.

33. K. Böckmann, B. Nellen, E. Paul, B. Wagini, I. Borecka, J. Diaz, U. Heeren, U. Liebermeister, E. Lohrmann, E. Raubold, P. Söding, S. Wolf, J. Kidd, L. Mandelli, L. Mosca, V. Pelosi, S. Ratti and L. Tallone, Nuovo Cimento 42 A, 954 (1966).

34. K.J. Foley, S.J. Lindenbaum, W.A. Love, S. Ozaki, J.J. Russel and L.C.L. Yuan, Phys. Rev. Letters 11, 503 (1963).

35. J. Berryhill and D. Cline, paper 280; Phys. Rev. Letters 21, 769 (1968).

36. W. Rarita, R.J. Riddell, Jr., C.B. Chiu and R.J.N. Phillips, Phys. Rev. 165, 1615 (1968).

37. L. Van Hove, Proc. XIIIth Int. Conf. on High-Energy Physics, Berkeley (1966), p. 253.

38. V. Barger, Proc. of the Topical Conf. on High-Energy Collisions of Hadrons, CERN (1968), CERN 68-7, p. 5.

39. M. Derrik, Proc. of the Topical Conf. on High-Energy Collisions of Hadrons, CERN (1968), CERN 68-7, p. 111.

40. E.W. Anderson, E.J. Blaser, H.R. Blieden, G.B. Collins, D. Garelick, J. Menes, F. Turkot, D. Birnbaum, R.M. Edelstein, N.C. Hien, T.J. McMahon, J. Mucci and J. Russ, Phys. Rev. Letters 20, 1529 (1968).

41. J. Orear et al., abstract 515; Phys. Rev. Letters 21, 389 (1968).

42. V. Barger and D. Cline, Phys. Rev. Letters 21, 392 (1968).

43. A.P. Contogouris, J. Tran Than Van and M. Le Bellac, Nuclear Phys. B5, 683 (1967).

44. C.B. Chiu and J. Finkelstein, paper 176; CERN preprint, TH 914 (1968).

45. J. Banaigs et al., paper 231 (submitted to Nuclear Phys.).

46. W.F. Baker et al., paper 229.

47. V. Barger, private communication.

48. V.D. Antopolsky et al., paper 929.

49. J. Mott, R. Ammar, R. Davis, W. Kropac, A. Cooper, M. Derrick, T. Fields, L. Hyman, J. Loken, F. Schweingruber and J. Simpson, Phys. Letters 23, 171 (1966).

50. A.S. Carroll et al., paper 14a (submitted to Phys. Rev. Letters).

51. A.S. Carroll, T. Fischer, A. Lundby, R.H. Phillips, C.L. Wang, F. Lobkowicz, A.C. Melissinos, Y. Nagashima and S. Tewksbury, Phys. Rev. Letters 20, 607 (1968).

52. A.S. Carroll et al., paper 14b (submitted to Phys. Rev. Letters).

53. D. Cline, C. Moore and D. Reeder, Phys. Rev. Letters 19, 675 (1967).

54. J. Banaigs, J. Berger, C. Bonnel, J. Duflo, L. Goldzahl, F. Plouin, W.F. Baker, P.J. Carlson, V. Chabaud and A. Lundby, "$K^{\pm}p$ elastic scattering in the backward hemisphere at 3.55 GeV/c" (submitted to Phys. Letters).

55. D. Birnbaum et al., paper 720.

56. E.W. Anderson et al., paper 723.

57. R.C. Chase et al., paper 949.

58. V. Glauber, High-Energy Physics and Nuclear Structure (North-Holland Pub. Co., Amsterdam, 1967), p. 311.

59. V. Franco and E. Coleman, Phys. Rev. Letters 15, 827 (1966).

60. H.C. Hsiung et al., paper 742; Phys. Rev. Letters 21, 187 (1968).

61. J.C. Vander Velde, paper 741.

62. The author is grateful to Professor R. Glauber for a fruitful conversation on these points.

63. L. Bertocchi et al., paper 118.

64. L. Bertocchi, private communication.

65. V.D. Antopolsky et al., paper 930.

66. R.C. Chase et al., paper 115.

67. V. Barger and D. Cline, paper 436; Phys. Letters 27 B, 312 (1968).

68. J. Schneider et al., paper 942.

69. H.R. Crouch, Jr. et al., paper 731.

70. P. Sonderegger, J. Kirz, O. Guisan, P. Falk Vairant, C. Bruneton, P. Borgeaud and A.V. Stirling, Phys. Letters 20, 75 (1966).

71. Y. Goldschmidt-Clermont et al., paper 443.

72. D.B. Cline et al., paper 281.

73. V. Barger and D. Cline, Phys. Rev. 156, 1522 (1967).

74. D.R.O. Morrison, Phys. Rev. 165, 1699 (1968); Phys. Letters 22, 187 (1966).

75. I. Butterworth, J. Brown, G. Goldhaber, S. Goldhaber, A. Hirata, J. Kadyk, B. Schwarzschild and G. Trilling, Phys. Rev. Letters 15, 734 (1965).

76. M. Borghini, G. Coignet, L. Dick, K. Kuroda, L. di Lella, P.C. Macq, A. Michalowicz and J.C. Olivier, Phys. Letters 24 B, 77 (1967).
For a comprehensive review on the subject, see L. Van Rossum, Proc. of the Topical Conf. on High-Energy Collisions of Hadrons, CERN (1968), CERN 68-7, p. 161.

77. N.E. Booth et al., paper 308; Phys. Rev. Letters 21, 651 (1968).

78. P. Grannis, J. Arens, F. Betz, O. Chamberlain, B. Dieterle, C. Schultz, G. Shapiro, H. Steiner, L. Van Rossum and D. Veldon, Phys. Rev. 148, 1297 (1966).

79. C. Daum, F.C. Erné, J.P. Lagnaux, J.C. Sens, M. Steuer and F. Udo, Nuclear Phys. B6, 617 (1968).

80. W.E. Frahn and R.H. Venter, Ann. Phys. (N.Y.) 27, 135, 385, 401 (1964).

81. R.T. Bell et al., paper 239.

82. R.J. Esterling et al., paper 311.

83. C. Daum, F. Erné, J.P. Lagnaux, J.C. Sens, M. Steuer and F. Udo, Nuclear Phys. B6, 273 (1968); Nuclear Phys. B7, 19 (1968).

84. N. Booth, G. Conforto and A. Yokosawa, private communication.

85. V. Barger and D. Cline, Phys. Rev. 155, 1792 (1967).
A. Dar and B. Kozlowsky, Phys. Letters 20, 314 (1966).

86. V. Barger, oral report given at this Conference.

87. A. Michelini et al., paper 522.

88. H. Högaasen, Nuovo Cimento 56 A, 915 (1968).

89. E.W. Anderson, E.J. Bleser, G.B. Collins, T. Fujii, J. Menes, F. Turkot, R.A. Carrigan Jr., R.M. Edelstein, N.C. Hien, T.J. McMahon and I. Nadelhaft, Phys. Rev. Letters 16, 855 (1966).

90. I.M. Blair, A.E. Taylor, W.S. Chapman, P.I.P. Kalmus, J. Litt, M.C. Miller, D.B. Scott, H.J. Sherman, A. Astbury and T.G. Walker, Phys. Rev. Letters 17, 789 (1966).

91. C.M. Ankenbrandt, A.R. Clark, B. Cork, T. Elioff, L.T. Kerth and W.A. Wenzel, Phys. Rev. 170, 1223 (1968).

92. J.V. Allaby et al., paper 605b.

93. S. Frautschi and B. Margolis, paper 728; Nuovo Cimento 57 A, 427 (1968).

94. S. Frautschi, O. Kofoed-Hansen and B. Margolis, "Large momentum transfer diffraction scattering and production", CERN preprint TH 936, to be published.

95. T.T. Chou and C.N. Yang, "A model of high-energy elastic scattering and diffractive excitation processes in hadron-hadron collisions", Stony Brook preprint.

96. E.L. Feinberg and I. Pomeranchuk, Suppl. Nuovo Cimento 3, 652 (1956).
M.L. Good and W.D. Walker, Phys. Rev. 120, 1857 (1960).

97. W. Ellis et al., papers 368 and 816; Phys. Rev. Letters 21, 697 (1968).

98. G. Cocconi, E. Lillethun, J.P. Scanlon, C.A. Stahlbrandt, C.C. Ting, J. Walters and A.M. Wetherell, Phys. Letters 8, 134 (1964).
C.M. Ankenbrandt, A.R. Clyde, B. Cork, D. Keefe, L.T. Kerth, W.M. Layson and A.M. Wenzel, Nuovo Cimento 35, 1052 (1965).
G. Bellettini, G. Cocconi, A.N. Diddens, E. Lillethun, J.P. Scanlon, A.M. Shapiro and A.M. Wetherell, Phys. Letters 18, 167 (1965).

99. L.D. Roper, Phys. Rev. Letters 12, 340 (1964). For the present status of this resonance, see C. Lovelace, Proc. Int. Conf. on Elementary Particles, Heidelberg (1967), p. 79.

100. F.R. Huson et al., paper 208.

101. E.L. Berger, E. Gellert, G.A. Smith, E. Colton and P.E. Schlein, Phys. Rev. Letters 20, 964 (1968).

102. R.M. Heinz, O.E. Overseth, D.E. Pellett and M.L. Perl, Phys. Rev. 167, 1232 (1968). Other references to previous measurements are contained in this publication.

103. D. Dekkers, B. Jordan, R. Mermod, C.C. Ting, G. Weber, T.R. Willits, K. Winter, X. de Bouard and M. Vivargent, Phys. Letters 11, 161 (1964).

104. H.L. Anderson et al., paper 638.

105. J.V. Allaby et al., paper 606.

106. T. Yao, Phys. Rev. 134 B, 454 (1964).
See also D.J. Brown, Nuclear Phys. B7, 37 (1968).

107. F. Turkot, G.B. Collins and T. Fujii, Phys. Rev. Letters 11, 474 (1963).
N.W. Reay, A.C. Melissinos, J.T. Reed, T. Yamanouchi and L.C.L. Yuan, Phys. Rev. 142, 918 (1966).
R.C. Lamb, R.A. Lundy, T.B. Novey, D.D. Yovanovitch and R. Lander, Phys. Rev. Letters 17, 100 (1966).
B.S. Neganov and L.B. Parfenov, Soviet Phys.-JETP 7, 528 (1958).
M.G. Mescheryakov, B.S. Neganov, N.P. Bogachev and U.M. Sidorov, Dokl.Akad.Nauk SSSR 100, 673 (1955).
M.G. Mescheryakov and B.S. Neganov, Dokl.Akad.Nauk SSSR 100, 677 (1955).

108. L. di Lella, Proc. Int. Conf. on Elementary Particles, Heidelberg (1967), p. 159.
D.C. Colley, Proc. of the Topical Conf. on High-Energy Collisions of Hadrons, CERN (1968), CERN 68-7, p. 60.

109. J.T. Donohue, Nuovo Cimento 55 A, 527 (1968).

110. Aachen-Berlin-CERN Collaboration and Aachen-Berlin-CERN-London (I.C.)-Vienna Collaboration, paper 451 (submitted to Phys. Letters).
The dependence of the slope on the mass of the produced particles was also studied by L. Marshall-Libby and S. Miyoshita, Phys. Rev. 168, 1779 (1968). See the discussion at the end of this talk.

111. W. De Baere et al., paper 445.

112. M. Aderholz et al., paper 461 (submitted to Nuclear Phys.).

113. For a discussion on this subject, see for example P.E. Schlein, Univ. Calif., Los Angeles, Report No. UCLA-1029.
G. Wolf, Phys. Rev. Letters 19, 925 (1967).
B. Haber, U. Maor, G. Yekutieli and E. Gotsman, Phys. Rev. 168, 1773 (1968).

114. K. Gottfried and J.D. Jackson, Nuovo Cimento 34, 735 (1964); 33, 309 (1964).

115. K. Buchner et al., paper 442.

116. Saclay-Amsterdam-Bologna-Rehovoth-Ecole Polytechnique (SABRE) Collaboration, paper 477.

117. R.L. Eiser et al., paper 812.

118. N. Armenise et al., paper 410.

119. N. Armenise et al., paper 412.

120. B.D. Hyams, W. Koch, D.C. Potter, J.D. Wilson, L. Von Lindern, E. Lorenz, G. Lütjens, U. Stierlin and P. Weilhammer, paper 737; Nuclear Phys. B7, 1 (1968).

121. M. Aderholz et al., paper 937.

122. G. Gidal et al., paper 808.

123. E. Bertolucci et al., paper 341.

124. D.D. Reeder and K.V.L. Sarma, Nuovo Cimento 53 A, 808 (1968), and University of Wisconsin preprint, 100-125, December (1967) (to be published in Phys. Rev.).

125. D. Birnbaum et al., paper 721.

126. Saclay-Amsterdam-Bologna-Rehovoth-Ecole Polytechnique (SABRE) Collaboration, paper 891.

127. M.A. Abolins et al., paper 224.

DISCUSSION

KRISCH: The CERN group has suggested that the break observed in the 90° cross-section is not evidence for the existence of several regions in the proton-proton interaction, but is an accident caused in some way by the more complicated diffraction wiggles that they claim to see in angular distributions.

I completely disagree with this suggestion for two reasons.

I first object on the grounds of aesthetics. In my opinion if you replace a simple model that fits the data well with a more complex model that fits the data less well, you have made little progress.

My second objection is on the grounds of kinematics. The 90° cross-section shows the break most clearly. I believe that this is because 90° is a special symmetry point: the effects of particle identity, whatever they are, are always the same. On the other hand, in the angular distribution near 90° the effects of particle identity are changing rapidly. This and the interference of the different regions complicate angular distributions.

However, if you take these effects into account in some way the breaks still show themselves clearly. An excellent fit to the data, including the recent CERN data, was shown in the session chaired by Dr. Mannelli.

CHEW: If the energy dependence of backward K^-p elastic scattering really has the power behaviour $\sim s^{-10}$, at least two qualitative conclusions can be drawn:

i) the leading Regge cuts are unimportant because they would lead to a higher power;
ii) the leading Regge pole coupled to K^+p has $J \approx -4$ at $u = 0$. With a "normal" slope, one would expect to see resonances on this trajectory beginning at $u = m^2 \sim 4$ GeV^2 or $m \sim 2$ GeV.

MARSHALL-LIBBY: The exponential dependence on mass for the differential cross-section for two-body production reactions discussed by Dr. Bellettini was fitted and interpreted and published in Phys. Rev. in early 1968 by S. Miyashita and L. Marshall-Libby, using a modification of the drop model of N. Byers and C.N. Yang. We put into the eikonal expression the measured AB elastic scattering amplitude and searched for a fit to the differential production cross-section for AB → CD, thus finding the CD elastic scattering amplitude. The radius of the CD interaction is related to this amplitude. These radii decrease as the mass and excitation of C and D increase. This general statement describes strange and non-strange baryons, and anti-baryons, and mesons. The radii approach constant values above 30 GeV.

BURKHARDT: I should like to stress the importance of the direct neutron-proton measurements in checking the validity of the Glauber formula at high energies. It seems that, if the scattering is dominated by moving singularities in the J-plane such as Regge poles, the usual elastic Glauber shadow correction should vanish and leave only a contribution from the third double spectral function due to inelastic intermediate states -- this should be about 1/3 the size. The data just presented show the np cross-sections about 5 mb less than those inferred from the Glauber formula, which supports this view. In view of the increasing use of these ideas, it is important to check these results, both experimentally and theoretically.

INTERMEDIATE AND HIGH-ENERGY COLLISIONS

Experimental 2

Chairman	J. OREAR
Rapporteur	O. CZYZEWSKI
Discussion Leader	D.R.O. MORRISON
Secretaries	D. LINGLIN
	M. STEUER
	P. VILLEMOES

MANY-BODY PROCESSES

O. Czyzewski

Institute of Nuclear Research, Cracow

1. INTRODUCTION

At the beginning I should define what I mean when referring to many-body processes; in the present context many means three or more. This subject of many-body collisions is essentially new at this Conference. Problems of characteristics of pion production were often discussed, but never were there so many papers on this subject -- about 90, in fact -- submitted to one conference. I believe there are two strongly correlated reasons for this increase in interest: first there is the dramatic growth of the amount of experimental data, relevant to the study of many-body processes, with good statistics in many individual channels. The second reason, also important, is the increased interest in this subject among theorists. It is correlated with the revival of the multiperipheral model by the introduction of Regge poles; this model helps in systematizing the data and maybe to understand them.

2. GENERAL PROPERTIES OF MANY-BODY PROCESSES

The general behaviour of particles produced in high-energy hadron collisions is very well visible on the plot from the paper of the Aachen-Berlin-Bonn-CERN-Cracow-Heidelberg-Warsaw Collaboration[1] (Fig. 1). This plot presents, for each kind of particle produced in a given channel of 16 GeV/c $\pi^- p$ interactions, a vector corresponding to an average value of the c.m. momentum. Its components are $\langle p_\perp \rangle$ and $\langle p_L^* \rangle$. One sees very well that:

a) $\langle p_\perp \rangle$ is essentially independent of multiplicity,

b) $\langle p_L^* \rangle$ depends strongly on multiplicity, being larger for smaller multiplicity,

c) $\langle p_L^* \rangle$ of protons is negative, $\langle p_L^* \rangle$ of pions is, in general, positive; the largest absolute values of $\langle p_L^* \rangle$ for π's are attained by negative pions (primary pions are negative).

It can be seen that the proton behaves differently from all other particles; even with higher multiplicities it retains part of its primary momentum -- it is a "leading particle". Now for the pion, this feature is less obvious, since the leading pion is hidden among many other pions. It would be expected that one can better see the leading meson in the case of Kp interaction. This problem was studied by the Aachen-Berlin-CERN-London-Vienna Collaboration. Figure 2 presents the longitudinal momentum versus $p_\perp$ distribution for protons, π mesons, and K^- mesons, produced in $K^- p$ interactions at 10 GeV/c incident momentum[2]. Behaviour of kaons is very similar to the behaviour of protons -- they are leading mesons. The peripheral behaviour of the proton becomes less pronounced when we look at higher multiplicities --

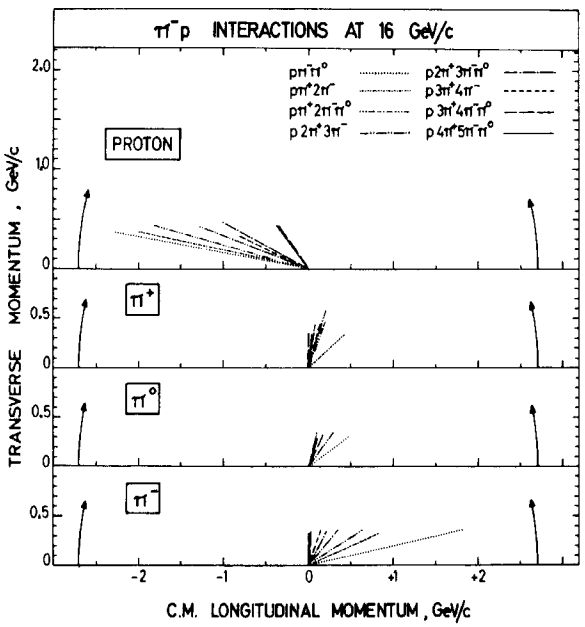

Fig. 1 Average c.m. momentum vectors composed of the average c.m. longitudinal momentum $\langle p_L^* \rangle$ and the average transverse momentum $\langle p_\perp \rangle$ for protons and different pions in the reactions $\pi^- p \to p + m\pi$. The circle line is the kinematic limit[1].

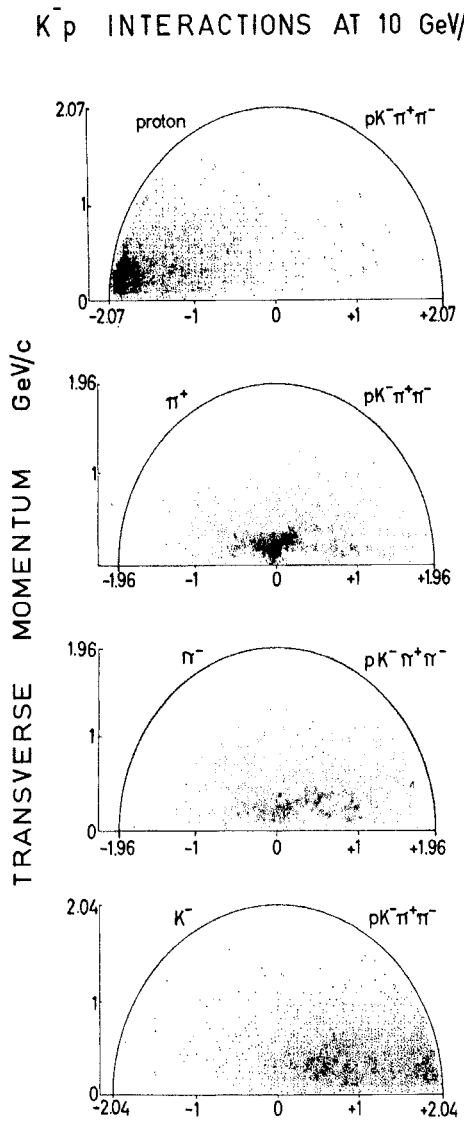

Fig. 2 Peyrou plots (p_t versus p_L^*) for particles produced in the reaction $K^-p \to pK^-\pi^+\pi^-$ at 10 GeV/c [2].

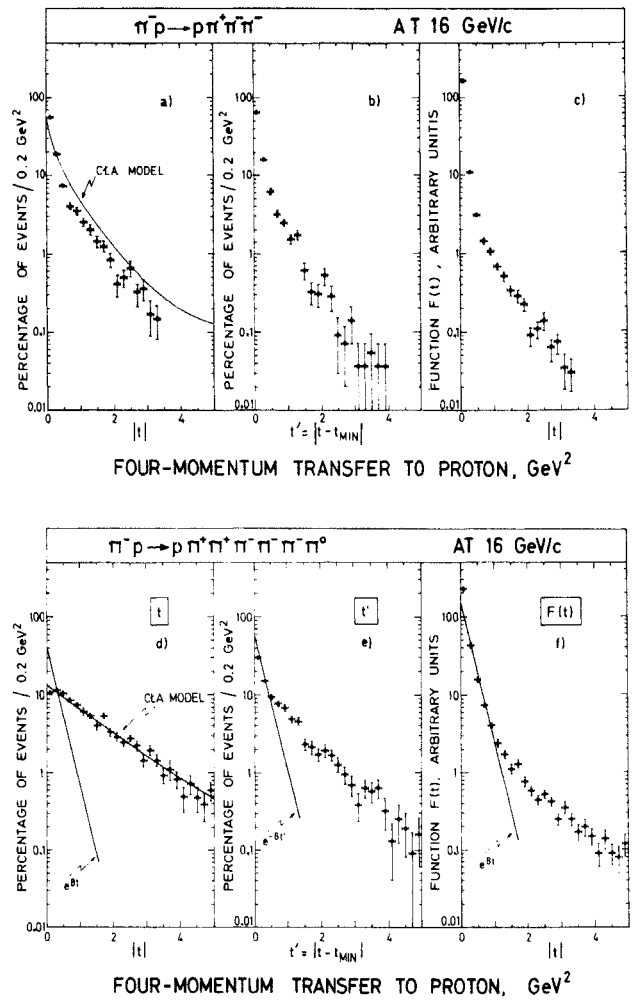

Fig. 3 t and t' distributions, and F(t) functions[3]:
a) b) c) $\pi^-p \to \pi^-p\pi^+\pi^-$
e) f) g) $\pi^-p \to \pi^-p2\pi^+2\pi^-\pi^0$ at 16 GeV/c [1].

this is to a large extent due to the influence of kinematics and phase-space factors. Figure 3 presents distributions of four-momentum transfers to nucleons for p3π and p6π channels of 16 GeV/c π^-p interactions[1]. They look very different, but their t' distributions [$t' = |t-t_{min}|$, where t_{min} is the threshold value of t for the production of the given mass of pion system (Fig. 4)] are similar; also F(t) functions[3], obtained by dividing the experimental t-distribution by the phase-space t-distribution, are similar. Even for very high multiplicity (eight-prong events at 8 GeV/c π^+ incoming momentum), the F(t) function looks similar to elastic scattering[4] (Fig. 5).

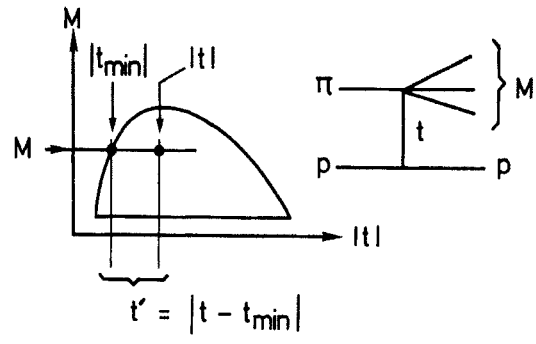

$$F(t) = \frac{\text{Experimental t-distribution}}{\text{Phase-Space t-distribution}}$$

Fig. 4 Definition of t' and of F(t). For two-body reactions A + B → C + D, Ph.Sp.(t) = const. and F(t) ∿ Expt(t).

The meaning of this seems to be the following: the part of the matrix element responsible for the behaviour of leading particles, is similar for different multiplicities.

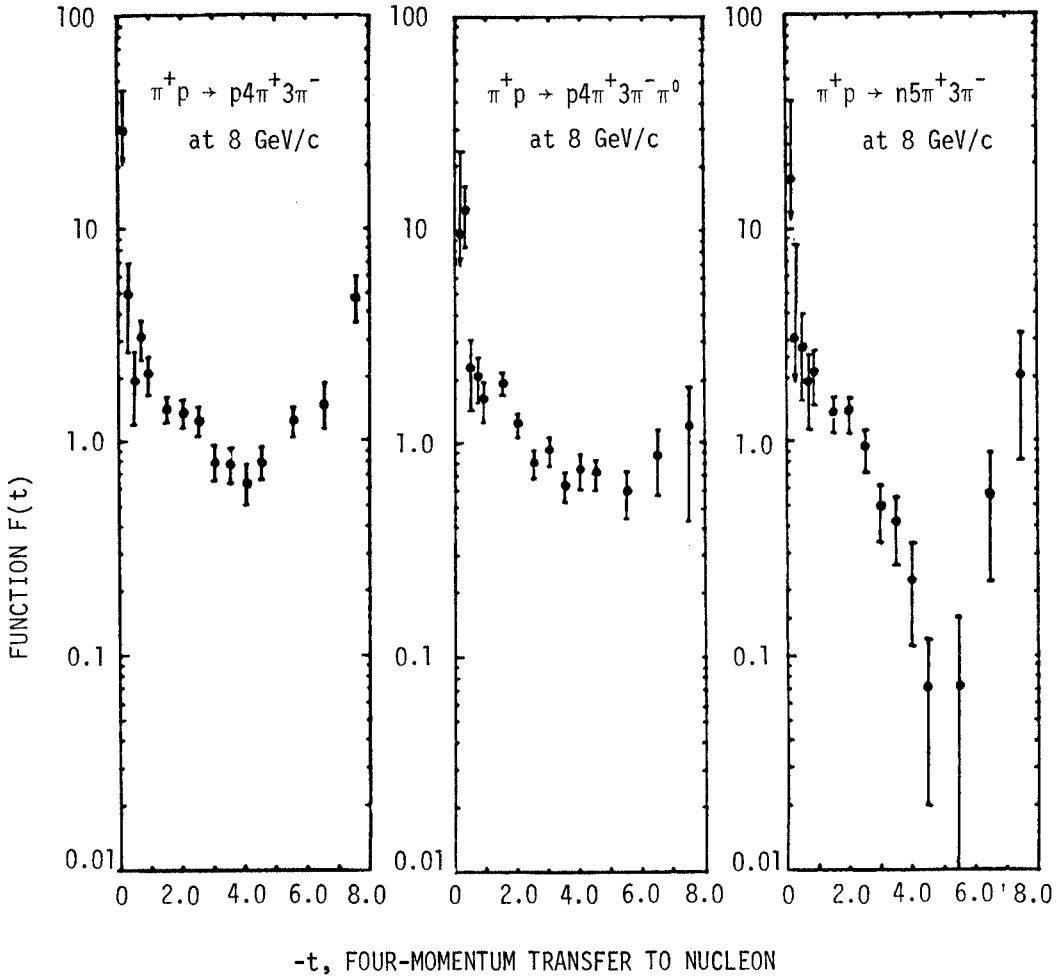

Fig. 5 F(t) functions for eight-prong π^+p reactions at 8 GeV/c [4].

Essentially all the properties of many-body processes, like the smallness of $p_\perp$, presence of leading nucleons, small inelasticity of the collision (fraction of energy transferred into pion production ~ 0.5) are well known from the study of cosmic-ray interactions [see, for example, a paper by Perkins[5]].

It seems that we have not learned much from the study of accelerator data, but these data are much more accurate than cosmic-ray data and therefore allowed us to make a detailed comparison with model predictions, thus we can maybe learn something about the dynamics of strong interactions.

3. MULTIPERIPHERAL REGGEIZED MODEL

For about a year we have had in our hands a model which allows us to compare experimental results in a quantitative way with a theory which is moderately simple -- namely the multiperipheral Reggeized model (MRM)[6]. The main features of this model can be seen by drawing simple Feynman diagrams:

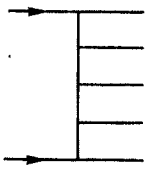

In parallel with the accumulation of data on resonances produced in high-energy collisions and on the data on two-body processes, there is an increasing amount of reliable experimental information on many-body processes. The MRM permits one to analyse them in a way similar to the analysis of two-body reactions; there are several papers on this subject submitted to the Conference.

3.1 Three-body reactions

MRM-type analysis of three-body processes is often difficult because an important part of the

cross-section of the three-particle final state, for example $p\pi^+\pi^0$, corresponds to quasi two-body processes.

There are three solutions to this problem:

a) one can choose for the analysis a channel without resonances in the final state. In such a case one has to believe that the description is correct even for very small energies of pairs of particles;

b) one can exclude resonances from the experimental data;

c) one can include resonance amplitudes in the calculation.

An example of the type (a) is the $K^+\omega^0 p$ final state, observed by a Berkeley group (Alexander et al.)[7] in the study of K^+p interactions at 9 GeV/c. They analyse the experiment in terms of three double Regge graphs.

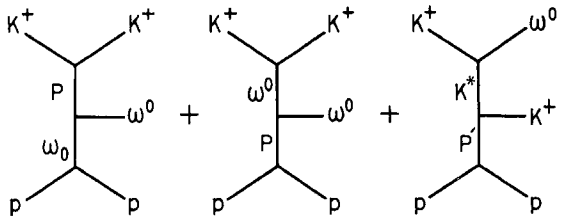

The agreement with data is very good, as shown in Fig. 6, which contains all the t-distributions and effective mass distributions of the channel in question.

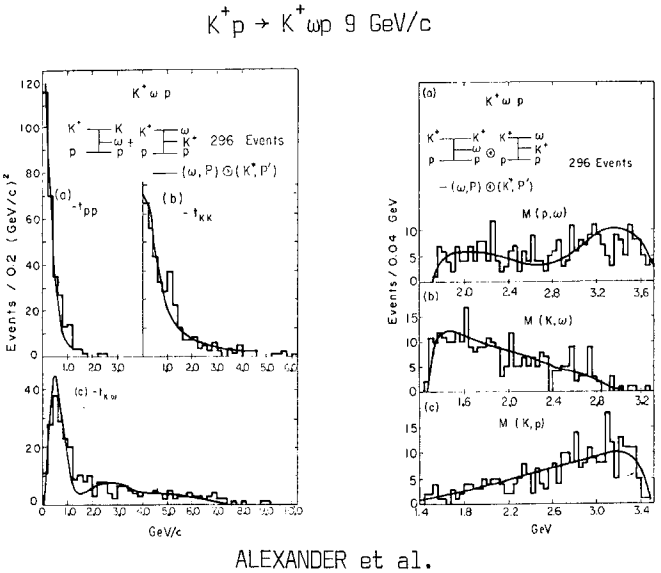

Fig. 6 t distributions and effective mass distributions for the reaction $K^+p \to K^+\omega^0 p$ at 9 GeV/c [7]; continuous lines give Regge fits.

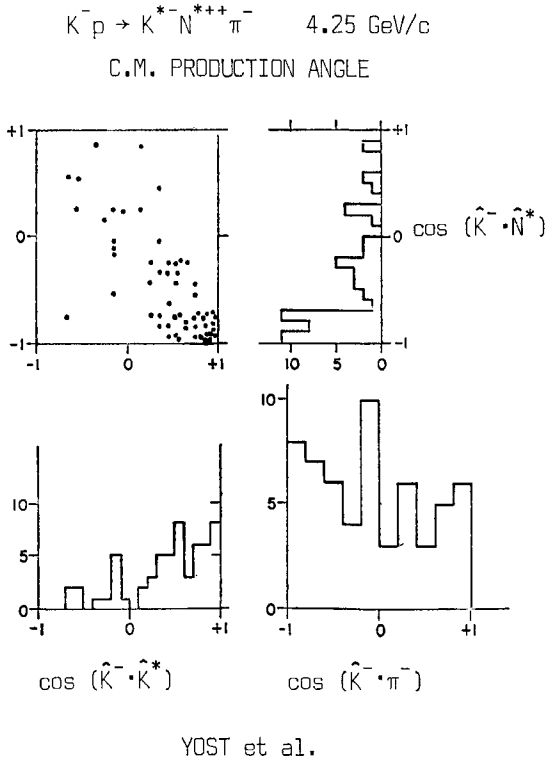

Fig. 7 c.m. angular distributions for K^{*-}, Δ^{++} and π^- for the reaction $K^-p \to K^{*-}\Delta^{++}\pi^-$ at 4.25 GeV/c [8].

Another reaction without obvious further resonances in the combinations of two out of three particles is the process $K^-p \to K^{*-}\pi^-\Delta^{++}$ studied at 4.25 GeV/c incident momentum by Yost et al.[8]. Figure 7 presents the c.m. angular distribution of K^{*-}, Δ^{++} and π^-. The shape of those distributions suggests that this reaction can be described by the double-peripheral graph; the analysis of decay distributions of K^* and Δ^{++} suggested that the dominant graph is:

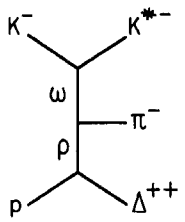

The second type of analysis was applied to the reaction $\pi^-p \to p\pi^-\rho^0$ at 25 GeV/c by Lips and Zweig (Wisconsin)[9]. Figure 8 presents a three-dimensional plot of t_{pp} versus $t_{\pi^-\pi^-}$, where strong correlation is visible. This type of correlation is expected for the MRM description of the reaction in question

in terms of a graph:

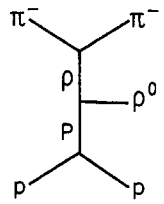

An analogous analysis was applied to the reactions $pp \to pn\pi^+$ or $p\Delta^{++}\pi^-$ at 28.5 GeV/c by a Brookhaven group (Ellis et al.)[10]. The authors used a Reggeized pion exchange and Pomeranchuk exchange; Figure 9 presents an excellent fit to the t-distribution of Δ^{++} and p for the second of the above-mentioned reactions. Similar results as to the validity of MRM are obtained by the Scandinavian Collaboration (Bøggild et al.)[11] in the study of four-prong pp interactions at 19 GeV/c.

There are, however, cases when the final state is dominated by resonances in such a way that one has to do drastic cuts on the effective masses of pairs of particles in order to apply a simple MRM calculation. The way out of this difficulty is to consider the whole sample of events, including in the calculation resonance effects, in a way more or less similar to the OPE model of Ferrari and Selleri[12]. In fact this model is still used to describe certain reactions where one-pion exchange dominates. Several

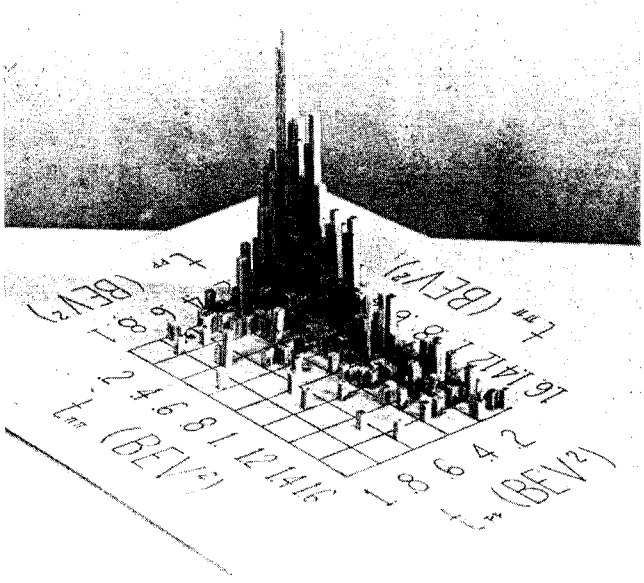

Fig. 8 Three-dimensional plot of t_{pp} versus $t_{\pi^-\pi^-}$ for the reaction $\pi^-p \to p\pi^-\rho^0$ at 25 GeV/c [9].

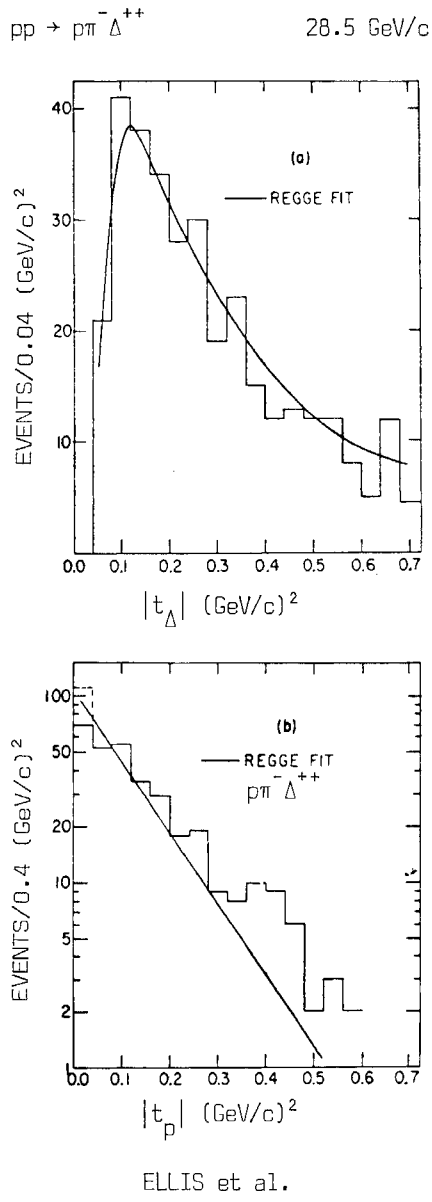

Fig. 9 t distributions, (a) to Δ^{++} and (b) to p, for the reaction $pp \to p\pi^-\Delta^{++}$ at 28.5 GeV/c [10]. Continuous lines give Regge fits.

papers on this subject were submitted. Its good agreement with the data on π^-p interactions at 13 and 20 GeV/c was found by a Harvard group (Brandenburg et al.)[13]. Also for the reaction $pp \to \Delta^{++}p\pi^-$, Colton et al.[14] find good general agreement with OPE model predictions. Figure 10 presents their data and fit to the $p\pi^-$ effective mass. [They observe also an interesting feature: the $N^*(1470)$ peak in the $\Delta^{++}\pi^-$ effective mass distribution is also well reproduced.] There is, however, one generally observed difficulty: OPE predicts isotopic, or at least symmetric (in the case of absorption) distribution of ϕ, the Treiman-Yang angle.

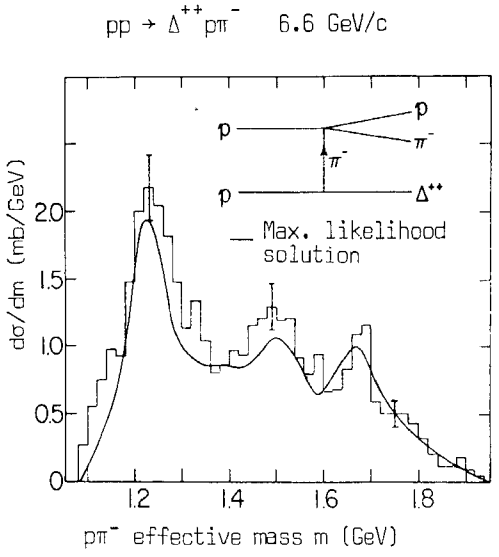

Fig. 10 $p\pi^-$ effective mass distribution for the reaction $pp \to \Delta^{++}p\pi^-$ at 6.6 GeV/c [14]. The continuous line corresponds to OPE model calculation.

Figure 11 presents three examples of these distributions taken from the papers by Rushbrooke et al.[15], Ellis et al.[10] and Berger et al.[16]. In all three cases experimental data are in disagreement with the simple one-pion exchange model, while very good agreement is found for Reggeized pion exchange (shown as a solid line in Fig. 11).

Analogous conclusions about the difficulties of comparing the OPE model with experiment, in this case for the reaction pp → YNK at 6 GeV/c, are reached by Dunwoodie et al.[17].

3.2 Analysis of several channels with the same set of parameters

Recently, Chan, Loskiewicz and Allison (CLA)[18] proposed a version of MRM which is supposed to describe all high-energy inelastic reaction channels simultaneously. For high values of the energy squared, s_i, of the pair of particles, the amplitude has Regge type behaviour, while for low energy the amplitude is constant and the essential role is played by phase space:

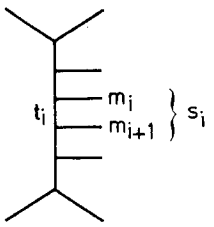

For high energy:

$$s_i \gg (m_i + m_{i+1})^2 \Rightarrow A_i \sim s_i^{\alpha_i(t)}$$

For low energy

$$s_i \approx (m_i + m_{i+1})^2 \Rightarrow A_i \sim \text{constants}$$

Total amplitude:

$$A \sim \prod_i A_i$$

Chan, Loskiewicz and Allison fitted with one set of parameters a large number of single-particle distri-

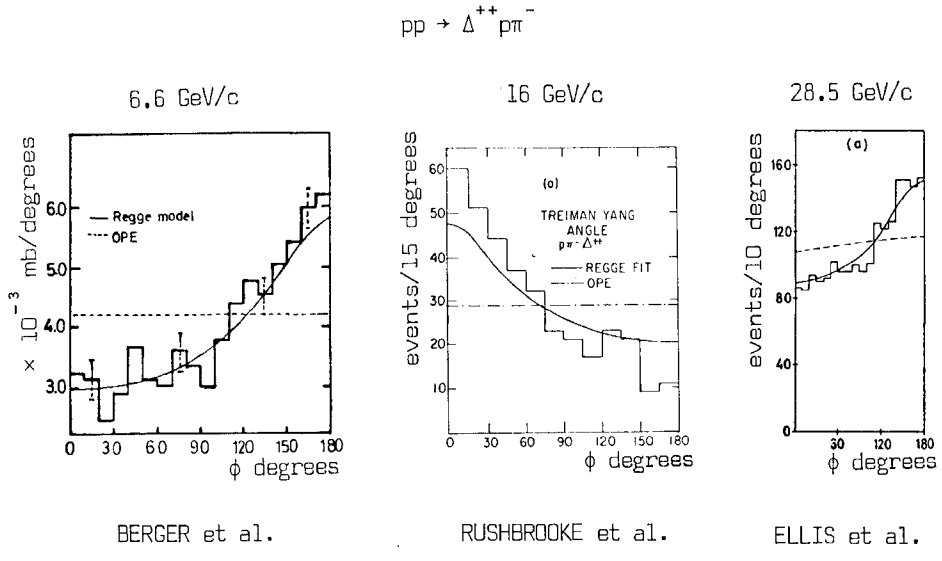

TREIMAN YANG ANGLE DISTRIBUTIONS

Fig. 11 Treiman-Yang angle distributions for the reactions $pp \to \Delta^{++}p\pi^-$: (a) at 6.6 GeV/c [16], (b) at 16 GeV/c [15], and (c) at 28.5 GeV/c [10]. The continuous line corresponds to Regge fits,. the broken line gives OPE model predictions.

butions for a variety of secondary particles produced in high-energy πp and Kp interactions.

New data for several energies of primary particles for many fitted inelastic channels have been presented to this Conference.

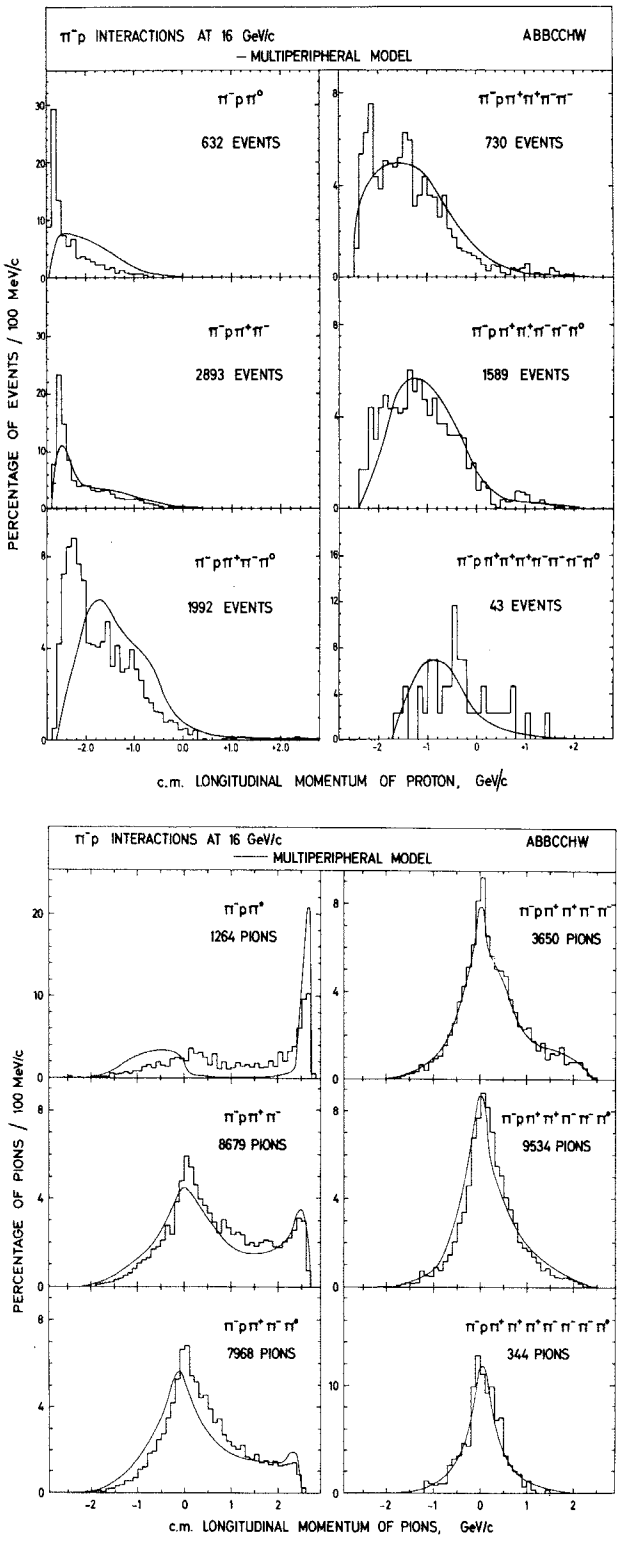

Fig. 12 Percentage distributions of protons and pions in c.m. longitudinal momentum from reactions $\pi^- p \to p + m\pi$ with m ranging from 2 to 8. The solid curves are calculated according to the CLA model[1].

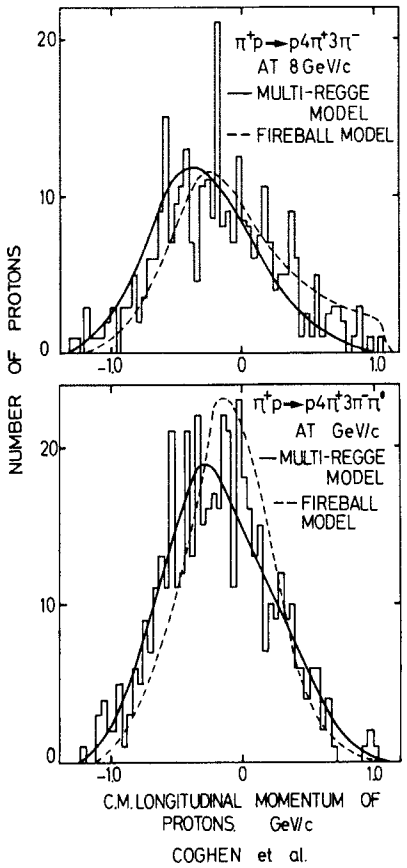

Fig. 13 c.m. longitudinal momentum distributions for protons from the reactions $\pi^+ p \to p4\pi^+3\pi^-$ and $\pi^+ p \to p4\pi^+3\pi^-\pi^0$ at 8 GeV/c [4]. Solid lines give the CLA model predictions.

The Aachen-Berlin-Bonn-CERN-Cracow-Warsaw Collaboration[1] presents a complete set of data on pion production in $\pi^- p$ interactions at 16 GeV/c for numbers of secondary pions ranging from two to eight. The comparison of the distributions of the longitudinal component of the c.m. momentum with the CLA model prediction is shown in Fig. 12. The same parameters as in the original paper of CLA were used in the calculation. One observes some disagreement for low multiplicity, partly due to pions being produced via resonant states. For higher multiplicities good agreement is obtained. In general, protons have their c.m. longitudinal momentum shifted towards negative values. The Cracow group (Coghen et al.)[4] shows that this effect persists even at high multiplicities (eight-prong events), where kinematic factors might be expected to dominate (Fig. 13).

More sophisticated analysis of a similar type is presented by the Genoa-Hamburg-Milan-Saclay Collaboration (Caso et al.)[19] in the study of

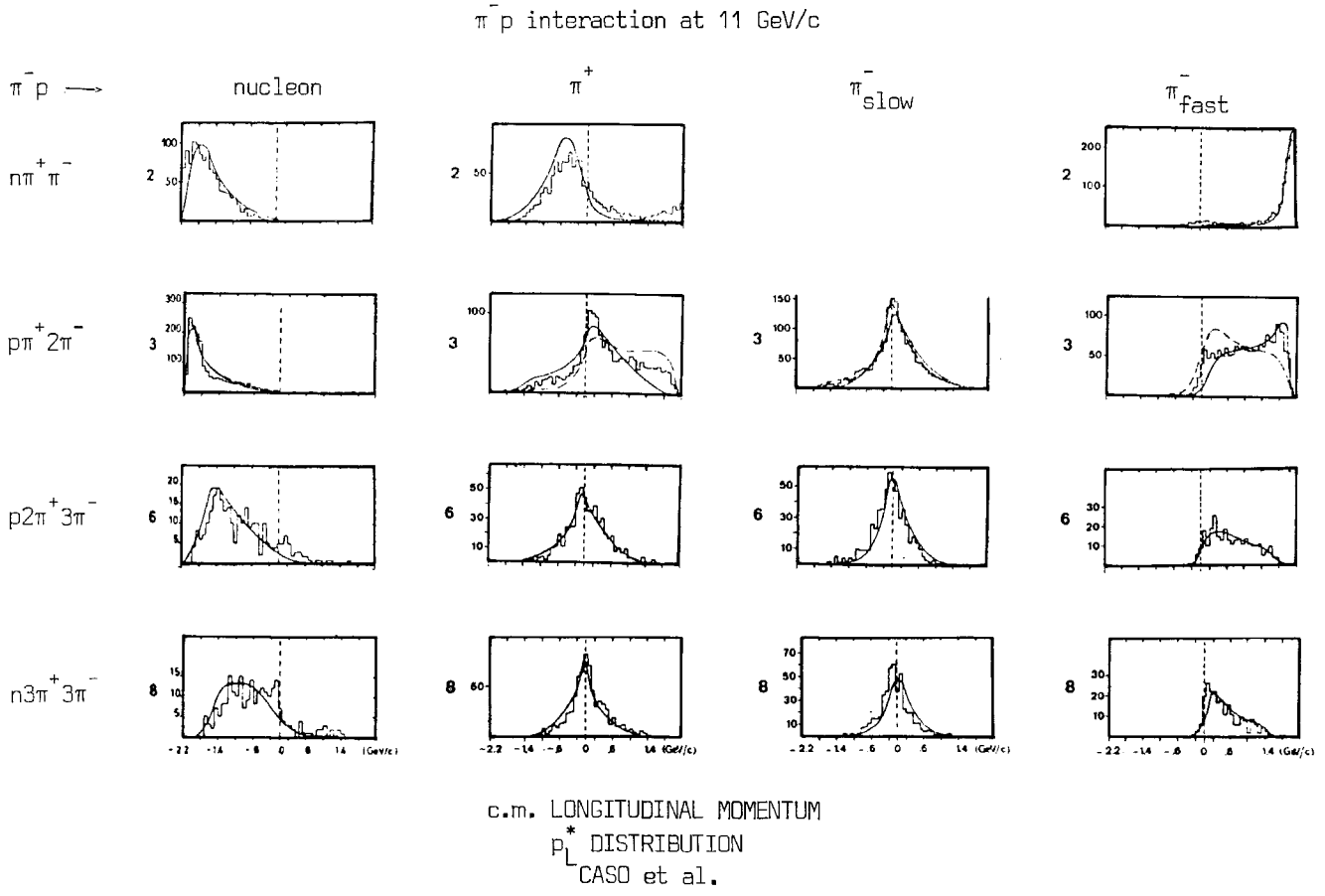

Fig. 14 c.m. longitudinal momentum distributions of particles produced in π^-p interactions at 11 GeV/c [19]. Solid lines correspond to CLA model predictions.

11 GeV/c π^-p interaction for final states containing two to six pions. The improvement consists in treating separately not only particles of different charges, but also the leading π^- which is defined as the fastest of all negative pions. Strong resonances are removed from experimental distributions. Figure 14 shows that also here there is good agreement between theory and experiment.

A very interesting and detailed study of K^+p interactions at 5 GeV/c was presented by the CERN-Brussels Collaboration[20]. The authors compare the CLA model with experimental data for three-, four-, five- and six-body final states. The general agreement is good; an example for the $K^+\pi^+\pi^-p$ final state is shown in Fig. 15, where cos θ* distributions for p, K^+, π^+ and π^- particles are presented. Five trajectories were used to describe the reactions: Pomeranchuk, strange meson, non-strange meson, nucleon and hyperon. Resonance effects were included in the calculations.

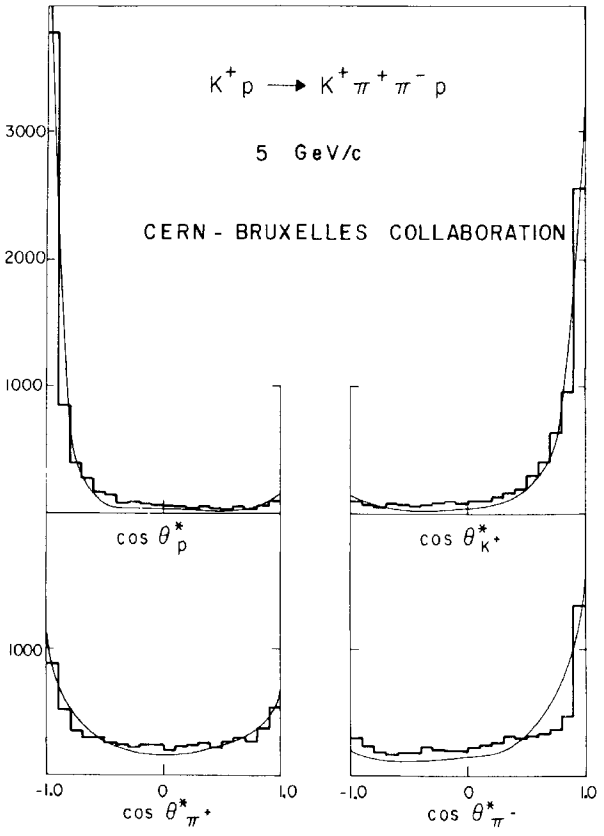

Fig. 15 Distribution of the cosine of the production angle for each of the final particles in reaction $K^+p \to K^+p\pi^+\pi^-$ at 5 GeV/c [20]. Solid lines give CLA model predictions.

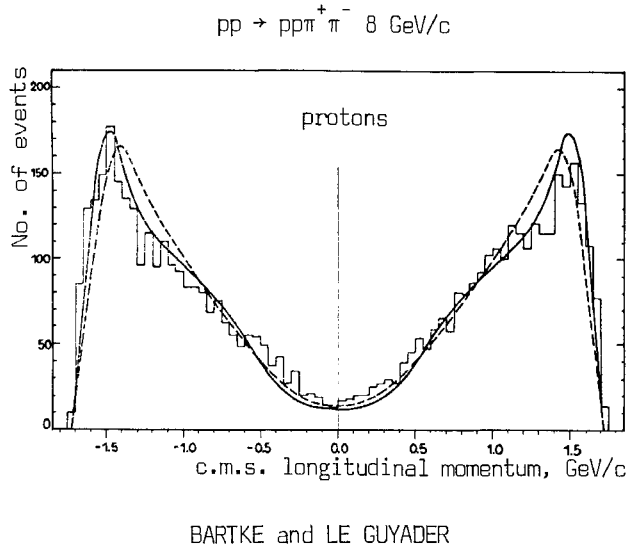

Fig. 16 Longitudinal c.m. momentum distribution for the reaction $pp \to pp\pi^+\pi^-$ at 8 GeV/c [23]. The full line gives the CLA model prediction with resonance effects included in the calculation; the broken line gives CLA model prediction without taking into account $N^*_{3/2,3/2}$ production.

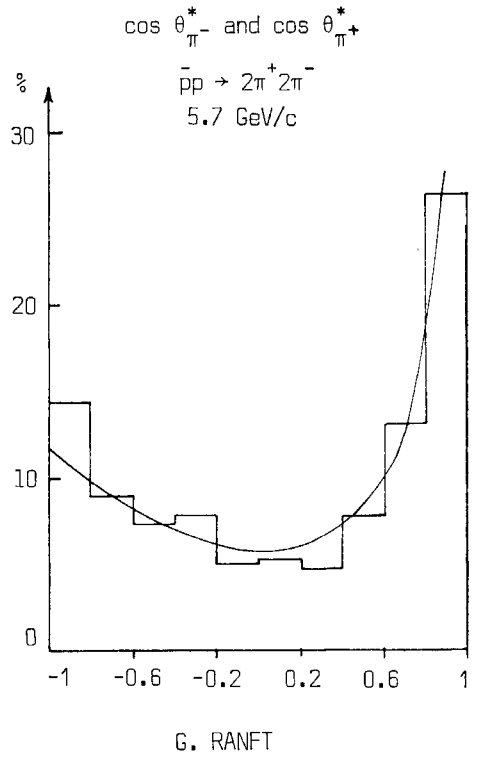

Fig. 17 $\cos\theta^*$ for π^- and $(-\cos\theta^*)$ for π^+ distribution for the reaction $\bar{p}p \to \pi^+\pi^+\pi^-\pi^-$ at 5.7 GeV/c [25]. The solid line gives Ranft multiperipheral Reggeized model calculation[24].

This question of how to include resonance production in MRM was extensively discussed by Plahte and Roberts[21]. These authors applied the CLA model with resonances included to π^+p and K^-p interactions, fitting with success several effective mass distributions.

The data of Kayas et al.[22] on the reaction $pp \to pp\pi^+\pi^-$ at 8 GeV/c are analysed with the same set of parameters in a paper by Bartke and Le Guyader[23]. Only one free parameter is used: it gives the amount of the N* production. They use a version of the MRM where at low energy the Regge amplitude is replaced by resonant (3/2,3/2) amplitude. Figure 16 shows the distribution of c.m. longitudinal momentum. The agreement with the predictions of MRM with resonance effects included is much better than for the version without resonances.

3.3 Annihilation in the frame of MRM

Ranft[24] analyses with success the CERN data on $\bar{p}p$ annihilations in flight at 5.7 GeV/c [25] with the same type of MRM; taking into account only a nucleon trajectory the author describes the data very well, as can be seen in Fig. 17 where $\cos\theta^*$ distribution for pions produced in four-pion annihilation is presented.

3.4 Multi-Regge fits to cross-sections

The MRM can also give definite predictions of the behaviour of the total cross-section for a given channel versus primary energy. Sosnowski and Wroblewski[26] have fitted compiled data on $\pi^\pm p$ interactions for a variety of channels, from two up to five pions in the final state. The general agreement in the shape of the cross-sections is fair; the authors used the same set of parameters as in the CLA paper. There is only one over-all normalization constant which is common to all channels. Cross-sections for the final states $\pi^-p\pi^0$, $p2\pi^+\pi^-$ and $p3\pi^+2\pi^-$ are to be seen in Fig. 18. At low multiplicities and low energy the predicted cross-section is much lower than the experimental one; this is partly due to the fact that s-channel resonances, abundant in this region, were not taken into account. Similar results are obtained for K^+p cross-sections by Bassompierre et al.[20].

3.5 Multiplicity distribution

The question of how often one finds a given number of secondary particles created in high-energy

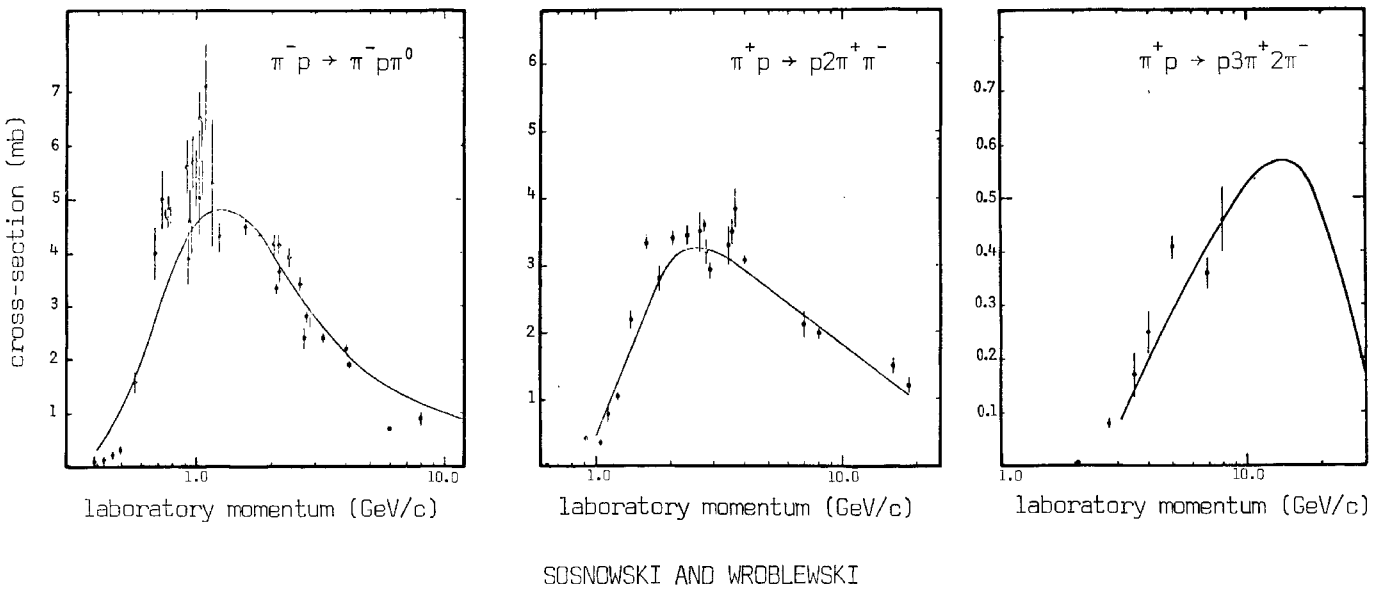

Fig. 18 Energy dependence of the cross-sections for the reactions $\pi^- p \to \pi^- p\pi^0$, $\pi^+ p \to p2\pi^+\pi^-$, and $\pi^+ p \to p3\pi^+2\pi^-$, in comparison with the CLA model predictions[26].

interaction is very important for checking the validity of models of particle production.

Brandt[27], in his paper, has made an analysis of present hydrogen bubble-chamber data for πp collisions. He uses distributions of total multiplicity (including neutral particles) reconstructed with the help of isospin statistical weight factors[28]. The data have been fitted with a Poisson distribution which, as can be seen in Fig. 19, gives reasonable agreement with experiment.

That the distribution of the number of pions produced in high-energy interactions was a Poisson one was predicted by Kajantie and Finkelstein[29], and Chew and Pignotti[30], on the basis of MRM.

The question of charged particle multiplicity distributions was also discussed by the Budapest

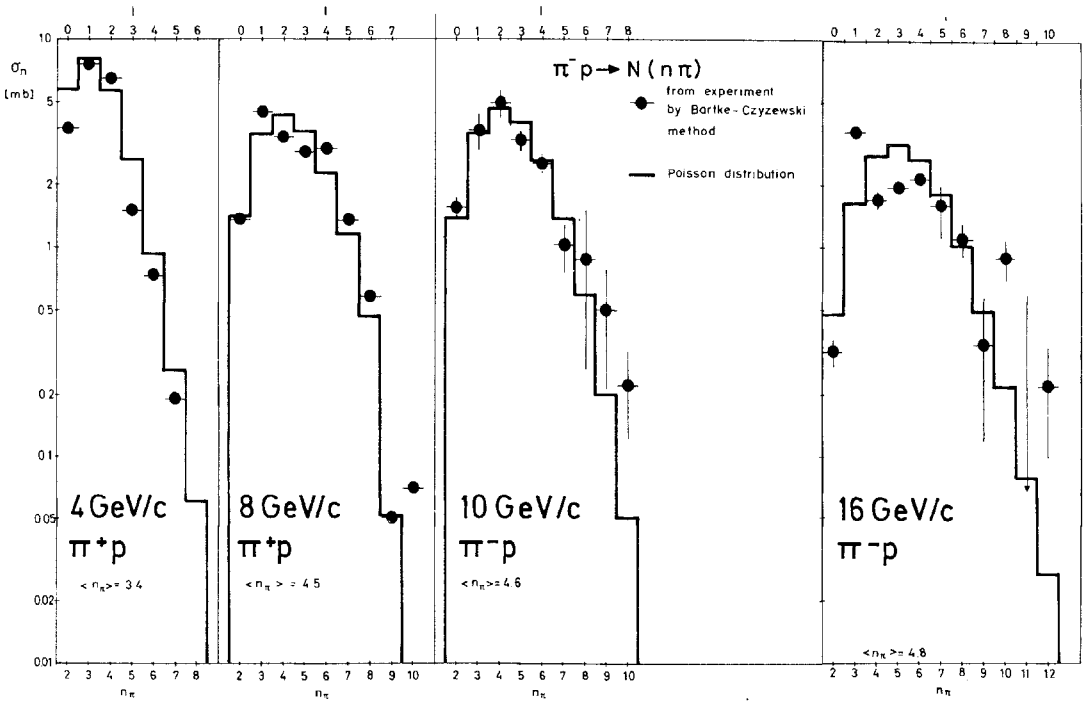

Fig. 19 Distributions of the number of secondary pions produced in $\pi^- p$ interactions compared to Poisson distributions[27].

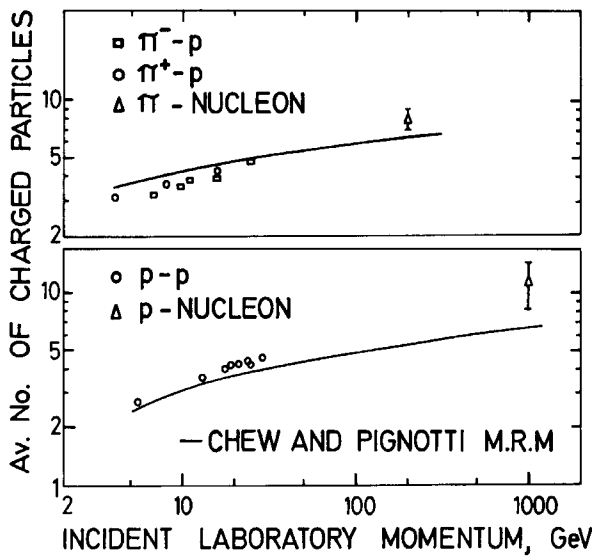

Fig. 20 Energy dependence of average multiplicity for $\pi^{\pm}p$ and pp interactions. The continuous curves correspond to the Chew and Pignotti model predictions[30].

group (Bozoki et al.)[31]. They used the formula of the exponential type

$$f(n) \sim n^b e^{-an^2}$$

and fit bubble-chamber and emulsion data.

3.6 Average multiplicity

Another interesting parameter is the average number of created particles, which is closely related to the average number of charged particles created in high-energy collisions. Figure 20 presents the energy dependence of this number for πp and pp interactions. Here the cosmic-ray point for 200 GeV/c average momentum of π-nucleon interaction was obtained by Gierula and Krzywdzinski[32] in a work based on the scanning of secondary tracks produced in very high energy interactions of nucleons in emulsion, while the nucleon-nucleon point at 1000 GeV/c [33] is also the result of scanning along the tracks of high-energy nucleons, produced in the disintegration of very high energy nuclei in emulsion.

The curves are the result of the bootstrap MRM calculation by Chew and Pignotti[30]; rough agreement is visible in the region where p_{lab} changes by two decades. This agreement is very good if one takes into account the approximations used in calculation.

3.7 Peripheral and central collisions

There is an interesting paper by Michejda[34], where he analyses the problem of angular momenta in high-energy collisions of high multiplicity. This problem relies heavily on the phases of the scattering amplitude which are unmeasurable. So the question is model dependent; Michejda shows that, for example, in MRM one can obtain higher average angular momenta for higher multiplicities. So the intuitive picture that high multiplicity collisions are more "central" than two-body ones may after all be wrong.

3.8 Conclusions of the analysis of experimental data in terms of MRM

a) The multiperipheral Reggeized model seems to describe reasonably well the main general features of many-body interactions.

b) It is, therefore, very important to analyse as much as possible of the experimental data in terms of the model. This would be particularly interesting for proton-proton interactions of high multiplicity.

c) The fine details of the interactions cannot be well reproduced in the framework of the existing versions of the model.

d) It is certainly worth while to try to develop a more sophisticated form of the model which could be substituted for the present very crude versions.

4. SATZ QUARK MODEL

Let me now discuss another approach to the problem of meson production, namely the quark model. Recently Satz[35] used the quark model to relate pp and πp inelastic cross-sections.

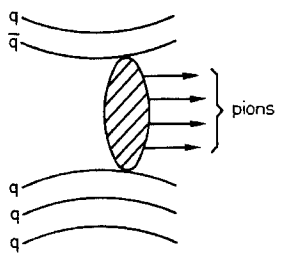

$$\sigma_{\pi N \to \pi N + k\pi}(p^{\pi}_{lab}) = \frac{2}{3}\,\sigma_{NN \to NN + k\pi}\left(\frac{3}{2}\,p^{\pi}_{lab}\right)$$

$(k = 1,2,3\ldots)$

Satz extended the quark model argument that $\sigma^{T}_{\pi p} = 2/3\sigma^{T}_{\pi pp}$ on partial cross-sections for the production of n pions and used statistical isospin weights to calculate cross-section for n-pion production from the observed charge configuration. [For

example, to obtain the cross-section for the reaction $\pi N \to \pi N + 2\pi$ one has to multiply $\sigma_{exp}(\pi^+ p \to p\pi^+\pi^+\pi^-)$ by the corresponding isospin weight factor.]

The comparison of πp and pp data is made for $p_\pi^{lab} = 2/3 p_p^{lab}$. This prescription follows from the argument that one should compare πp and pp data at equal laboratory momenta of the quarks. For the production of two and three pions, Satz found very good agreement between the weighted πp and pp cross-sections.

Hofmokl and Szeptycka[36] have extended this to show that also for high multiplicities, for four and five pions produced, the agreement is good. (Figure 21.)

Kittel et al. (CERN) [37] made a comparison of πp and Kp data, and also found general agreement with Satz predictions.

There is, however, evidence that at least in the region just above threshold, where cross-sections increase rapidly, the relation between πp and pp cross-sections is the result of the fact that for $p_\pi^{lab}/p_p^{lab} = 2/3$ the available phase space for the production of n pions is in both cases similar. Bartke and Sosnowski[38] have calculated phase-space predictions for several channels; an example for

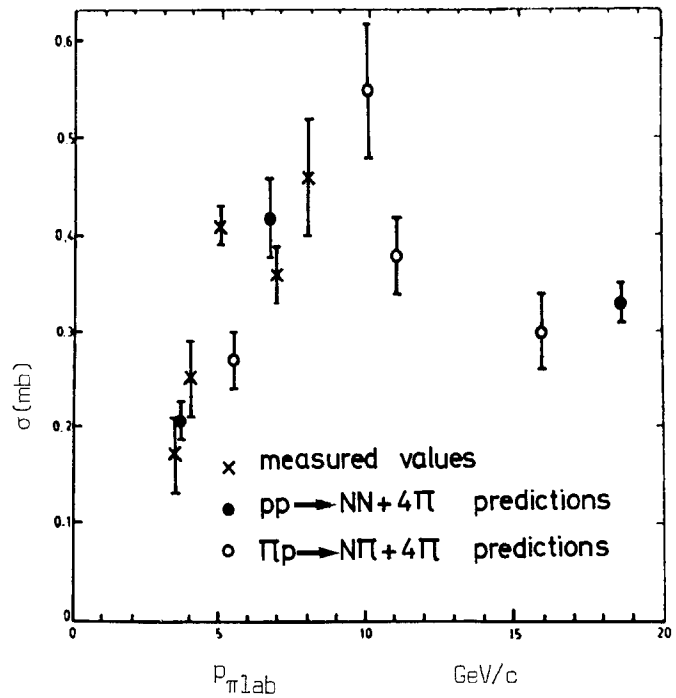

Fig. 21 Comparison of the cross-sections for the production of four and five pions in πp and pp interactions in the frame of the Satz model[36].

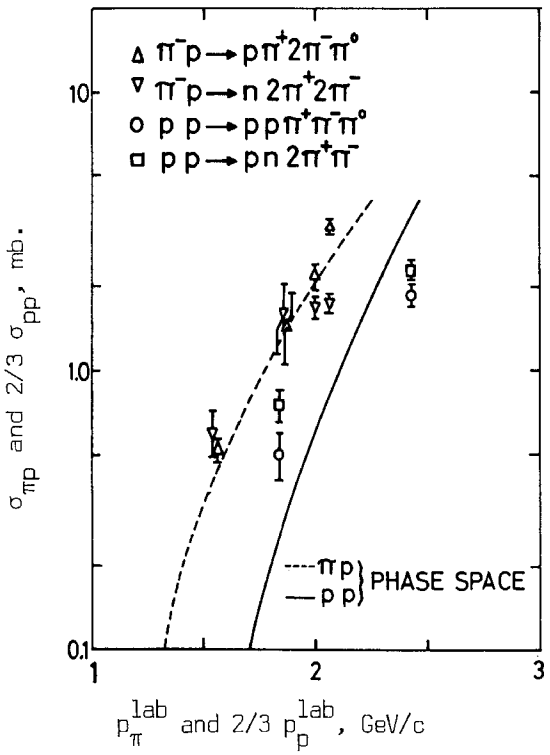

Fig. 22 Cross-sections for the production of three pions in π^-p and pp interactions in comparison with phase-space predictions[38].

production of three pions is presented in Fig. 22. Although points for primary pions and protons follow roughly the same curve, the points for pions tend to be nearer to the phase-space curve for π^-p interactions, whereas proton points follow their phase-space curve, i.e. phase-space or kinematic effects are important. At higher energy the predictions of the Satz model can be derived from the MRM. Figure 23

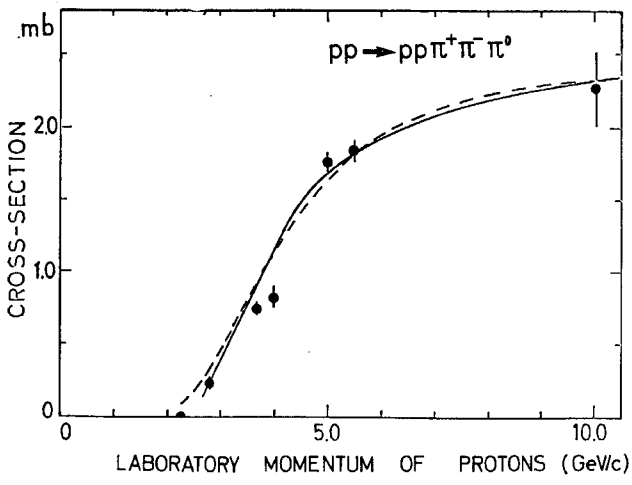

Fig. 23 Cross-section for the reaction $pp \to pp\pi^+\pi^-\pi^0$ plotted versus the laboratory momentum of incident proton. The full curve shows the predictions of the Reggeized multiperipheral model. The dashed curve shows the predictions of the same model for the reaction $\pi p \to \pi N + (3\pi)$ plotted versus the laboratory momentum of incident pion equal to 3/2 of the incident proton momentum[39].

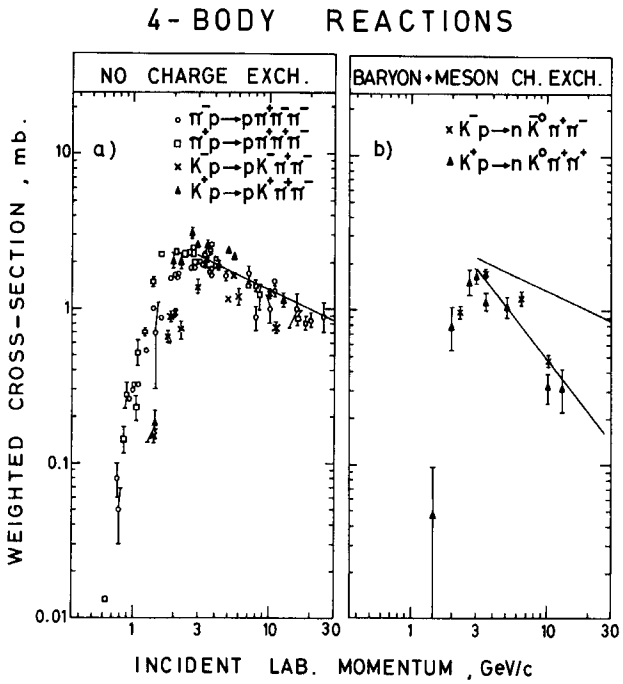

Fig. 24 Energy dependence of the cross-sections for the reactions $\pi^{\pm}p \to p\pi^{\pm}2\pi$ and $K^{\pm}p \to K^{\pm}p2\pi$, in comparison with the reaction $K^{\pm}p \to K^0n2\pi$ [37].

[Sosnowski[39]] presents the comparison in the framework of the Satz model of calculated πp and pp cross-sections for the production of three pions. The agreement is very good.

These arguments show that the predictions obtained by Satz from the quark model do not provide a sensitive test of the model.

5. CHARGE EXCHANGE OF LEADING PARTICLES

Kittel et al. (CERN) [37] made a comparison of the energy dependence of the cross-sections of the following reactions:

$$\pi^{\pm}p \to \pi^{\pm}p\,\pi^{+}\pi^{-} \qquad (a)$$

$$K^{\pm}p \to K^{\pm}p\,\pi^{+}\pi^{-} \qquad (b)$$

with the reaction:

$$K^{\pm}p \to K^0n\,\pi^{+}\pi^{-}. \qquad (c)$$

In this last reaction both "leading particles" undergo charge exchange. Figure 24 shows the comparison. One sees that the cross-section for the reaction (c) falls with increasing energy much faster than the cross-section for channels (a) and (b).

The interpretation of this picture seems to be the following (see Fig. 25):

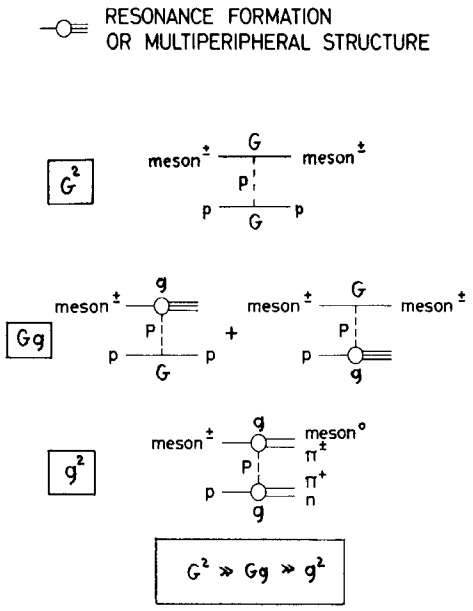

Fig. 25 Presentation of the reactions of the previous figure in terms of graphs with Pomeranchuk exchange.

a) processes where at least one of the primary particles undergoes quasi-elastic scattering (Pomeranchuk exchange) are important (dominate?) at high energy;

b) processes where Pomeranchuk exchange takes place between two groups of particles are not important at high energy.

6. PRODUCTION OF ANTIBARYONS BY MESONS

Similar observation on the importance of the Pomeranchuk exchange for inelastic processes can be made when one compares the cross-sections for the reactions in which Pomeranchuk exchange is possible, for example:

$$\text{meson} + p \to B\bar{B} + p$$

with processes where it is not possible, for example:

$$\pi^{-}p \to \Lambda\,\bar{\Lambda}\,n\,.$$

Figure 26 summarizes the cross-section for the creation of baryon pairs by mesons. The new data for $K^{+}p$ interaction at 8.25 GeV/c are presented by Bassompierre et al. (CERN-Brussels Collaboration)[40]. Beusch et al. (ETH-CERN-I.C. London)[41] present spark-chamber data on the process $\pi^{-}p \to \Lambda\bar{\Lambda}n$ at 5, 7 and 12 GeV/c. Also new Aachen-Berlin-CERN-London-Vienna data[42] for the reaction

$$K^{-}p \to p\bar{p}\Lambda \quad \text{at 10 GeV/c}$$

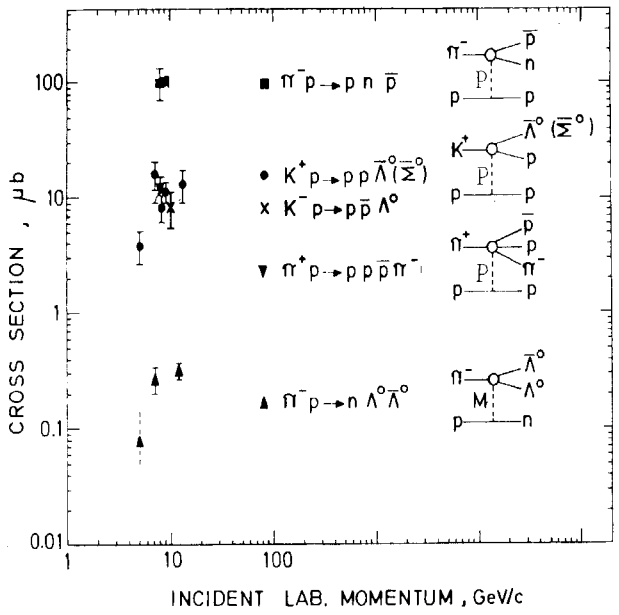

Fig. 26 Cross-sections versus energy for the reactions $K^+p \to pp\bar{\Lambda}^0(\bar{\Sigma}^0)$ [40], $\pi^-p \to \Lambda\bar{\Lambda}n$ [41], $\pi^-p \to pp\bar{p}n$, $\pi^+p \to ppp\bar{p}\pi^+$ and $K^-p \to p\bar{p}\Lambda^0$ [42].

and Aachen-Berlin-CERN data for the process:

$$\pi^+p \to pp\bar{p}\pi^+ \text{ at } 8 \text{ GeV/c}$$

have been included. An interesting fact is seen: when the production of the $B\bar{B}$ pair is possible via diffraction dissociation-- no quantum number exchange, Pomeranchuk exchange-- the cross-section is an order of magnitude larger than in the case when charge or strangeness has to be exchanged.

7. COHERENT PRODUCTION ON NUCLEI

In general the word "coherent" applied to a reaction means that the nucleus emerges from the collision in the same state as before the collision. The most characteristic feature of such a reaction [see, for example, a paper by the Berkeley-Milan-Orsay-Saclay Collaboration[43]] is a narrow peak in the distribution of the four-momentum transfer t. This distribution can be described by the formula:

$$d\sigma/dt \sim e^{at}$$

with $a \propto A^{2/3}$, A being the atomic number of the nucleus in question. Most of the information about inelastic coherent processes was obtained from heavy liquid bubble-chamber data; several papers about coherent production on a target composed of one kind of nuclei, and not a mixture (i.e., on deuterons and Ne nuclei), were submitted to this Conference.

Several groups have reported data on K-deuterium interactions:

$$K^-d \to K^-\pi^+\pi^-d$$

at 3 GeV/c by the SABRE collaboration[44]; the same reaction at 5.5 GeV/c was observed by Phelan et al. (Argonne-Northwestern)[45]. The reaction:

$$K^+d \to K^+\pi^+\pi^-d$$

at 3 GeV/c was studied by Buchner et al. (Munich-Brussels-CERN Collaboration)[46].

The main features of both reactions are found to be as follows: the mass of the created $K^\pm\pi^+\pi^-$ system is rather low; it is a broad enhancement of about 300 MeV width, centred at $\sim$ 1.25 GeV (Fig. 27). K^+ and π^- (or K^- and π^+) form in a high percentage of events a $K^*(890)$, so that the reaction in question is mostly a three-body one:

$$K^\pm d \to K^{*0}\pi^\pm d.$$

Figure 28 presents p_L^*, $p_\perp$ plots, also called Peyrou plots, for this reaction[46] at 3 GeV/c. Deuterons are seen to be produced mostly backward, near the kinematic limit; K^* are emitted forward; also π's are produced in the forward direction, but this is less marked than for K^*'s.

The analysis of the decay angular distribution inside the $K^*\pi$ system leads to the conclusion that the mechanism responsible for its production is of the Deck type:

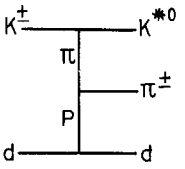

The spin and parity of the created system are most probably 1^+, in accordance with Morrison's rule:

$$P_f = P_i(-1)^J$$

where $P_f(P_i)$ denotes the parity of final (initial) state of the outgoing (incoming) particle and J is the change in the angular momentum.

Very similar conclusions are reached in the paper by Cnops et al. (Brookhaven-Oak Ridge-Philadelphia Collaboration)[47] on the mechanism of the coherent production of $\pi^+\pi^+\pi^-$ system by 8 GeV/c π^+ mesons on deuterons.

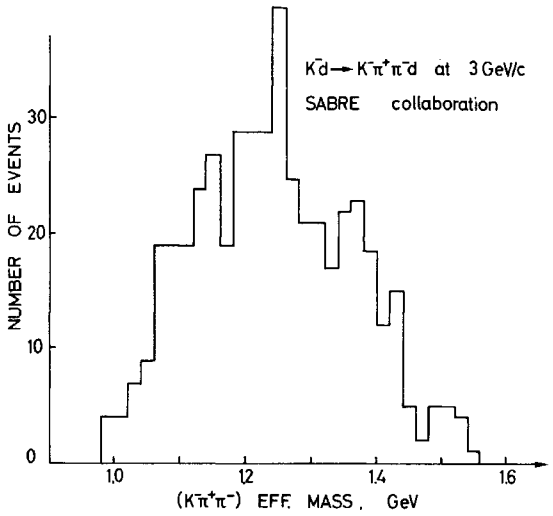

Fig. 27 Effective mass distribution of the $K^-\pi^+\pi^-$ system for the reaction $K^-d \to K^-\pi^+\pi^-d$ at 3 GeV/c laboratory incident momentum[44].

Data on the coherent production on neon were presented by Bingham et al. (Berkeley-Brookhaven-Milan-Orsay-Saclay Collaboration)[48]. The reaction studied was:

$$K^- \, Ne \to K^-\pi^+\pi^- \, Ne$$

at 5.5 and 12.7 GeV/c incident momentum in an exposure of the 80 in. BNL bubble chamber, filled with a mixture of H_2 and Ne. Figure 29 shows the t' distribution: the slope a = 90 GeV^{-2}, corresponding to the radius of $\sim$ 3.2 f.

A similar experiment, but with a 28 GeV/c proton beam,was performed by Huson et al.[49] at Brookhaven.

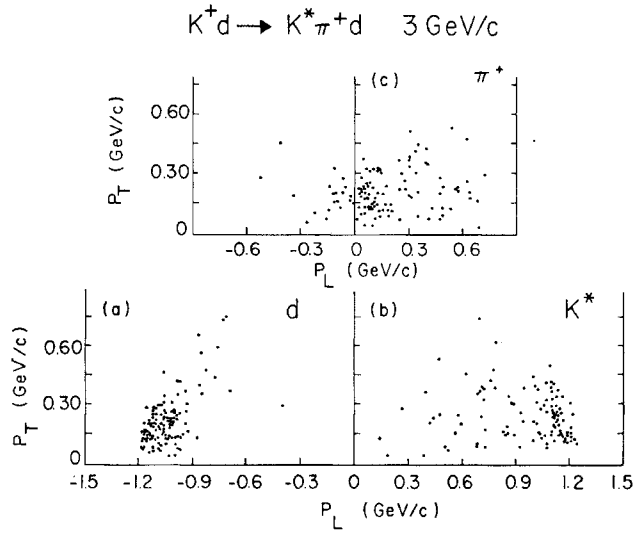

Fig. 28 Transverse (T) versus longitudinal (L) momenta for: (a) d, (b) K^*, and (c) π^+ in the over-all c.m. for the reaction $K^+d \to K^{*0}\pi^+d$ at 3 GeV/c [46].

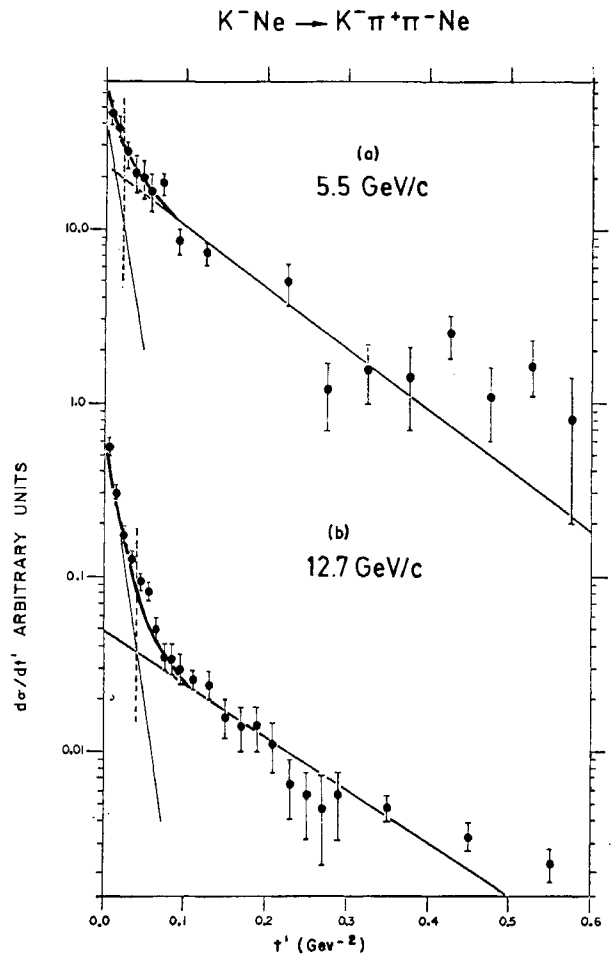

Fig. 29 Distribution of the t'($t'=|t-t_{min}|$) to the $K\pi\pi$ system for the reaction $K^-Ne \to K^-\pi^+\pi^-Ne$, (a) at 5.5 GeV/c and (b) at 12.7 GeV/c [48].

The reaction was:

$$p \, Ne \to p \, \pi^+\pi^- \, Ne \, .$$

Figure 30 gives the t' distribution; the slope is a = (110 ± 50) GeV^{-2}.

Using a nuclear absorption model, the authors tried to calculate the total interaction cross-section of the emerging $p\pi^+\pi^-$ system on the nucleon. The average mass of this system is about 1470 MeV; the question whether it is a resonance or kinematic enhancement remains unsettled. The result is:

$$\sigma(1470) = 30 \text{ to } 70 \text{ mb.}$$

The accuracy is not high, but measurements of this type are extremely important. They can be made in a reliable way only when one knows exactly what the target is; this is the case here. Obviously much higher statistics are necessary.

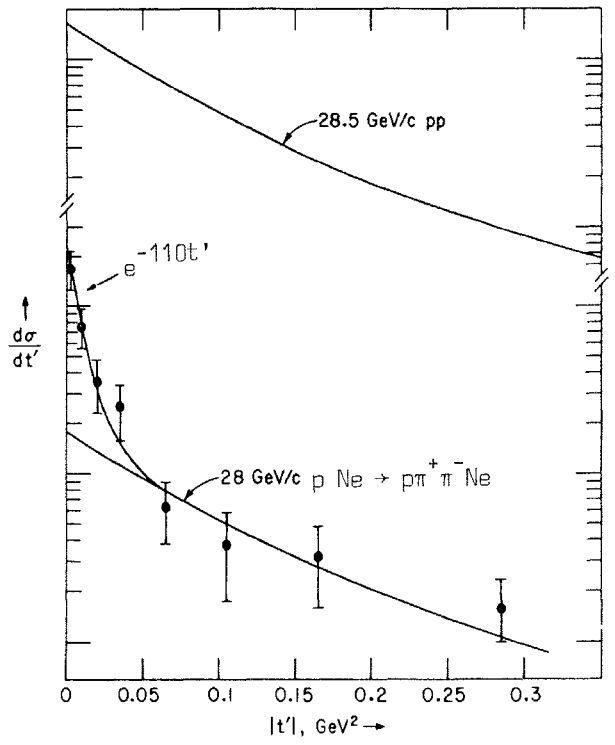

Fig. 30 t' distribution to the $p\pi^+\pi^-$ system for the reaction $pNe \to p\pi^+\pi^-Ne$ at 28 GeV/c [49]. Upper curve corresponds to the reaction $pp \to pp\pi^+\pi^-$, $M(p\pi^+\pi^-) < 1.6$ GeV [71].

Finally, let me mention the cosmic-ray paper by Hébert and Molloy[50] from Ottawa University; they find in nuclear emulsions three events, which are interpreted as coherent interactions of high-energy nuclei (Z of the order of 20, energy 10-20 GeV per nucleon) in an emulsion.

8. ANGULAR CORRELATIONS

Several years ago, Goldhaber et al.[51] (GGLP) discovered in $\bar{p}p$ annihilations that correlations existed in the distributions of the angle between two pions: the average value of the angle between pions of equal charge was smaller than in the case of pairs of opposite charge. As a measure of the effect the parameter γ was introduced:

$$\gamma = \frac{\text{number of pairs with } \theta_{\pi\pi} > 90°}{\text{number of pairs with } \theta_{\pi\pi} < 90°}$$

$\gamma^{+-} > \gamma^{\pm\pm}$ (gamma "unlike" is greater than gamma "like").

There is now certainly a revival of the interest in this subject, the same type of correlations being found[52] in π^+p interactions at 8 GeV/c. Evidence has been presented by Eskreys[53] of the existence of these correlations for π^0-π^0 pairs. Eskreys shows that in π^- interactions at 9 GeV/c primary momentum in a xenon bubble chamber, the average value of the angle between the two π^0 mesons is significantly smaller than expected for non-correlated production.

New results for this type of correlation for charged pions were presented by Bellini et al. (Milan and Orsay Collaboration)[54] for 8 and 16 GeV/c π^--proton and π^--nucleus interactions, by the Aachen-Berlin-Bonn-CERN-Warsaw Collaboration[55] for the 16 GeV/c π^--proton interactions, and by Fridman et al. (Strasbourg group)[56] for the eight-prong $\bar{p}p$ annihilations at 5.7 GeV/c. The general impression is that the effect depends rather strongly on details of the interaction mechanism, especially on resonance production.

To summarize briefly:

a) annihilation

the effect is strongest at rest, $(\gamma^U - \gamma^L)$ decreases when c.m. energy increases;

b) π-p interactions

i) effect is better seen if γ's are calculated in the c.m. system of pions, not in the over-all c.m. system;

ii) $\gamma^{++} > \gamma^{--}$ for primary π^+;
$\gamma^{--} > \gamma^{++}$ for primary π^-;

iii) there are $\pi^0\pi^0$ correlations.

Conclusion: if one knew the matrix element describing the pion system, one could reproduce these effects.

It is my belief that this is proved by Diaz et al. (CERN-Collège de France Collaboration)[57] in the study of $\bar{p}p \to \pi^+\pi^+\pi^-\pi^-$ annihilations at rest. This process is analysed in terms of amplitudes, dominated by the $^3S_1$ $\rho\pi\pi$ amplitude. The GGLP correlations are very strong. Figure 31 presents the distributions of cos $\theta_{\pi\pi}$ for like and unlike pion pairs. The fit is very good; the effect is probably mainly due to the $\rho\rho$ interference terms[58]. This type of analysis, if it could be extended to higher multiplicities and higher energies, could give valuable information on the detailed structure of final states.

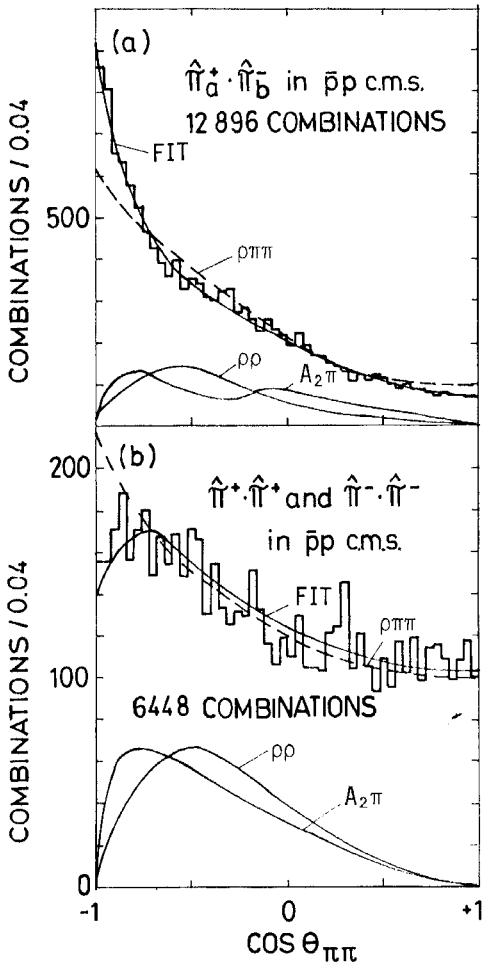

Fig. 31 Distributions of the cos $\theta_{\pi\pi}$ angle for $\pi^+\pi^+$, $\pi^-\pi^-$ and $\pi^+\pi^-$ pion pairs for the annihilation at rest $pp \to \pi^+\pi^+\pi^-\pi^-$. The curves represent model calculations[57].

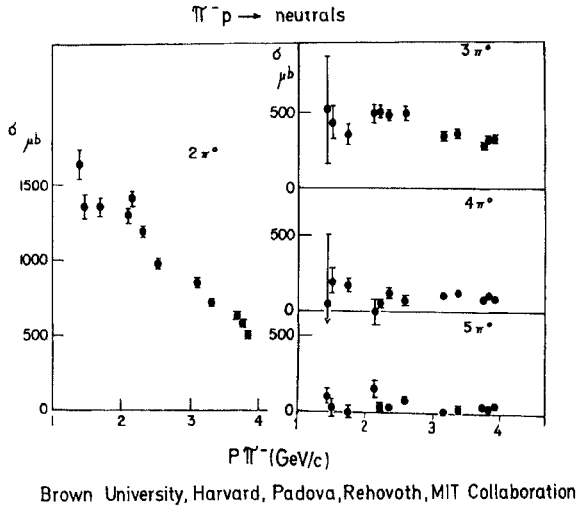

Fig. 32 Energy dependence of the cross-sections for the production of two, three, four and five neutral pions by π^- mesons on protons[59].

9. NEUTRAL PARTICLE PRODUCTION

A new class of experimental data is presented by the Brown University-Harvard-Padua-Rehovoth-MIT Collaboration in the paper by Crouch et al.[59]. The authors present energy dependences of the cross-section for the reaction $\pi^- p \to$ neutrals for different neutral pion multiplicities. Measurements are performed using a spark-chamber technique. Figure 32 presents cross-sections for the production of two, three, four and five neutral pions in the energy range 1.4-4.0 GeV/c. Higher multiplicity channels [reactions $\pi^- p \to n + (3,4,5)\pi^0$] show very little, if any, energy dependence. It would be of considerable interest to have more detailed data on those interactions, also at higher energy.

10. $p_\perp - p_L^*$ CORRELATIONS FOR STRANGE PARTICLES

The longitudinal and transverse momentum distributions for the reaction $\pi^- p \to K\bar{K}Nm\pi$ and $\pi^- p \to K\Lambda m\pi$ at 4 GeV/c incident momentum were studied by a Dubna group (Bannik et al.)[60] in the JINR propane bubble chamber. Correlation between p_L^* and $p_\perp$ for K^0 mesons, similar to that observed in many experiments for pions, has been found (Fig. 33).

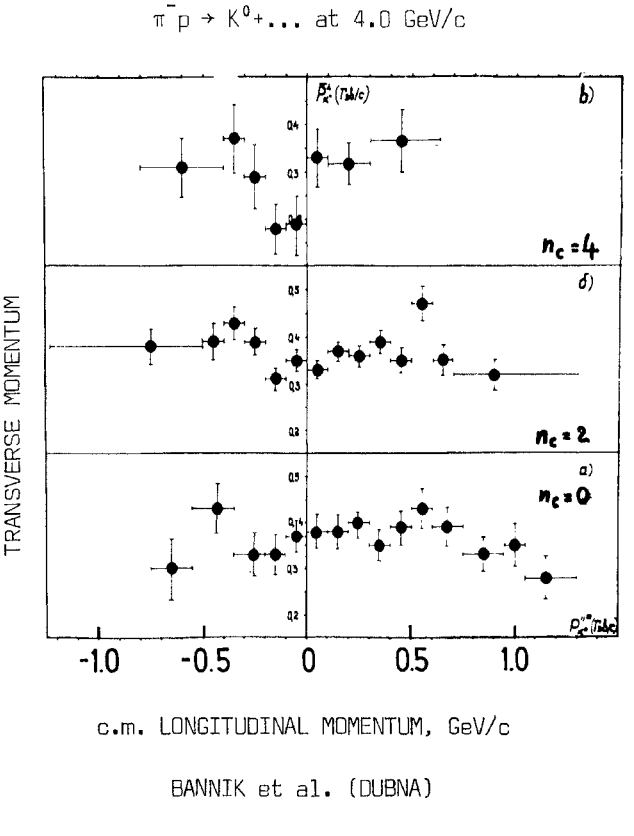

Fig. 33 $\langle p_\perp \rangle$ versus $\langle p_L^* \rangle$ plot for K^0 mesons, produced in $\pi^- p$ interactions at 4 GeV/c [60].

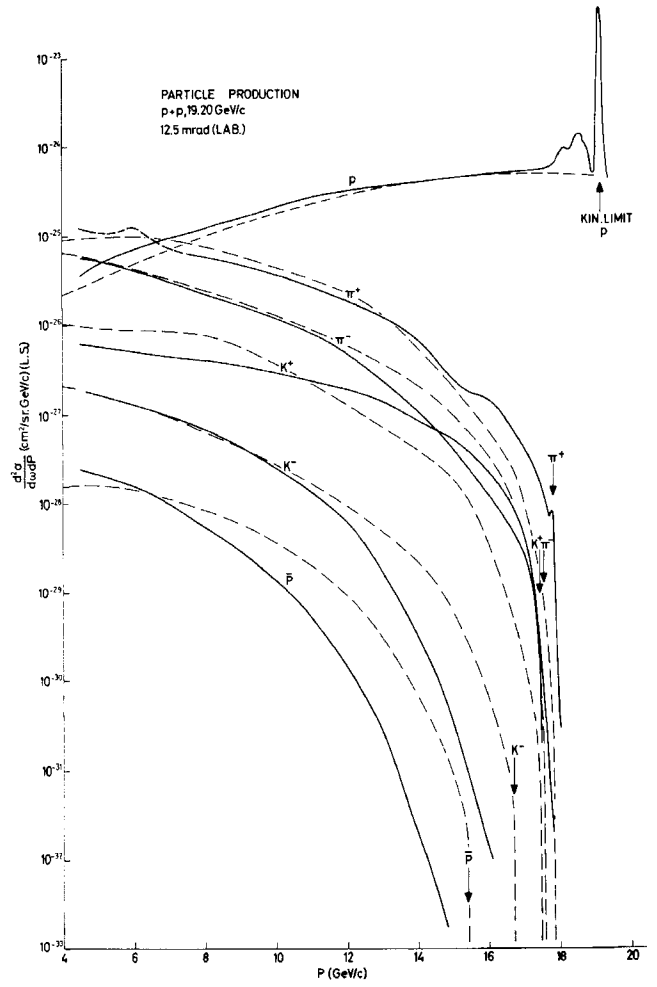

Fig. 34 Comparison of the particle spectra produced in 19 GeV/c pp interactions at 12.5 mrad production angle (solid lines)[61] with the predictions of the thermodynamics model of Hagedorn and Ranft[62] (broken lines).

11. PROTON-PROTON COUNTER EXPERIMENTS AND PHENOMENOLOGICAL FITS TO THE DATA

Allaby et al.[61] present new data on the spectra of particle production in pp interactions at 19 GeV/c. Figure 34 shows the comparison of these data with the thermodynamical model of Hagedorn and Ranft[62]. The agreement is not very good. It can be probably improved by changing the parameters of the model.

G. Yen[63] presents the fits to the data of Ratner et al.[64] and of Anderson et al.[65] on pp interactions at 12.5 and 30 GeV/c, respectively. The fit is based on the assumption that pp interactions are dominated by two-body reactions:

$$pp \to N^* + N^* .$$

Qualitative agreement with experimental data was found.

Friedländer[66] analysed the $p_\perp$ distributions of particles produced in 16 GeV/c $\pi^- p$, 25 GeV/c $\pi^- p$ and 5.7 GeV/c $\bar{p}p$ interactions. His conclusions are the following:

a) the often-used formula:

$$f(p_\perp) \sim p_\perp \, e^{-p_\perp/p_0}$$

is not adequate to describe the data;

b) the formula:

$$f(p_\perp) \sim p_\perp \, e^{-p_\perp^2/p_0^2}$$

describes moderately well $p_\perp$ distributions for protons; it does not describe the distributions for emitted pions.

c) pion data can be well reproduced by the formula

$$f(p_\perp) \sim a p_\perp \, e^{-p_\perp^2/p_1^2} + b p_\perp \, e^{-p_\perp^2/p_2^2}.$$

12. INELASTIC Kπ INTERACTIONS

Trippe et al.[67] use the OPE model to extract information on the Kπ interaction. They have studied energy dependence of the cross-section for single and double pion production in $K^+\pi^-$ interactions.

The validity of this method was previously tested on inelastic πp interaction cross-sections [Colton et al.[68]] derived from the study of pp interactions.

Figure 35 presents the energy dependence of the cross-sections for the reactions:

$$K^+\pi^- \to K^+ \pi^0$$
$$\to K^0 \pi^+ \pi^-$$
$$\to K^0 \pi^0 \pi^+ \pi^- .$$

Obviously the results of this type based on larger statistics will be very interesting; for example it will be possible to study the reaction:

$$K^+\pi^- \to K^{*0}\rho^0, \text{ etc.}$$

13. ISOTOPIC SPIN DEPENDENCE OF THE ANNIHILATION CROSS-SECTION

Camerini et al. (Wisconsin)[69] have determined the ratio of I = 1 to I = 0 $\bar{N}N$ annihilation cross-sections, comparing the data on $\bar{p}d$ and $\bar{p}p$ annihilations.

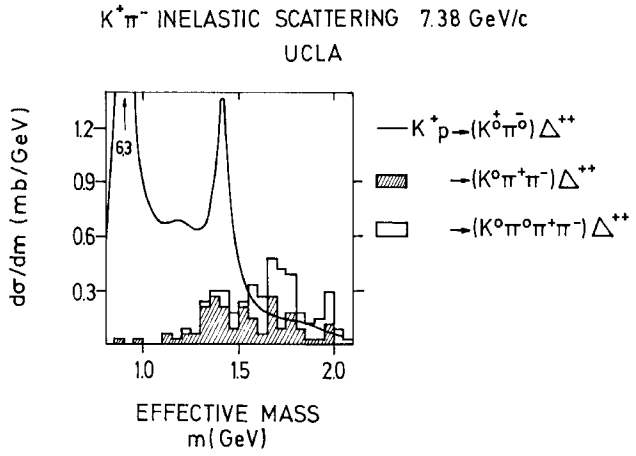

Fig. 35 $K^+\pi^-$ inelastic scattering from Trippe et al.[67]. The histogram shows data for the two indicated reactions for the Δ^{++} and $|t| < 0.5$ GeV^2 selections.

In the energy range 1.2-5.5 GeV/c the ratio $\sigma_{ANN}(I=0)/\sigma_{ANN}(I=1)$ is much larger than one, varying from about 4 at low momenta down to about 3 at 5.5 GeV/c.

14. RARE $\bar{p}d$ PROCESSES

I would like to mention now the experiment of Bizzarri et al. (Rome-Syracuse University Collaboration)[70] who found that lambdas can be produced by antiprotons stopping in a deuterium-filled bubble chamber, although this is below the threshold for two-body reactions, which one normally assumes, taking one of the baryons in the deuteron to be a spectator. Hence it must be concluded that all three particles are involved in the reaction. Another striking result is the presence of the reaction: $\bar{p}d \to p\pi^-$, observed at the rate of $(1.0 \pm 0.4) \times 10^{-5}$ per annihilation. This is also a three-body initial state interaction; $\bar{p}$ reacts with both nucleons of the deuteron.

Acknowledgements

It is a pleasure to thank Dr. D.R.O. Morrison for many helpful discussions and for reading the manuscript; thanks are due also to the scientific secretaries, especially to Dr. P. Villemoes, for their help.

I would like to express my gratitude to Professor C. Peyrou for the hospitality extended to me at the CERN Track Chamber Division, where a great part of the work on this report was done.

REFERENCES AND FOOTNOTES

1. Aachen-Berlin-Bonn-CERN-Cracow-Heidelberg-Warsaw Collaboration, paper 465.
2. Aachen-Berlin-CERN Collaboration and Aachen-Berlin-CERN-London-Vienna Collaboration, abstract 450.
3. G. Bialkowski and R. Sosnowski, Phys. Letters 25 B, 519 (1968).
4. T. Coghen et al., paper 755.
5. D.H. Perkins, in Proc. Int. Conf. on Theoretical Aspects of High Energy Phenomena, CERN 61-22 (1961).
6. For the detailed list of references, see, for example, G.F. Chew and A. Pignotti, UCRL-18275, to be published in Phys. Rev.
7. G. Alexander et al., paper 659.
8. G.B. Yost et al., paper 64.
9. Lips and Zweig, Analysis of the data of the University of Wisconsin (Walker-Erwin Group), private communication by Dr. Zweig.
10. E.W. Ellis et al., paper 368.
11. H. Bøggild et al., paper 779.
12. See, for example, E. Ferrari and F. Selleri, Nuovo Cimento Suppl. 24, 453 (1962).
13. G.W. Brandenburg et al., paper 36.
14. E. Colton et al., paper 541 and UCLA-1023 Rev.
15. J.G. Rushbrooke et al., paper 560.

16. E.L. Berger, E. Gellert, G.A. Smith, E. Colton and P.E. Schlein, Phys. Rev. Letters 20, 964 (1968).

17. W.M. Dunwoodie et al., paper 696.

18. Chan Hong-Mo, J. Loskiewicz and W.W.M. Allison, CERN preprint TH.866 (1968).

19. Genoa-Hamburg-Milan-Saclay Collaboration, paper 326.

20. G. Bassompierre et al., paper 440.

21. E. Plahte and R.G. Roberts, CERN preprint TH.919, 1968.

22. G. Kayas, J. Le Guyader, M. Sene, T.P. Yiou, J. Alitti, Nguyen Thuc Diem, G. Smajda, J. Ginestet, D. Nanerse and Tran Ha Anh, Nuclear Physics B5, 169 (1968).

23. J. Bartke and J. Le Guyader, paper 485.

24. G. Ranft, paper 798.

25. A. Accensi, V. Alles-Borelli, B. French, Å. Frisk, J.M. Howie, W. Krischer, L. Michejda, W.G. Moorhead, B.W. Powell, P. Seyboth and P. Villemoes, Phys. Letters 20, 557 (1966).

26. R. Sosnowski and A. Wroblewski, paper 203.

27. S. Brandt, paper 775.

28. J. Bartke and O. Czyzewski, Nuclear Phys. B5, 582 (1968).

29. J. Finkelstein and K. Kajantie, CERN preprint TH.857 (1968).

30. G.F. Chew and A. Pignotti, UCRL 18275 (1968).

31. G. Bozóki et al., abstract 38.

32. J. Gierula and S. Krzywdziński, paper 574 (submitted to Nuovo Cimento).

33. F. Abraham, J. Gierula, R. Levi Setti, K. Rybicki, C.H. Tsao, W. Wolter, R.L. Fricken and R.W. Muggett, Phys. Rev. 159, 1110 (1967).

34. L. Michejda, paper 577 (to be published in Fortschritte der Physik).

35. M. Satz, Phys. Letters 25 B, 220 (1967);
M. Satz, Phys. Rev. Letters 19, 1453 (1967).

36. T. Hofmokl and M. Szeptycka, paper 575, and Phys. Letters 26 B, 546 (1968).

37. E.W. Kittel et al., abstract 469.

38. J. Bartke and R. Sosnowski, paper 201.

39. R. Sosnowski, paper 202.

40. G. Bassompierre et al., paper 448.

41. W. Beusch et al., paper 520.

42. Aachen-Berlin-CERN-London(I.C.)-Vienna Collaboration, private communication from Dr. D.R.O. Morrison.

43. Berkeley-Milan-Orsay-Saclay Collaboration, Topical Conference on High-Energy Collisions of Hadrons, CERN 68-7, (1968), vol. 1, p. 537.

44. Saclay-Amsterdam-Bologna-Rehovoth-Ecole Poly. Collaboration, paper 477.

45. J. Phelan et al., paper 954.

46. K. Buchner et al., paper 442.

47. A.M. Cnops et al., paper 209.

48. Berkeley-Brookhaven-Milan-Orsay-Saclay Collaboration, paper 401.

49. F.R. Huson et al., paper 208.

50. H. Hébert et al., paper 364.

51. G. Goldhaber, S. Goldhaber, W. Lee and A. Pais, Phys. Rev. 120, 300 (1960).

52. J. Bartke, O. Czyzewski, J.A. Danysz, A. Eskreys, J. Loskiewicz, P. Malecki, J. Zaorska, K. Eskreys, K. Juszczak, D. Kisielewska, W. Zielinski, M. Szeptycka, K. Zalewski, G. Pichon and M. Rumpf, Phys. Letters 24 B, 163 (1967).

53. K. Eskreys, paper 882.

54. G. Bellini et al., paper 894.

55. Aachen-Berlin-Bonn-CERN-Warsaw Collaboration, paper 467.

56. A. Fridman et al., paper 578.

57. J. Diaz et al., paper 439.

58. K. Zalewski, Proceedings of the VIIth Cracow School of Theoretical Physics, June 1967, vol. 2, p. 31.

59. H.R. Crouch Jr. et al., paper 820.

60. B.P. Bannik et al., paper 69.

61. J.V. Allaby et al., paper 604.

62. R. Hagedorn and G. Ranft, preprint CERN TH.851 (1967).

63. E. Yen, paper 529.

64. L.G. Ratner et al., paper 546 and Phys. Rev. 166, 1353-1364 (1968).

65. E.W. Anderson, E.J. Bleser, G.B. Collins, T. Fujii, J. Menes, F. Turkot, R.A. Carrigan Jr., R.M. Edelstein, N.C. Hien, T.J. McMahon and I. Nadelhaft, Phys. Rev. Letters 19, 198 (1967).

66. E.M. Friedländer, Shape of the transverse momentum distribution from high energy inelastic interactions, unpublished.

67. T.G. Trippe et al., paper 542 and UCLA 1024 (1968).
P.E. Schlein, $K\pi$ scattering and normal parity K^*'s, UCLA-1029 (1968).

68. E. Colton et al., paper 543.

69. U. Camerini et al., paper 283.

70. R. Bizzarri et al., paper 380.

71. P.L. Connolly, W.E. Ellis, P.V.C. Hough, D.J. Miller, T.W. Morris, C. Quannes, R.S. Panvini and A.M. Thorndike, Third Topical Conference on Resonant Particles, Athens, Ohio, November 1967.